P H D T H E S I S

presented to

University of Cergy-Pontoise
École Doctorale Sciences et Ingénierie

to obtain the title of

Doctor of Science of the University of Cergy-Pontoise

Specialty: Sciences and Technologies of Information and Communication

Defended by

Abdel Nasser ASSIMI

Diversity Techniques for HARQ Transmissions over Frequency-Selective Channels

prepared at
Equipes Traitement de l'Information et Systèmes (ETIS) - UMR8051
ENSEA - Université de Cergy-Pontoise - CNRS

defended on December 17, 2009

Jury:

Reviewers:	M.	Zhi DING	University of California Davis
	M.	Dirk SLOCK	Eurecom Sophia Antipolis
Examinators:	M.	Pierre DUHAMEL	LSS/Supelec-CNRS
	M.	Philippe LOUBATON	Université de Marne la Vallée
Advisor:	Mme.	Inbar FIJALKOW	ETIS/ENSEA-UCP-CNRS
Co-advisor:	M.	Charly POULLIAT	ETIS/ENSEA-UCP-CNRS
Invited:	M.	Christophe LE MARTRET	THALES

Résumé

Nous considérons dans cette thèse le problème de la transmission fiable de données par paquets en utilisant une transmission mono-porteuse sur des canaux sélectifs en fréquence à évanouissements. Notre objectif est de concevoir des couples émetteurs-récepteurs permettant d'améliorer les performances de la détection en l'absence d'information sur le canal à la transmission et ceci en exploitant la diversité temporelle disponible dans le cadre des protocoles de retransmission hybrides (HARQ).

En analysant les performances du système de transmission avec un récepteur à maximum de vraisemblance, nous établissons un critère pertinent pour l'étude des performances du système basé sur les statistiques de la distance Euclidienne à la sortie du canal sélectif en fréquence. A partir de ce cadre théorique, nous proposons un nouveau schéma de diversité entre les différentes retransmissions, nommé précodage de phase, qui permet de combattre l'interférence entre symboles pour les canaux lentement variables dans le temps. Puis, à l'aide de nos outils d'analyse, nous revisitons un autre schéma de diversité qu'est la diversité d'entrelacement. En particulier, nous soulignons le double avantage offert par ce schéma, à savoir la diversité de modulation et la réduction de l'interférence entre symboles. Nous réalisons ensuite une étude comparative entre les deux schémas de diversité précédents sous traitement itératif ou non itératif au récepteur. Enfin, nous introduisons un nouveau protocole de retransmission adaptative pour les transmissions dîtes multi-couches afin de réduire l'interférence entre couches pour les canaux rapidement variant dans le temps utilisant des informations de retour limitées.

Abstract

In this thesis, we consider the problem of reliable data packets transmission using single-carrier signaling over frequency-selective fading channels. Our objective is to design enhanced transceivers with improved detection performance in the absence of channel state information at the transmitter by exploiting the available time-diversity in Chase combining Hybrid Automatic Repeat reQuest (HARQ) protocols.

By analyzing the performance of the transmission scheme using an optimal maximum-likelihood receiver, we establish a suitable criterion for the study of system performance based on the statistics of the Euclidean distance at the output of a frequency-selective channel. From this theoretical framework, we propose a novel transmit-diversity scheme between subsequent HARQ transmissions, called phase-precoding, which allows the mitigation of intersymbol interference for slow time-varying channels. Then, with the help of our analytical tools, we revisit another transmit-diversity scheme which is the bit-interleaving diversity scheme. In particular, we emphasize the double advantage offered by this diversity scheme including the inherent modulation diversity in addition to the intersymbol interference reduction. Subsequently, we perform a comparative study between phase-precoding and bit-interleaving diversity schemes under iterative and non-iterative receiver structures. Finally, we introduce a new adaptive retransmission protocol for a multi-layer transmission scheme for the mitigation of inter-layers interference for rapidly time-varying channels using limited feedback information.

Contents

List of Figures

List of Tables

Glossary

3GPP	Third Generation Partnership Project
APP	A *Posteriori* Probability
AC	Auto-Correlation
ARQ	Automatic Repeat reQuest
AWGN	Additive White Gaussian Noise
BER	Bit-Error Rate
BICM	Bit-Interleaved Coded Modulation
BID	Bit-Interleaving Diversity
BPSK	Binary Phase-Shift Keying
CC	Chase-Combing
CP	Cyclic Prefix
CSI	Channel State Information
DFT	Discrete Fourier Transform
EDGE	Enhanced Data rate for GSM Evolution
EXIT	EXtrinsic Information Transfer
FD	Frequency-Domain
FER	Frame-Error Rate
FIR	Finite Impulse Response
FFT	Fast Fourier Transform
GSM	Global System for Mobile communications
HARQ	Hybrid Automatic Repeat reQuest
IC	Interference Canceller
IR	Incremental Redundancy
IT	Identical Transmission
ISI	Intersymbol Interference
LDPC	Low Density Parity Check (code)
LLR	Log-Likelihood Ratio
LTE	Long-Term Evolution
LTSC	Long-Term Static Channel
MAP	Maximum A Posteriori
MFB	Matched-Filter Bound
MIMO	Multiple-Input Multiple-Output
MISO	Multiple-Input Single-Output

ML	Maximum Likelihood
MLSD	Maximum-Likelihood Sequence Detection
MMSE	Minimum Mean-Square Error
MSE	Mean-Square Error
OFDM	Orthogonal Frequency-Division Multiplexing
OFDMA	Orthogonal Frequency-Division Multiple Access
OSED	Output Squared Euclidean Distance
PAPR	Peak-to-Average Power Ratio
PPD	Phase-Precoding Diversity
PSK	Phase-Shift Keying
QAM	Quadrature-Amplitude Modulation
QPSK	Quaternary Phase-Shift Keying
RSC	Recursive Systematic Convolutional (Code)
SC-FDMA	Single Carrier Frequency Division Multiple Access
SIC	Successive Interference Canceller
SIMO	Single-Input Multiple-Output
SISO	Soft-Input Soft-Output
SNR	Signal to Noise Ratio
STSC	Short-Term Static Channel
TC	Turbo-Code
TD	Time-Domain
TE	Turbo-Equalization
TSC	Total Squared Correlation
WBE	Welch Bound Equality
WiMAX	Worldwide Interoperability for Microwave Access
UMTS	Universal Mobile Telecommunications System

General Introduction

NOWADAYS, we are witnessing a significant growth in the use of personal communications services, including voice, video, and data transmission. According to the ICT (International Telecommunication Union), the number of mobile telephone subscribers around the world had reached 49% of the number of inhabitants at the end of the year 2007. At the same time, this percentage had even reached 97% in the developed countries. There is continuous development of portable wireless terminals for various types of applications such as traditional mobile telephony, wireless Internet, and traffic information. The demand for high data rate broadband services in cellular and local area wireless communication systems is increasing steadily. This growing demand is not only in terms of the number of users, but also in terms of data rate and quality of service.

Reliable communications through wireless channels are particularly rough due to the effects of multi-path fading, shadowing, path-loss, noise, etc. In order to combat these effects, advanced signal processing techniques are required such as transmit diversity techniques, channel precoding, and equalization. Even though, errors occur in the received packets due to the unexpected behavior of the communication channel. In order to protect the transmitted information against errors introduced by the channel, error correction codes are commonly used in modern communication systems. The degree of protection provided by the channel code to the useful information depends on the code type and its coding rate. The quality of the communication link is usually expressed in terms of *bit error rate* (BER) or in terms of *frame error rate* (FER). Depending on the underlaying application, other performance measures may also be required such as *transmission delay* and *data throughput*.

A need for retransmissions

A major concern in data communication systems is how to control transmission errors caused by the transmission channel. For one-way communication systems, as in broadcast applications for example, the channel code rate must be suitably chosen to match the worst channel conditions. The said "worst channel conditions" are to be determined as function of the error rate which can be tolerated by the underlaying application. This results in small *throughput efficiency* due to the wasted redundancy when channel conditions are good. For two-way communication systems, Automatic Repeat

reQuest (ARQ) [1] is another error control method which uses an error detection code and acknowledgments to achieve reliable data transmission. This method provides better throughput efficiency than error correcting codes for good channel conditions, but for bad channel conditions, the inverse is true. Hybrid ARQ (HARQ) protocols combine error correction codes and ARQ protocols in order to benefit from the advantages of both error control methods. In this case, the code rate in the first transmission can be chosen to match the typical channel conditions while HARQ retransmissions operate for bad channel realizations. This results in an improved throughput efficiency in the system. In the case of a decoding failure of the received packet, the receiver discards the erroneous packet and sends a negative acknowledgment to the transmitter requesting for a retransmission. This continues until a maximum number of allowable retransmissions has been achieved. This type of HARQ protocols is called type-I. In type-II HARQ protocols, the notion of *packet combining* [2, 3] was introduced. The previous erroneous receptions of the same packet are stored at the receiver in order to be combined with the current reception. This increases the probability of correct recovery of the transmitted information message. Type-II HARQ protocols have two main modes: namely *Chase Combining* [2] which is based on the retransmission of the same codeword, and *Incremental Redundancy* [4] which is based on the retransmission of additional parity bits. Chase combining HARQ protocols are simple to implement in comparison with incremental redundancy HARQ protocols. However, they have in general lower performance. In this work, we focus on Chase combining HARQ protocols with the goal of improving their performance while keeping their relative implementation simplicity.

Various transmission systems

An efficient communication system provides the required quality of service using the minimum of available resources including signal bandwidth (in frequency and time), power consumption and system cost. Early cellular mobile communication systems, which was commercially launched on the GSM standard in 1991, used narrow-band single carrier transmission with TDMA/FDM multiplexing for sub-channels. In GSM systems, GMSK was selected over other modulation schemes for GSM systems as a compromise between spectral efficiency and spurious emissions. GSM users enjoy data rates of only 9.6 kbp/s used for short message service (SMS) and Multimedia Message Service (MMS). In GPRS systems, the data rate was artificially increased up to a maximum of 114 kbp/s by allocating the eight time slots in GSM systems to one user. This solution is impractical because only one user at a time can benefit of this improved data rate. With the increasing demand for high data rate services, an efficient utilization of the available resources has become of premium importance. Resort has been made to high order modulations (8-PSK, 16-QAM, 32-QAM) with multiple coding schemes in Evolved EDGE systems allowing a maximum of 1 Mbit/s and a typical bit-rate of 400 kbit/s. The price for this enhancement is a less immunity to noise.

For higher bandwidth efficiency, MIMO transmission schemes with spatial multiplex-

ing were introduced. However, a more sophisticated signal processing at the receiver is required in order to remove the resulting spatial interference. Many space-time coding schemes were proposed which sacrify the bandwidth efficiency in order to remove inter-channel interference in a simple way as in [5]. The advantage of space-time coding schemes is a higher degree of transmit *diversity*. Between spatial multiplexing and transmit diversity, there is some diversity-multiplexing trade-off [6]. However, space-time coding schemes are not robust in frequency-selective channels due to the destroyed orthogonality by the effect of inter-symbol interference.

Inter-symbol interference is a well known problem in digital communication systems resulting from multi-path propagation and linear filtering at the transmitter and the receiver. In order to overcome this problem, new forms of data signaling were introduced such as CDMA and OFDMA signaling which are more robust to inter-symbol interference and allow a simple multiuser access scheme. On the other hand, they have their own problems. For example, wideband CDMA signaling has been adopted in UMTS, the third generation of mobile cellular systems (3G). In CDMA systems, the signal is processed at the chip-rate which is much higher than the data rate. This results in a higher power consumption and a higher components cost. Moreover, the quality of the communication link depend on network loading due to the problem of inter-user interference.

In recent years, OFDMA has been considered as a strong candidate for the broadband air interface for its robustness to multipath fading, higher spectral efficiency and bandwidth scalability. It has been selected for WiMAX and 3GPP LTE downlink radio access technology. On the other hand, the OFDMA waveform exhibits very pronounced envelope fluctuations resulting in a high peak-to-average power ratio (PAPR). Signals with a high PAPR require highly linear power amplifiers to avoid excessive inter-modulation distortion. The result is a low power efficiency which places a significant burden on portable wireless terminals in the uplink direction. Another problem with OFDMA in cellular uplink transmissions derives from the inevitable offset in frequency references among the different terminals that transmit simultaneously [7]. Frequency offset destroys the orthogonality between different subcarriers, thus introducing multiple access interference.

The renewal of single-carrier transmission

OFDMA signaling is suitable for down-link transmissions because power efficiency is not of major concern at the base station. In order to overcome the disadvantages of OFDMA signaling for uplink transmissions, a modified form of OFDMA is under investigation for the 3GPP LTE systems [8], which is referred to as Single Carrier FDMA (SC-FDMA). As in OFDMA, different users in an SC-FDMA system share M different orthogonal frequencies (subcarriers) to transmit the information symbols. However, the N transmitted symbols by one user are not directly mapped to the allocated subcarriers. Instead, this is the N-DFT points of the modulated symbols which are mapped to the allocated subcarriers. It was shown in [9] that the received signal after carrier demapping

follows the same model as for a single carrier transmission with a modified channel response depending on the subcarriers scheduling strategy. Therefore, SC-FDMA signals have inherently lower PAPR than OFDMA signals. This reduces the burden of linear amplification and improves the power efficiency in mobile terminals. There are two main subcarriers scheduling strategies including localized and distributed subcarriers mapping schemes. A distributed mapping scheme provides better frequency diversity and lower PAPR than a localized mapping scheme, but the latter one is less sensitive to frequency offset [10]. The possible use of TDMA multiplexing is not discarded to resolve this trade-off problem. However, in cellular systems with severe multipath propagation, SC-FDMA signals arrive at the base station with substantial inter-symbol interference. Consequently, equalization techniques must be used at the receiver in order to cancel this interference.

Since SC-FDMA is a single-carrier system, classical equalization algorithms used in single carrier systems are applicable. An optimal maximum likelihood (ML) receiver [11, 12] for joint equalization and channel decoding can not be implemented in practical systems due to its huge complexity. However, near ML-performance can be achieved in a reasonable complexity using iterative equalization and channel decoding as in turbo-equalization [13, 14].

A turbo-equalizer uses Soft-input Soft-Output (SISO) modules [15] for its constituent blocks including equalization, mapping/demapping, and channel decoding. As it will be seen through this dissertation, the use of SISO equalization is not only fundamental for turbo-equalization, but also is very useful for packet combining in HARQ protocols. Actually, the equalization performance can be enhanced even in a non-iterative receiver by using the available *a priori* information from previous transmissions of the same packet.

Context and objectives

We consider in this thesis a point-to-point data packet communication system with a feedback channel limited to acknowledgments. The system uses single carrier transmission with cyclic-prefix insertion over multipath fading frequency-selective channels. The context of this work is very similar to the context of the 3GPP LTE uplink except that we consider a single-user system. However, the obtained results can be applied to the case of multi-user LTE system system due to the complete separation between users in the frequency-domain. Since the feedback channel is limited, we assume that the transmitter has no knowledge of channel state information (CSI). The feedback channel is assumed to be error-free.

Our objective is to perform a cross-layer optimization between the physical layer and the link layer. At the physical layer, we consider the equalization, while at the link layer we consider HARQ protocols. More precisely, we investigate the optimization of the system performance in terms of frame error rate and in terms of data throughput, taking into account the frequency-selective nature of the propagation channel. The

error correction code is assumed given and is not subject to our optimization. As it is previously mentioned, HARQ protocols are the result of combining classical ARQ protocols with channel coding. On the other hand, turbo-equalization is the result of combining channel coding with equalization. We search for possible combining between all of equalization, channel coding, and ARQ protocols in order to improve the overall system performance in comparison with separate processing of each functional block in the communication system.

The main questions in this thesis are how to optimize the signal processing in the physical layer by taking advantage from the inherent time diversity in HARQ protocols? Inversely, how to modify HARQ protocols in order to improve the performance of detection in the physical layer? We mainly focus on Chase combining HARQ protocols due to their low implementation complexity in comparison with incremental redundancy HARQ protocols.

In order to answer these questions, we start by studying the theoretical performance of the classical bit-interleaved coded modulation scheme with HARQ retransmissions over a frequency selective channel assuming an optimal ML receiver in order to determine the effects of different system parameters on system performance. This leads us to the study of the statistical characteristics of the Euclidean distance spectrum at the output of the transmission channel. From this theoretical study, we get some insights for the optimization of the transmission scheme at the transmitter side. In particular, we focus on two HARQ transmit-diversity schemes having the advantage of preserving the PAPR of the transmitted signal. These two schemes are the *phase-preceding diversity* scheme and the *bit-interleaving diversity* scheme. We analyze and compare the performance of both diversity schemes in the context of time-varying channels.

The above diversity schemes are particularly useful for slow-time varying channels. For rapidly time-varying channels, we turn our attention onto a different transmission scheme which is the *multi-layer* transmission scheme using superposed coded modulations coding with successive interference cancellation (SIC) receiver. In order to facilitate the optimization of HARQ protocols for layered HARQ transmissions, we derive an equivalent MIMO model for the received signal. Based on this model, we optimize the power allocation problem at each retransmission. This transmission scheme with the optimized retransmission protocol can be viewed as a form of adaptive modulation scheme based on the returned HARQ acknowledgments.

Outline of this thesis

This dissertation is organized in five chapters. We assume that the reader is familiar with the different types of channel coding such as convolutional codes, turbo-codes and low density parity check codes.

Chapter 1 is devoted to the presentation of the considered communication system and some background materials regarding turbo-equalization and packet combining for

single-carrier transmission over frequency selective channels. After a brief review over the basic types of HARQ protocols used to ensure data reliability, we present the various channel models encountered along this thesis. At the receiver side, we present the turbo-equalizer structure using two types of equalizers including maximum *a posteriori* probability (MAP) [16] and *minimum mean square error* (MMSE) [17] equalizers. In particular, we focus on the low complexity MMSE equalizer and we present its implementation in the time-domain as well as in the frequency-domain. We present the semi-analytical EXIT charts tools which are useful for the study and the comparison of iterative receivers. After a brief survey of different types of basic Hybrid ARQ protocols, we discuss various packet combining strategies for single-carrier transmission over a frequency-selective channels. We conclude this chapter by presenting a performance comparison between different HARQ retransmission protocols.

Chapter 2 establishes the theoretical bases of this thesis. We investigate the performance of the bit interleaved coded modulation system using an optimal maximum-likelihood receiver in order to determine the limiting performance of any practical receiver and to get some insights about the design of the system and the effect of different system parameters such as the channel code, the interleaving length and the channel correlation. To this end, we carry out an error probability analysis which inevitably leads us to the study of the Euclidean distance spectrum at the output of the frequency-selective channels. By establishing a suitable formulation for the evaluation of the Euclidean distance, and based on the uniform interleaver concept, we derive an approximation for the output Euclidean distance distribution. The approximated distribution is used with the union bound in order to obtain an upper bound on the FER performance of the system. This study is performed in the case a static channel as well as in the case of a time-varying channel with uniform power-delay profile.

In chapter 3, we exploit the results obtained in chapter 2 in order to propose a new transmit diversity scheme among subsequent HARQ transmissions in chase combining mode for slowly time-varying channels in the purpose of improving data throughput in the system. This diversity scheme is called phase-precoding because only the phases of the transmitted symbols are changed in each retransmission according to some specific precoding pattern responding to a suitable performance criterion.

In chapter 4, we study another transmit diversity scheme which is the bit-interleaving diversity. By using an Euclidean distance based analysis, we show the potential of this diversity scheme for various channel models in comparison with classical HARQ retransmission protocol using joint equalization. We compare the performance of this diversity scheme with the performance of the phase-precoding diversity scheme in terms of the achievable performance and the implementation complexity. We also extend the usage of the bit-interleaving diversity to MIMO frequency-selective channels. We emphasize how bit-interleaving exploits the additional space dimension with a suitable interleaving design.

In chapter 5, we turn our attention to the problem of packet retransmission for multi-layered transmission which is an efficient transmission scheme in terms of data

throughput for time-varying channels. Multi-layered transmission can be seen as a MISO transmission system. Therefore, we establish an equivalent MIMO channel model for HARQ retransmission system using multi-layered signals. Based on MMSE MIMO detection with successive decoding, we optimize the linear superposition coefficients at each HARQ retransmission. Since few layers can be used in practice, we focus on the practical solutions for the case of two layers.

Finally, we conclude this work by giving some concluding remarks and some possible perspectives for future research.

Contributions and Publications

We summarize below the main contributions of this work:

- In chapter 2, we propose a new theoretical formulation for the evaluation of the Euclidean distance at the output of a frequency-selective channels. By using this formulation, we have given the main statistical properties of the the squared Euclidean distance at the output of a frequency-selective channel.
- In chapter 3, we propose a novel phase-precoding diversity scheme between subsequent HARQ transmission for intersymbol interference mitigation.
- In chapter 4, we compare the phase-precoding diversity with bit-interleaving diversity under iterative and non-iterative receivers.
- In chapter 5, we establish a MIMO model for layered HARQ transmissions in Chase combining mode. Based on this model, an adaptive HARQ protocol is proposed.

At the present date, this thesis has led to the following publications:

International Journals

1. A. Assimi, C. Poulliat, and I. Fijalkow, "Phase-precoding without CSI for packet retransmissions over frequency-selective channels," *Accepted to IEEE Trans. Commun.*, 2009.
2. A. Assimi, C. Poulliat, and I. Fijalkow, "Diversity techniques for single-carrier packet retransmissions over frequency-selective channels," *Accepted to EURASIP Journal on Wireless Communications and Networking Special Issue on "3GPP LTE and LTE Advanced"*, 2009.

International Conferences

3. A. Assimi, C. Poulliat, and I. Fijalkow, "Distance distribution for turbo-equalized systems over static frequency-selective channels," in *IEEE Int. Conf. Acoust. Speech Signal Process. (ICASSP)*, Las Vegas, USA, March 2008, pp. 2949–2952.

4. A. Assimi, C. Poulliat, I. Fijalkow, and D. Declercq, "Periodic Hadamard phase precoding for HARQ systems over intersymbol interference channels,"(*Invited paper*) in *Int. Symp. on Spread Spectrum Techniques and Applications (ISSSTA)*, Bologna, Italy, August 2008, pp. 714 –718.

5. A. Assimi, C. Poulliat, and I. Fijalkow, "Performance analysis of turbo-equalized systems over frequency-selective block-fading channels," in *Eur. Signal Process. Conf.(EUSIPCO)*, Lausanne, Switzerland, August 2008.

6. A. Assimi, C. Poulliat, and I. Fijalkow, "Packet combining for turbo-diversity in HARQ systems with integrated turbo-equalization," in *Int. Symp. Turbo Codes (ISTC)*, Lausanne, Switzerland, September 2008, pp. 61–66.

7. A. Assimi, C. Poulliat, and I. Fijalkow, "Phase precoding with integrated turbo-equalization for packet retransmissions," in *IEEE Int. Symp. Pers., Indoor Mob. Radio Commun.(PIMRC)*, Cannes, France, September 2008.

8. A. Assimi, C. Poulliat, and I. Fijalkow, "Bit-interleaving diversity for HARQ transmission over MIMO frequency-selective channels," in *IEEE International Workshop on Signal Processing Advances in Wireless Communications (SPAWC)*, Perugia, Italy, June 2009, pp. 310–314.

9. A. Assimi, C. Poulliat, and I. Fijalkow, "On cyclic frequency diversity for single-carrier packet retransmissions," in *IEEE Int. Symp. Inf. Theory*, Seoul, Korea, June 2009.

10. A. Assimi, C. Poulliat, and I. Fijalkow, "Reliable communications using multi-layer transmission," in *EuropeComm*, London, UK, August 2009.

11. A. Assimi, C. Poulliat, and I. Fijalkow, "Packet combining for multi-layer hybrid-ARQ over frequency-selective fading channels," in *Eur. Signal Process. Conf. (EUSIPCO)*, Glasgow, Scotland, August 2009, pp. 671-675.

National Conferences

12. A. Assimi, C. Poulliat, and I. Fijalkow, "ARQ-hybride avec turbo-égalisation sur les canaux sélectifs en fréquence à évanouissements par bloc," in *Groupe de recherche et d'études du traitement du signal et des images (GRETSI)*, Troyes, France, September 2007, pp. 1145–1148.

Notations

The following notations are used throughout this dissertation:

- Variables and scalars are denoted by italics (a, A).
- Vectors are denoted by lowercase boldface letters ($\mathbf{a}$).
- Matrices are denoted by uppercase boldface letters ($\mathbf{A}$).
- An ensemble of elements is represented with calligraphic fonts ($\mathcal{A}$).

Les main used notations are summarized in the following table:

Operators and functions:

$\oplus$	Binary addition
$*$	Linear convolution
$\odot$	Hadamard product between vectors and matrices (or element-wise product).
$(.)^*$	Complex conjugate.
$(.)^\top$	Transpose.
$(.)^H$	Hermitian transpose.
$\Re(.)$	Real part of the complex argument.
$\Pr(.)$	probability.
$E(.)$	Statistical expectation.
$\mu(X)$	Mean of the random variable X.
$\sigma^2(X)$	Squared standard deviation of the random variable X.
$\underline{\mathbf{x}}$	Discrete Fourier transform of $\mathbf{x}$.
$R_\ell(.)$	Deterministic auto-correlation function for lag ℓ.

Symbols:

K_b	Number of information bits in a packet.
N_b	Number of coded bits in a packet.
N_s	Number of modulation symbols in a packet.
t, T	Index of HARQ (re)transmission.
$T_{\max}$	Index of HARQ (re)transmission.
ρ	Signal-to-noise ratio
$\mathbf{h}, \mathbf{H}$	Channel response.
$\mathbf{c}$	Coded block.
$\mathbf{x}$	Transmitted signal.
$\mathbf{f}$	Forward MMSE filter.
$\mathbf{b}$	Backward interference cancellation filter.
$\mathbf{z}$	Received signal.
$\mathbf{w}$	Gaussian white noise vector.
$\mathbf{e}$	Error sequence.
Π	Bit-interleaver.
r	Coding rate.
P_e	Error probability.
P_2	Pairwise error probability.
T_h	Throughput.
Δ	Output squared Euclidean distance.

Chapter 1

Reliable Communications over Frequency-Selective Channels

THIS chapter presents the model of the considered communication system for data packet transmission over a frequency-selective channel with some background materials regarding HARQ protocols and detection methods including iterative signal detection and decoding. We pay particular attention to packet combining techniques with integrated channel equalization.

1.1 Introduction

In high speed data packet transmission systems using single-carrier signaling over frequency-selective fading channels, the received signal is a distorted version of the transmitted signal due to the effects of the communication channel including fading, inter-symbol interference (ISI), and background noise. The presence of ISI in the received signal results from multipath propagation or a limited bandwidth of the channel. In order to recover the transmitted data from the received signal, equalization techniques and error correcting codes are usually used in modern digital communication systems. In particular, there is an interest in iterative signal processing methods such as turbo-equalization which combine equalization and channel decoding in an iterative manner leading to a remarkable performance gain in comparison with classical methods using separate equalization an channel decoding. This performance gain of iterative methods is achieved at the expense of higher computational complexity at the receive end. However, with the continuous technological advances in terms of processing speed, this barrier is not of major concerns for future use in practical systems.

Even with a sophisticated receiver, errors may occur in the received data due to multiple reasons such as an instantaneous high level of noise or the mismatch between the system-design parameters and the actual channel behavior. Hence the need for error control techniques in order to ensure the reliability of the received data. The main

used error control techniques are forward error correction (FEC), and ARQ protocols for two-way communication links. Hybrid ARQ protocols combine both of these two methods for better throughput performance.

Basic types of HARQ protocols ensure data reliability through the retransmission of the same packet after error detection at the receive end thanks to an embedded error detection code in the transmitted packet. The receiver discards the erroneous received signal and retries again to decode the transmitted packet from the most recent received transmission. Most advanced HARQ protocols improve the system performance by incorporating packet combining techniques such as signal combining in *Chase combining* (CC) HARQ and code combining in *incremental redundancy* (IR) HARQ. All received signals concerning the same packet are stored at the receiver memory to be jointly processed in order to fully exploit the available information about the transmitted packet. Therefore, the design of HARQ protocols becomes directly related to the code design in the case IR-HARQ, while it becomes related to the signal processing in the physical layer in the case of CC-HARQ. This thesis focuses on signal combining for data transmission over frequency-selective channels in the context of CC-HARQ. The IR-HARQ and the optimization of code design is out of the scope of this work.

In this chapter, we review the basics HARQ protocols and some packet combining techniques for single carrier transmission over frequency-selective channels.

1.2 Single-carrier packet transmission

We consider a typical single-carrier communication system over a frequency-selective channel whose the block diagram is shown in Figure 1.1.

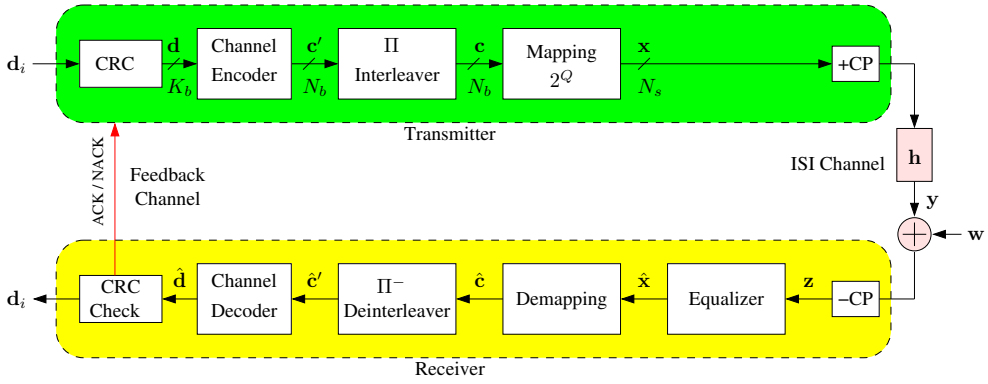

FIGURE 1.1: System model for single-carrier transmission over a frequency-selective channel.

At the transmitter side, the information data bits to be transmitted are first segmented into blocks of equal lengths. To each data block $\mathbf{d}_i$ is added a signature sequence of length L_{crc} bits for the purpose of error detection at the receiver. The signature sequence is obtained by an error detection code which is traditionally a Cyclic Redundancy

Check (CRC) code. The obtained block $\mathbf{d}$ containing K_b bits including the information bits and the CRC bits, are encoded by a rate-K_b/N_b error correction code giving a codeword $\mathbf{c}$ having N_b coded bits. The coded bits are interleaved using a bit-interleaver Π. Then, the coded and interleaved bits are mapped into a sequence $\mathbf{x}$ of N_s symbols using, unless otherwise mentioned, a complex modulation alphabet $\mathcal{S}$ of size $|\mathcal{S}| = 2^Q$ symbols. For convenience, we assume $N_b = QN_s$. Finally, a cyclic-prefix (CP) formed by the last L_{cp} symbols of $\mathbf{x}$ is inserted at the beginning of $\mathbf{x}$ before being transmitted through the communication channel.

The communication channel is frequency-selective and modeled by its equivalent discrete-time finite impulse response (FIR), denoted by $\mathbf{h} = [h_0, \cdots, h_{L-1}]$, of length L and assumed constant during one block transmission but it may vary from one block to the next depending on the considered channel model. In addition, some background noise is added to the received signal as in all communication systems.

At the receiver side, the CP is first removed from the received signal. The obtained sequence is first processed by a channel equalizer in order to remove the inter-symbol interference caused by the frequency-selective channel. Then, the receiver performs the inverse operations that have been performed at the transmitter including symbol demapping, bit de-interleaving and channel decoding. The integrity of the decoded packet $\hat{\mathbf{d}}$ is checked thanks to the CRC signature. In the case of a correct decoding, the decoded packet is delivered to the front-end application and a positive acknowledgment signal ACK is returned to the transmitter through the feedback channel. Otherwise, a negative acknowledgment signal NACK is returned back to the transmitter requesting for a retransmission.

We give in the following the description of each constituent block of the transmitter scheme and the general adopted assumptions.

1.2.1 Error detection code

In most of communication systems a systematic CRC code is usually used as an error detection code. For example, in CCITT (Consultative Committee of International Telephone and Telegraph) standards, a CRC code with 16 parity bits ($L_{crc} = 16$) is adopted. Its generator polynomial is defined by $g(D) = D^{16} + D^{12} + D^5 + 1$, where D stands for bit delay operation.

CRC codes are easy to implement, but it is not easy to evaluate their performance. However, there are some meaningful measures for the performance of CRC codes, such as the "burst-error detection capability" and "error-detection coverage." In general, a binary CRC code with L_{crc} parity bits can detect all burst errors of length L_{crc} or less, and also the fraction $1 - 2^{-L_{crc}}$ of all the error patterns [18]. Thus, the performance of CRC codes are mainly determined by L_{crc}. The longer L_{crc}, the better the performance. For example, the 3GPP standard [19] defines 3 possible CRC lengths which are 8, 16, and 24. The CRC code with $L_{crc} = 16$ can provide adequate detection for most applications.

In this work, we assume a perfect error detection code and the undetected error

probability is zero. For more details about the performance of binary error detections codes, the reader may refer for example to [20, 21].

1.2.2 Channel coding

There are many types of error correcting codes which are used in digital communication systems such as convolutional codes [22], turbo codes [23], and low density parity check codes (LDPC) [24, 25]. In this thesis, without loss of generality, we present and illustrate our results using convolutional codes since they are the basic channel coding feature on modern communication systems. This is mainly due to their low implementation complexity compared to other types of codes. In addition, the distance spectrum of the convolutional codes can be computed in straightforward manner which facilitates the evaluation of the theoretical performance of the communication system (cf. Chapter 2). However, we show at some particular occasions some numerical results using turbo codes as well as LDPC codes. The decoder is based on the maximum a posteriori probability (MAP) criterion and implemented by the forward-backward BCJR algorithm [16]. This algorithm allows soft-input soft-output (SISO) decoding which necessary for iterative signal processing as it will be see later in this chapter.

1.2.3 Bit-interleaving

Bit-interleaving is usually used in communication systems in order to locally decorrelate the coded bits. Thus, the neighboring coded bits in the interleaved block can be considered as statistically independent. This property enhances the error correction capability of the channel code. Beside this, bit-interleaving is necessary for iterative signal detection and decoding methods. The achieved performance gain due to interleaving is called the *interleaving-gain*. In general, the interleaving gain increases with the interleaver length, but at the expense of an increased latency, because the entire interleaved block must be received before it can be processed. In the literature, there are several types of bit-interleavers. Based on the construction method, they can be classified in three categories:

- Random interleaver: The interleaved bits are obtained by applying a pseudo-random permutation on the original bits.

- Semi-random interleaver: A typical example of this type of interleaver is the S-random interleaver [26] which has one design parameter S called the spreading factor. It was originally introduced to improve the performance of turbo-codes. It is defined according to the following rule: Any two adjacent bits in the original packet are found in the interleaved packet separated from each other by more than S bit locations. There are some construction algorithms which converge in a reasonable time if $S < \sqrt{N_b/2}$, where N_b is the interleaver length as in [27].

- Deterministic interleaver: the data bit are redistributed according to a deterministic permutation function. The uniform interleaver and the quadratic polynomial interleaver used as the internal interleaver in the 3GPP turbo-code [28] are two examples of this type of interleavers.

1.2.4 Symbol mapping

The symbol mapper associates to each group of bits $(b_1, b_2, \cdots, b_Q)$ a symbol x taken from the mapping constellation $\mathcal{S}$ such as BPSK, QPSK, or QAM constellations. Thanks to the bit-interleaver, we assume that the coded bits are statistically independent and consequently, the modulation symbols are have equal probability to be transmitted. In addition, we assume that the transmitted symbols have a unit average signal power i.e. $E_s = E(|x|^2) = 1$ and a Gray mapping scheme is used through this work.

1.2.5 Cyclic-prefix insertion

The cyclic-prefix insertion provides a guard time between consecutive transmitted blocks in order to avoid inter-block interference. Therefore, the length of the cyclic-prefix is chosen, in general, to be equal to the maximum channel delay-spread in terms of symbol period, i.e $L_{cp} = L$. Consequently, the linear channel convolution can be viewed as a circular convolution after the removal of the cyclic-prefix. The advantage of the circular convolution that it becomes a simple multiplication in the frequency-domain by a discrete Fourier transform (DFT) operation. This allows performing the equalization in the frequency-domain which has in general less computational complexity compared to the equalization in the time-domain.

1.3 Hybrid ARQ protocols

Early wired communication systems used ARQ protocols to ensure data reliability for non-coded packets. Based on retransmission strategies, there are three basic types of ARQ schemes: stop-and-wait, go-back-N, and selective-repeat.

The stop-and-wait scheme represents the simplest ARQ procedure and was implemented in early error-control systems. In this protocol, the transmitter sends a data packet to the receiver and waits for an acknowledgment before proceeding with the next transmission. The receiver responds by a positive acknowledgment signal ACK in the case of correct CRC check on the received packet. Otherwise, the receiver discards the erroneous packet and responds by a negative acknowledgment signal NACK requesting for a retransmission of that packet. The acknowledgment for a packet arrives after a *round-trip delay*, defined as the time interval between the transmission of a packet and the receipt of an acknowledgment for that packet. If an ACK signal has been returned from the receiver, the transmitter sends the next packet in the queue. Otherwise, the transmitter resends the same packet in error and waits again for an acknowledgment.

This operation continues until the correct reception of the packet or a maximum number of allowable retransmissions $T_{\max}$ has been reached. If a packet is still in error after $T_{\max}$ trials, an error is declared at the receiver to the upper network layer. This scheme is simple but inherently inefficient because of the idle time spent waiting for an acknowledgment of each transmitted packet. This is actually a real problem for communication systems with long round-trip delay such as in deep-space telecommunications. In order to overcome this problem, Go-Back-N and selective-repeat ARQ protocols have been introduced. In these two ARQ schemes, packets are transmitted continuously. We are not going to describe these protocols, and the reader may refer to [1] for a detailed description. We only give some useful remarks concerning their relative performance. Among these three ARQ protocols, selective-repeat ARQ offers the best throughput performance as function of the error probability. However, it requires a larger storage memory at the transmitter and packets ordering at the receiver. It can be viewed as multiple stop-and-wait ARQ processes running in parallel. Thus, we assume in this work a stop-and-wait retransmission protocol with zero delay.

After the introduction of error correcting codes in digital communication systems, the information message including the CRC bits is encoded by a channel encoder giving a coded packet. Consequently, the CRC check is performed at the receiver after the decoding of the packet. The modified ARQ protocols by the incorporation of error correcting codes in this manner are called Hybrid ARQ (HARQ) protocols of type-I.

Type-II HARQ is an advanced form of HARQ which uses the concept of packet combining. The rational behind packet combining is as follows: Even if a received signal has led to a detection failure, it contains, however, some useful information about the transmitted packet. Therefore, it is stored in the receiver memory to be combined with other retransmissions which leads to enhanced detection performance. Depending on the retransmission scheme and the combining method, HARQ protocols of type-II can be classified into two categories: namely Chase combining (CC-HARQ) which is based on the retransmission of the same coded packet, and incremental redundancy (IR-HARQ) mode which is based on the retransmission of additional redundancy bits. In the following we give a brief description of these HARQ schemes.

1.3.1 Chase combining HARQ

This HARQ scheme takes its name from D. Chase for his published works [2] on the combining an arbitrary number of noisy packets in a single packet based on a maximum-likelihood criterion. In Chase combining HARQ, a coded and modulated packet $\mathbf{x}$ is initially transmitted to receiver. The same packet $\mathbf{x}$ is retransmitted in response to a NACK receipt for the previous transmission. The ensemble of received copies of the same packet are combined at the receiver in a single signal which contains the accumulated information about the transmitted packet from all received signals.

In order to clarify the combining method, we consider the case of packet transmission over a flat block-fading channel as shown in Figure 1.2. The received signal at the t-th

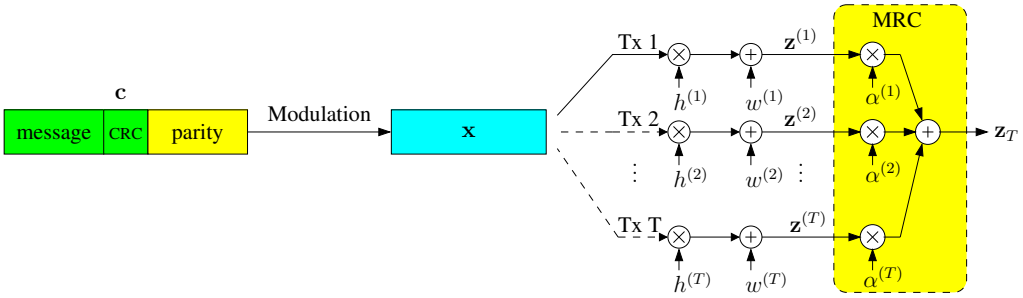

FIGURE 1.2: Chase combining HARQ scheme.

transmission can be written as

$$\mathbf{z}^{(t)} = h^{(t)}\mathbf{x} + \mathbf{w}^{(t)} \tag{1.1}$$

where $h^{(t)}$ is the corresponding complex channel gain, and $\mathbf{w}^{(t)}$ is the noise vector whose elements are i.i.d. complex Gaussian random variables with zero mean and variance σ_w^2. After the T-th HARQ round, the receiver combines the T received packets at the symbol level in a single packet denoted by $\mathbf{z}_T$. The combined packet is obtained by weighting each packet by an estimate of its reliability before being summed with the other packets.

$$\mathbf{z}_T = \sum_{t=1}^{T} \alpha^{(t)} \mathbf{z}^{(t)}\,, \tag{1.2}$$

where $\alpha^{(t)}$ is the reliability of each received packet which is given under maximum-likelihood decoding by

$$\alpha^{(t)} = \frac{(h^{(t)})^*}{\sigma_w^2} \tag{1.3}$$

This method of combining is also referred to as the *maximum-ratio combining* (MRC). The MRC method is known to be an optimal combining scheme for independent Gaussian channels. Other sub-optimal combining methods exists with lower complexity compared to MRC combining such as *equal-gain combining* and *selective combining* [29].

Actually, MRC combining provides the maximum possible SNR at the output of the linear combiner [29]. The combined signal can be written as

$$\mathbf{z}_{\text{mrc}}(T) = \left(\sum_{t=1}^{T} \frac{|h^{(t)}|^2}{\sigma_w^2} \right) \mathbf{x} + \sum_{t=1}^{T} \frac{(h^{(t)})^*}{\sigma_w^2} \mathbf{w}^{(t)} \tag{1.4}$$

The SNR of the combined signal, denoted by ρ_T, is given by

$$\rho_T = \sum_{t=1}^{T} \frac{|h^{(t)}|^2 E_s}{\sigma_w^2} = \sum_{t=1}^{T} \rho^{(t)} \tag{1.5}$$

where $E_s = E(|x_n|^2)$ and $\rho^{(t)}$ is the instantaneous received SNR at each HARQ transmission. Therefore, CC-HARQ takes advantage from the accumulated SNRs from the individual transmissions which improves the decoding performance of the transmitted packet.

1.3.2 Incremental redundancy HARQ

Incremental redundancy HARQ generalizes the CC-HARQ scheme by considering that each transmission is a punctured version of a low rate mother code denoted by $\mathcal{C}_0$.

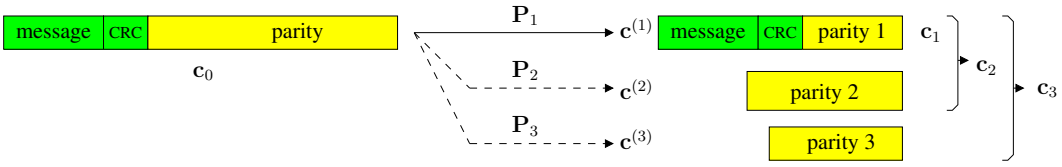

FIGURE 1.3: Incremental redundancy HARQ scheme.

In the IR-HARQ scheme shown in Figure 1.3, the information data packet is first encoded by a mother code $\mathcal{C}_0$ of rate r_0 giving the codeword $\mathbf{c}_0$. At the first transmission, only some coded bits of $\mathbf{c}_0$ are selected according to a predetermined bit-puncturing pattern $\mathbf{P}_1$. The selected bits are grouped in a single block $\mathbf{c}^{(1)}$ which is modulated and then transmitted to the receive end. The ensemble of all possible blocks $\mathbf{c}^{(1)}$ defines a certain code $\mathcal{C}_1$ having a rate $r_1 \geq r_0$. The bit-puncturing pattern $\mathbf{P}_1$ must be suitably selected in order to have a decodable code $\mathcal{C}_1$. We denote by $\mathbf{c}_1 = \mathbf{c}^{(1)}$ the transmitted codeword.

The receiver tries to recover the information data by decoding the mother code from the received codeword $\mathbf{c}_1$ after bit de-puncturing. In the case of a decoding failure, a NACK signal is returned to the transmitter requesting for a retransmission. The transmitter responds by sending a second block $\mathbf{c}^{(2)}$ containing additional coded bits taken form remaining bits of $\mathbf{c}_0$ which *have not been transmitted yet*. This time, the receiver retries to recover the information data by joint decoding of both received blocks $\mathbf{c}^{(1)}$ and $\mathbf{c}^{(2)}$. The combined codeword $\mathbf{c}_2 = [\mathbf{c}^{(1)}, \mathbf{c}^{(2)}]$ defines a codeword of a code $\mathcal{C}_2$ of a lower rate $r_2 \leq r_1$. This enhances the decoding performance due to the additional coding gain provided by the lower rate code $\mathcal{C}_2$. This continues until the correct decoding of the information data or the maximum number of transmissions $T_{\max}$ has been achieved.

Thus, we have $\mathcal{C}_1 \subseteq \mathcal{C}_2 \subseteq \cdots \subseteq \mathcal{C}_{T_{\max}} \subseteq \mathcal{C}_0$ which express the rate-compatibility restriction between the punctured codes in IR-HARQ protocols. The puncturing patterns are optimized for convolutional codes in [4], and for turbo-codes in [30]. We illustrate the IR-HARQ scheme by an example taken from [4].

Example 1. A family of three rate-compatible punctured codes $\mathcal{C}_1$, $\mathcal{C}_2$, and $\mathcal{C}_3$ are generated from a rate-$1/4$ convolutional mother code $C(31, 27, 35, 33)_8$ (in octal notations)

by applying three bit puncturing patterns of period 4 defined as follows

$$\mathbf{P}_1 = \begin{bmatrix} 1111 \\ 1000 \\ 0000 \\ 0000 \end{bmatrix}, \quad \mathbf{P}_2 = \begin{bmatrix} 0000 \\ 0111 \\ 1100 \\ 0000 \end{bmatrix}, \quad \mathbf{P}_3 = \begin{bmatrix} 0000 \\ 0000 \\ 0011 \\ 1110 \end{bmatrix} \tag{1.6}$$

where each row in the puncturing matrix is applied periodically to one of the outputs of the mother encoder. This defines three rate-compatible codes of rates $r_1 = 4/5$, $r_2 = 4/10$, and $r_3 = 4/15$, respectively.

1.3.3 Data throughput

The performance of HARQ protocols are usually expressed in terms of data *throughput* which is defined by the average number of correctly received information bits per channel use (bit/cu). It is given by

$$T_h = \frac{Qr_1}{E(T)} \tag{1.7}$$

where r_1 is the coding rate at the first transmission, Q is the number of bits per transmitted symbol, and $E(T)$ is the average delivery delay per packet which can be computed using the renewal theory [31, 32] as follows. We first define the following probabilities

$$p(T) \triangleq \Pr(\text{NACK}_1, \cdots, \text{NACK}_{T-1}, \text{NACK}_T) \tag{1.8}$$

$$q(T) \triangleq \Pr(\text{NACK}_1, \cdots, \text{NACK}_{T-1}, \text{ACK}_T) \tag{1.9}$$

giving respectively, the probability of decoding failure, and the probability of decoding success at the T-th round. Then, the average delivery delay can be calculated as

$$E(T) = \sum_{T=1}^{T_{\max}} Tq(T) \tag{1.10}$$

At round $T_{\max}$, since even in the case of NACK the transmitters moves on to the next packet, we have

$$q(T_{\max}) = 1 - \sum_{T=1}^{T_{\max-1}} q(T) \tag{1.11}$$

We can verify that $q(T) = p(T-1) - p(T)$ assuming $p(0) = 1$. By substituting in 1.10, this yields to

$$E(T) = \sum_{T=1}^{T_{\max}} p(T-1) = 1 + \sum_{T=1}^{T_{\max}-1} p(T) \tag{1.12}$$

By substituting this in (1.7), we obtain

$$T_h = \frac{Qr_1}{1 + \sum_{T=1}^{T_{\max}-1} p(T)} \tag{1.13}$$

Equation 1.13 shows that data throughput is directly related to FER at each HARQ round. Throughput is sometimes expressed in terms of *throughput efficiency* which is the data throughput normalized to the transmission rate in the first transmission Qr_1 which is the maximum possible throughput. The probability $p(T_{\max})$ is called the *dropping rate* which is the frame error rate at the last HARQ round.

1.3.4 Performance comparison between CC and IR

From coding viewpoint, CC can be considered as a special case of IR by using a mother code formed by the concatenation of the channel code with a rate-$1/T_{\max}$ repetition code with an appropriate bit puncturing patterns. Consequently, the performance of the IR are potentially superior to the performance of CC due to the superior coding gain which can be obtained by using a suitably selected mother code in comparison with a simple repetition of a higher rate code. However, there is a major difference between CC and IR from signal processing viewpoint. The difference is that the transmitted signals in CC are the same in all HARQ transmissions which allows performing packet combining at the signal level, while this is not possible in IR where the combining is performed at the bit level by joint decoding after symbol detection and demodulation.

From the information theory point of view, it has been shown in [33] that the gain of IR over CC using ideal codes increase with the initial coding rate r_1 for static channels. For example, for initial coding rate $r_1 = 0.5$, IR provides 1 dB of gain over CC. For block-fading channels, the gain is less important and the performance of both schemes become almost comparable. Moreover, in some particular situations, CC can even outperforms IR. This occurs when the first transmitted block $\mathbf{c}^{(1)}$ falls in deep fading and the retransmitted block $\mathbf{c}^{(2)}$ is not decodable, even in the best channel conditions.

To overcome this problem, beside the rate compatibility restriction, an additional constraint on the design of IR codes is added which is the *self-decodability* of each transmitted blocks. The IR-HARQ scheme with self-decodable codes are sometimes referred to as type-III HARQ [34].

1.4 Channel models

The communication channel must be suitably modeled in order to obtain accurate estimations of the system performance leading to a proper design of the communication system. In this thesis, we distinguish between three channel models that are commonly used in the evaluation of HARQ performance.

1.4.1 Short-term static channel model

In short-term static (STSC) channel model, the channel response remains the same during the period of one block transmission, but changes independently from one block

transmission to the next. This model can be found in practice when the coherence time of the channel is longer than the time period of one block transmission but smaller than the round-trip delay.

1.4.2 Long-term static channel model

In long-term static channel (LTSC) model, the channel response does not change between subsequent HARQ transmissions of the same packet and changes independently from one packet to another. Actually, this model does not rely on a physical or system justification. It is only used for the purpose of evaluating the average system performance over all possible channel realizations in slowly time-varying channel conditions comparing to the round-trip delay.

In practice, channel may change slowly between subsequent transmissions. We model the channel variations by a first order auto-regressive random process (AR1) with a correlation coefficient α as

$$\mathbf{h}^{(t)} = \alpha \mathbf{h}^{(t-1)} + \mathbf{u}^{(t)},\ t = 1, \cdots, T_{max} \tag{1.14}$$

with $\mathbf{h}^{(0)} = 0$, where $\alpha \in [0, 1]$ and $\mathbf{u}^{(t)} = [u_0^{(t)} \cdots u_{L-1}^{(t)}]^\top$ is a vector of length L whose components are complex-valued i.i.d. Gaussian noise with variance $\sqrt{1 - |\alpha|^2}/L$ in order to have unit average channel gain, i.e. $E[||\mathbf{h}^{(t)}||^2] = 1$. The correlation coefficient α is usually expressed in terms of Doppler frequency according to Jakes' model [35] as $\alpha = J_0(2\pi f_d \tau)$, where $J_0(\cdot)$ is the zero-order Bessel function of the first kind, f_d denotes the maximum Doppler frequency, and τ is the time delay between two subsequent HARQ transmissions. The limiting case when $\alpha = 0$ corresponds to the STSC model, whereas the case of $\alpha = 1$ corresponds to the LTSC model.

1.4.3 Spatial channel model extended

The Spatial Channel Model Extended (SCME) is a model developed by the European WINNER[1] project as specified in [36] and its Matlab implementation in [37]. It is an extension of the implementation of the 3GPP Spatial Channel Model (SCM) [38]. This channel model is suitable for both short range and wide area communications including wireless local area network (WLAN), wireless metropolitan area networks (WMAN), 3GPP long term evolution, and Beyond 3G.

In this model, the frequency-selective channel is characterized by six non-zero taps with varying delays per link with a decreasing power-delay profile. The channel length L in terms of symbol duration is a random variable and can take large values depending in the transmission speed. We use this model in some of our simulations in order to validate our results in more realistic channel conditions.

[1] Wireless World Initiative New Radio

Now, we present the receiver structure including a turbo-equalizer for iterative equalization and channel decoding. The resort to turbo-equalization in our study is motivated by the desire of investigating the performance limits of the system. The case of separate equalization and channel decoding is considered as a particular case of this general receiver structure.

1.5 Turbo-equalization

An optimal ML receiver for joint sequence detection and decoding can not be implemented in practice due to its huge complexity. In a traditional receiver scheme based on separate equalization and channel decoding scheme, the equalizer does not benefit from the coded nature of the received sequence. By using an iterative approach for signal detection and decoding as in a turbo-equalization scheme [13], near ML-performance can be achieved with reasonable complexity. Turbo-equalization is based on the turbo-decoding principle of serially concatenated codes by viewing the frequency-selective as a trellis code of unit-rate in concatenation with the channel code. While it is yielding to superior performance when compared with separate equalization and channel decoding, turbo-equalization has the disadvantage of higher computational complexity. However, we envision that this equalization technique will eventually be implemented in future communication systems.

The received signal is modeled as

$$z_n = \sum_{i=0}^{L-1} h_i x_{n-i} + w_n,\ n = 0, \cdots, N_s - 1 \tag{1.15}$$

where the signal indexes $(n-i)$ are taken modulo N_s due to the cyclic prefix insertion, and w_n is an independent additive white complex Gaussian noise with variance σ_w^2 (or $\sigma_w^2/2$ per real dimension). Figure 1.4 shows the block diagram of the turbo-equalizer. The equalizer and the channel decoder are connected iteratively by the intermediate of the interleaver. They exchange soft information about the transmitted coded sequence. We use the following notations: $P(x)$ for the probability of the symbol x and $L(c)$ for the log-likelihood ratio (LLR) of the bit c. The lower indexes a, p, and e indicate respectively a priori, a posteriori, and extrinsic probabilities, while the upper indexes E and D designate equalizer and decoder respectively.

From the received signal $\mathbf{z}$ and the available a priori on the transmitted symbols from the channel decoder at the previous turbo-iteration $\{P_a^D(x_n = x) : x \in \mathcal{S}, n = 0, \cdots, N_s - 1\}$, the equalizer produces the a posteriori probabilities $\{P_p^E(x_n) = \Pr(x_n = x|\mathbf{z}) : x \in \mathcal{S}, n = 0, \cdots, N_s - 1\}$. The soft-demapper converts these a posteriori probabilities into LLRs for the coded bits $L_p^E(\mathbf{c})$. Assuming the independence between the coded bits within each symbol, the soft demapper computes from the symbol probabilities $\{P_p^E(x_n)\}$ the LLRs of the corresponding coded bits $\{c_{n,1}, \cdots, c_{n,Q}\}$ defined

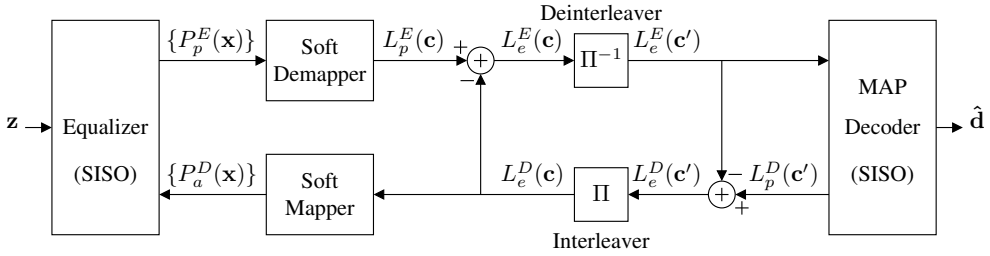

FIGURE 1.4: Turbo-equalizer scheme.

by

$$L_p^E(c_{n,q}) \triangleq \log \frac{\Pr(c_{n,q}=0|\mathbf{z})}{\Pr(c_{n,q}=1|\mathbf{z})} \tag{1.16}$$

where $\Pr(c_{n,q}=b|\mathbf{z})$ are computed by using the following marginalization

$$\Pr(c_{n,q}=b|\mathbf{z}) = \sum_{x_n \in \mathcal{S}: c_{n,q}=b} \Pr(x_n|\mathbf{z}) = \sum_{x_n \in \mathcal{S}: c_{n,q}=b} P_p^E(x_n) \tag{1.17}$$

According to the turbo principle, the extrinsic LLRs are computed by $L_e^E(\mathbf{c}) = L_p^E(\mathbf{c}) - L_e^D(\mathbf{c})$ to be fed to the channel decoder after de-interleaving. The channel decoder consists of a MAP decoder which produces the a posteriori LLRs $L_p^D(\mathbf{c}')$. The extrinsic LLRs from the channel decoder are computed as $L_e^D(\mathbf{c}') = L_p^D(\mathbf{c}') - L_e^E(\mathbf{c}')$ to be fed back to the equalizer after interleaving and soft mapping. The soft mapper computes the symbol probabilities $\{P_a^D(x_n = x) : x \in \mathcal{S}, n = 0, \cdots, N_s - 1\}$ by

$$P_a^D(x_n) = \prod_{q=1}^{Q} \Pr(c_{n,q}) \tag{1.18}$$

with

$$\Pr(c_{n,q}=0) = \frac{e^{L_e^D(c_{n,q})}}{1+e^{L_e^D(c_{n,q})}}, \quad \Pr(c_{n,q}=1) = \frac{1}{1+e^{L_e^D(c_{n,q})}} \tag{1.19}$$

The probabilities $P_a^D(x_n)$ are used by the equalizer as a priori in the next turbo-iteration. The iteration between the equalizer and the decoder continues until the correct decoding of the received packet or a maximum number of turbo-iterations has been executed.

We present in the following the description of the SISO equalizer under the MAP and the MMSE equalization criteria.

1.5.1 MAP equalization

The MAP equalizer employs the Forward-Backward BCJR algorithm [16] which is a trellis based algorithm that maximizes the a posteriori probability for each transmitted symbol.

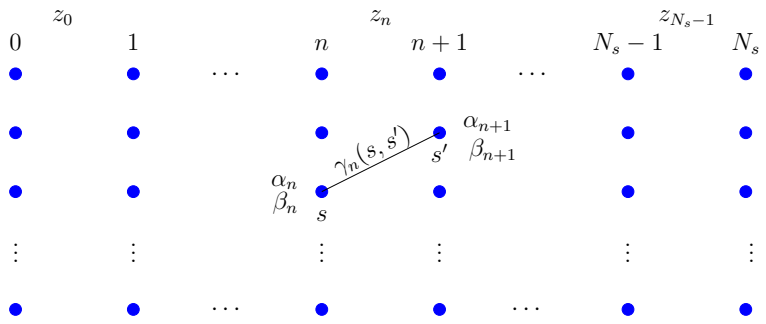

FIGURE 1.5: Forward-Backward equalization algorithm.

On the trellis representation of the channel, shown in Figure 1.5, each state S_n is identified by the previous $L-1$ transmitted symbols $(x_{n-1}, \cdots, x_{n-L+1})$. Consequently, there are $2^{Q(L-1)}$ different states. For a given channel state $S_n = s$, the output of the noiseless channel corresponding to the transmission of a symbol $x_n \in \mathcal{S}$ is

$$\psi(x_n, s) = h_0 x_n + \sum_{i=1}^{L-1} h_i x_{n-i} \tag{1.20}$$

The MAP equalizer computes the a posteriori probabilities $\Pr(x_n = x \in \mathcal{S}|\mathbf{z})$, using the conventions of Figure 1.5, as

$$\Pr(x_n = x \in \mathcal{S}|\mathbf{z}) \propto \sum_{(s,s'):x_n=x} \alpha_n(s) \times \gamma_n(s,s') \times \beta_{n+1}(s') \tag{1.21}$$

where

$$\alpha_n(s) = \Pr(s; z_0, \cdots, z_{n-1}) \tag{1.22}$$
$$\beta_{n+1}(s') = \Pr(z_{n+1}, \cdots, z_{N_s-1}|s') \tag{1.23}$$
$$\gamma_n(s,s') = \Pr(s', z_n|s) \tag{1.24}$$

The variable $\gamma_n(s,s')$ is the transition probability between two stats $S_n = s$ and $S_{n+1} = s'$ at the n-th section of the trellis and given by

$$\gamma_n(s,s') = \Pr(x_n|s,s') \times \Pr(x_n) \times \Pr(z_n|x_n,s) \tag{1.25}$$

where $\Pr(x_n|s,s') = 1$ if s and s' are connected, and zero otherwise. The term $\Pr(x_n)$ is the a priori on x_n, and the last term is computed for Gaussian noise by

$$\Pr(z_n|x_n,s) = \frac{1}{\pi\sigma_w^2} e^{-|z_n-\psi(x_n,s)|^2/\sigma_w^2} \tag{1.26}$$

The variables $\alpha_n(s)$ and $\beta_{n+1}(s')$ are computed by the following forward and backward recursions

$$\alpha_{n+1}(s') = \sum_{s} \alpha_n(s)\gamma_n(s,s') \tag{1.27}$$

$$\beta_n(s) = \sum_{s'} \beta_{n+1}(s')\gamma_n(s,s') \tag{1.28}$$

MAP equalization provides superior performance compared to other equalization techniques. However, it has prohibitive complexity when dealing with a high modulation order or a long channel due to the exponential increase of the number of states versus the channel length L and the modulation alphabet size. An alternative to MAP equalization with very lower complexity consists of using linear filtering equalization presented in the next section.

1.5.2 MMSE equalization

Linear equalization based on the minimum mean square error (MMSE) criterion has linear complexity with the channel length and practically independent of the modulation order. The MMSE equalizer can be implemented in the time-domain using finite-length filters or in the frequency-domain if cyclic-prefix insertion is used. We describe in the following both of these methods.

1.5.2.1 Time-domain MMSE equalization

The problem of MMSE equalization with *priors* was addressed by many works, as in [39, 40], using different approaches but leading to equivalent results. The structure of the soft-input soft-output (SISO)MMSE equalizer is shown in Figure 1.6 including a forward linear filter $\mathbf{f}$ and an interference canceler filter $\mathbf{b}$. The forward filter $\mathbf{f}$ is implemented using a finite number of taps $L_f = l_1 + l_2 + 1$, where the parameters l_1 and l_2 specify, respectively, the length of the non-causal and the causal part of the forward filter.

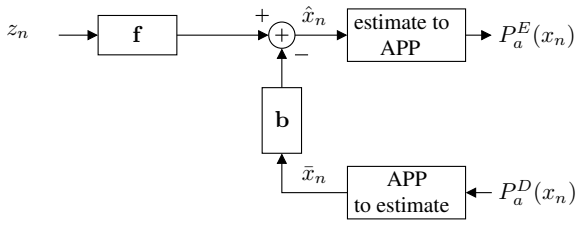

FIGURE 1.6: Time-domain SISO MMSE equalizer with interference canceler.

The linear estimate $\hat{x}_n$ of the transmitted symbol x_n is given by

$$\hat{x}_n = \mathbf{f}^H \mathbf{z}_n - \mathbf{b}^H \bar{\mathbf{x}}_n \tag{1.29}$$

where $\mathbf{z}_n = [z_{n-l_2}, \cdots, z_{n+l_1}]^\top$ are the required observation samples around the estimated symbol. The vector $\mathbf{z}_n$ can be modeled in matrix form by

$$\mathbf{z}_n = \mathbf{H}\mathbf{x}_n + \mathbf{w}_n \tag{1.30}$$

where

$$\begin{aligned} \mathbf{z}_n &= [z_{n-l_2}, \cdots, z_{n+l_1}]^\top \\ \mathbf{x}_n &= [x_{n-l_2-L+1}, \cdots, x_{n+l_1}]^\top \\ \mathbf{w}_n &= [w_{n-l_2}, \cdots, w_{n+l_1}]^\top \end{aligned} \tag{1.31}$$

and $\mathbf{H}$ is the channel matrix of dimensions $L_f \times (L_f + L - 1)$ having the following form

$$\mathbf{H} = \begin{bmatrix} h_{L-1} & \cdots & h_0 & 0 & \cdots & 0 \\ 0 & h_{L-1} & \cdots & h_0 & \ddots & \vdots \\ \vdots & \ddots & & \ddots & \ddots & 0 \\ 0 & \cdots & 0 & h_{L-1} & \cdots & h_0 \end{bmatrix}, \tag{1.32}$$

The derivation of the expression of the linear filters that minimize the mean squared error $E[|\hat{x}_n - x_n|^2]$ can be found in [40]. We only provide here the solution which is given by

$$\mathbf{f} = \alpha(\sigma_w^2 \mathbf{I} + v\mathbf{H}\mathbf{H}^H)^{-1}\mathbf{h} \tag{1.33}$$

$$\mathbf{b} = \mathbf{H}^H \mathbf{f} - \mu \mathbf{u} \tag{1.34}$$

where

$$\mathbf{u} = [\mathbf{0}_{1\times(l_2+L-1)}\ 1\ \mathbf{0}_{1\times l_1}]^\top \tag{1.35}$$

$$\mathbf{h} = \mathbf{H}\mathbf{u} \tag{1.36}$$

$$\mu = \mathbf{f}^H \mathbf{h} \tag{1.37}$$

$$v = \frac{1}{N_s} \sum_{n=0}^{N_s-1} E(|x_n|^2) - |\bar{x}_n|^2 \tag{1.38}$$

$$E(|x_n|^2) = \sum_{x\in\mathcal{S}} |x|^2 \Pr(x_n = x) \tag{1.39}$$

$$\bar{x}_n = E(x_n) = \sum_{x\in\mathcal{S}} x \Pr(x_n = x) \tag{1.40}$$

$$\alpha = \frac{1}{1 + (1-v)\mu'} \tag{1.41}$$

$$\mu' = \mathbf{h}^H(\sigma_w^2 \mathbf{I} + v\mathbf{H}\mathbf{H}^H)^{-1}\mathbf{h} \tag{1.42}$$

The variable v reflects the reliability of the decoder feedback. For a perfect feedback $v = 0$, and for no a priori we have $v = 1$.

The estimated symbol at the output of the equalizer can be modeled by a Gaussian model as

$$\hat{x}_n = \mu x_n + \eta_n \tag{1.43}$$

where η_n is complex Gaussian noise with variance $\sigma_\eta^2 = \mu(1-\mu)$. Based on this model, the output extrinsic a posteriori probabilities (APPs) are then computed

$$P_a^E(x_n) = \Pr(x_n|\hat{\mathbf{x}}) = \Pr(x_n|\hat{x}_n) = \Pr(\hat{x}_n|x_n)\Pr(x_n)/\Pr(\hat{x}_n) \tag{1.44}$$

where second equality results from the independence of noise η_n and the last equality comes from the Bayes rule. Thus,

$$P_a^E(x_n) \sim \Pr(\hat{x}_n|x_n)\Pr(x_n) \tag{1.45}$$

The term $\Pr(x_n)$ is the a priori on x_n, and $\Pr(\hat{x}_n|x_n)$ an be computed from the noise distribution as

$$\Pr(\hat{x}_n|x_n) = \kappa_n \exp(-\frac{|\hat{x}_n - \mu x_n|^2}{\sigma_\eta^2}) \tag{1.46}$$

where κ_n is a normalization constant chosen to have a true probability mass function, i.e. $\sum_{x_n \in \mathcal{S}} P_a^E(x_n) = 1$ at the output of the estimator.

The complexity of the finite-length MMSE equalizer increases with the length of the forward filter L_f. Therefore, L_f must be properly chosen as a compromise between complexity and the performance loss due to the finite-length implementation. In general, an adequate choice could be $L \leq L_f \leq 3L$.

As an example, we have simulated the FER performance of the transmission over the Proakis-C channel defined by $\mathbf{h} = [0.227, 0.460, 0.688, 0.460, 0.227]$. Simulation parameters are the following: The packet length is $N_b = 1024$ bits obtained by a rate-1/2 convolutional code (5,7). We use a pseudo random interleaver and BPSK modulation. The MMSE filter length is $L_f = 15$ ($l_1 = 5$, $l_2 = 9$). Figure 1.7 shows the FER performance up to five turbo-iterations for both MAP and MMSE turbo-equalizers. The performance of the channel code over AWGN are reported on the same figure as a reference.

We can observe the remarkable gain achieved by turbo-equalization and the superiority of the MAP equalizer where it performs close to the AWGN performance after 5 iterations.

Finally, it is worth to note that the performance of the MMSE turbo-equalizer can be improved by feeding the a posteriori LLRs from the channel decoder to the MMSE equalizer instead of the extrinsic LLRs. Actually, as explained in [41], by using the full available information on the transmitted symbols, the performance of the interference canceler is improved.

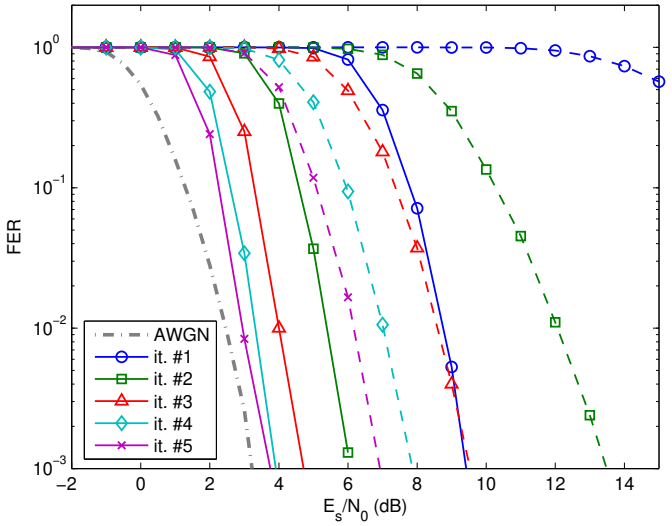

FIGURE 1.7: Turbo-equalization performance over proakis-C channel using BPSK modulation. Solid curves for MAP equalization, and dotted curves for MMSE equalization.

1.5.2.2 Frequency-domain MMSE equalization

Thanks to the cyclic prefix insertion, the time domain convolution becomes a simple multiplication in the frequency domain. Thus, after removing the CP from the received blocks, a discrete Fourier transform (DFT) is applied on the obtained signal $\mathbf{z}$. The obtained signal can be modeled in the frequency domain as

$$\underline{\mathbf{z}}[n] = \underline{\mathbf{h}}[n]\,\underline{\mathbf{x}}[n] + \underline{\mathbf{w}}[n] \tag{1.47}$$

where the DFT vector of a signal vector $\mathbf{x}$ is denoted by $\underline{\mathbf{x}}$, and $\underline{\mathbf{x}}[n]$ is the n-th element of the vector $\underline{\mathbf{x}}$. Based on this model, the MMSE equalization problem reduces in the frequency-domain to scalar multiplication. The corresponding receiver structure is shown in Figure 1.8.

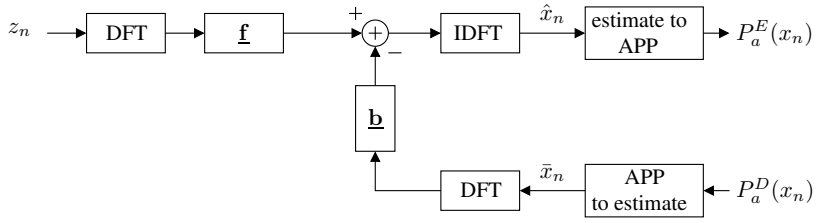

FIGURE 1.8: Frequency-domain SISO MMSE equalizer with interference canceler.

According to this structure, the linear estimate $\hat{\mathbf{x}}$ of $\mathbf{x}$ is given in [42] by

$$\underline{\hat{\mathbf{x}}}[n] = \underline{\mathbf{f}}^*[n]\,\underline{\mathbf{z}}[n] - \underline{\mathbf{b}}^*[n]\,\underline{\bar{\mathbf{x}}}[n] \tag{1.48}$$

In a similar way to the time-domain equalizer, the solution for the linear filters is given by

$$\underline{\mathbf{f}}[n] = \alpha \frac{\underline{\mathbf{h}}[n]}{\sigma_w^2 + v|\underline{\mathbf{h}}[n]|^2} \tag{1.49}$$

$$\underline{\mathbf{b}}[n] = \underline{\mathbf{f}}^*[n]\,\underline{\mathbf{h}}[n] - \mu \tag{1.50}$$

$$\alpha = \frac{1}{1 + (1-v)\mu'} \tag{1.51}$$

$$\mu = \alpha\mu' \tag{1.52}$$

$$\mu' = \frac{1}{N_s} \sum_{n=0}^{N_s-1} \frac{|\underline{\mathbf{h}}[n]|^2}{\sigma_w^2 + v|\underline{\mathbf{h}}[n]|^2} \tag{1.53}$$

From the performance viewpoint, the frequency-domain MMSE equalization is equivalent to the time-domain counterpart with $L_f = N_s$. From the complexity viewpoint, frequency-domain MMSE implementation requires two initial DFT operations for the received sequence and the channel response and two DFT operations per turbo-iteration. These DFT operations can be efficiently implemented by using the FFT algorithm. From the results of [42], the complexity of the time-domain MMSE turbo-equalization is roughly of the order $N_s(L_f+L)$ per turbo-iteration, while it is of the order $N_s \log_2(N_s)$ for the frequency-domain MMSE turbo-equalization. This shows clearly the advantage of the frequency-domain solution when dealing with a long channel response.

1.5.3 EXIT charts analysis

The analytical assessment of the performance of the iterative receivers is difficult in general. However, the convergence behavior of the turbo-equalizer can be studied using a semi-analytical tool called extrinsic information transfer (EXIT) charts [43]. EXIT charts are particularly useful for the prediction of system performance in terms of BER assuming large interleaving length. In practice, the interleaver has a finite length, and the system performance in terms of FER can not be predicted using this kind of analysis. However, EXIT charts analysis give an idea about the asymptotic system performance which is very useful for the comparison between two different iterative receivers.

The EXIT function for the equalizer is a function which gives the mutual information with the transmitted data at the output of the equalizer I_{out}^E as a function of the mutual information at its input I_{in}^E. The EXIT function for the channel decoder is defined in a similar way giving I_{out}^D as function of I_{in}^D. Practical methods for the computation of EXIT charts are given in details in the tutorial paper [44].

In order to show the convergence behavior of the turbo-equalizer through iterations, the transfer function of the equalizer and the the inverse transfer function of the decoder

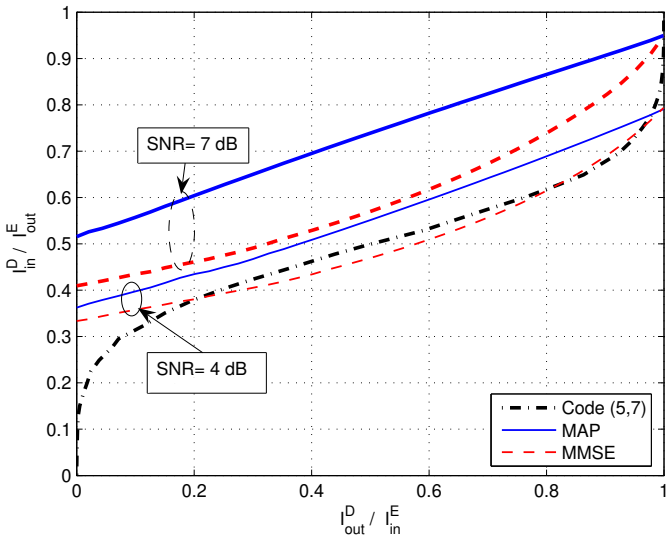

FIGURE 1.9: EXIT charts for MAP and MMSE turbo-equalizers for different SNR values.

are traced on the same figure. The convergence point is the intersection point between the two curves. Figure 1.9 shows the Exit charts for both MAP and MMSE turbo-equalizers for different values of SNR. We can see that the output of the MAP equalizer has higher reliability than the MMSE equalizer but they converge into the same point for high a priori. For SNR=4 dB, the convergence point for the MMSE turbo-equalizer has low reliability than the MAP equalizer. This explains the performance superiority of the MAP turbo-equalizer. For SNR=7 dB, both MMSE and MAP equalizer converge to almost the same point. however, the MMSE equalizer need more iterations to reach the convergence point.

1.6 Packet combining for frequency-selective channels

As it has been noted previously, IR uses code combining which is performed at the bit level after equalization and symbol demapping. In the context of CC, There is various methods to perform packet combining. We presents some of these methods which are different in the position of performing the combining.

1.6.1 Maximum-ratio combining

A simple way for packet combining over frequency selective channel is to equalize each received packet separately, and then combine the various received copies of the same packet at the output of the equalizer as shown in Figure 1.10. The combining can be made either at the symbol level before soft-demapping or at the bit level after soft-

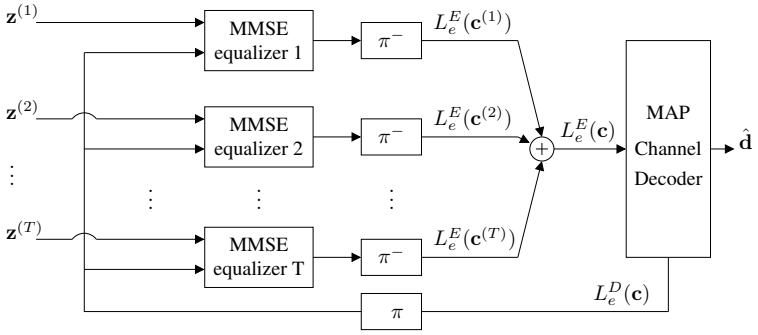

FIGURE 1.10: MMSE turbo-equalization with maximum ratio combining.

demapping. Maximum ratio combining at the symbol level requires the knowledge of the equivalent Gaussian channel model (channel gain and noise variance). This is actually the case when using MMSE equalization. When we do not have a direct access to the equivalent Gaussian channel model at the equalizer output as for MAP equalization, MRC can be performed at the bit level in an approximated way assuming the independence between the transmitted bits within each symbol. This is performed by adding the LLRs at the output of the symbol soft-demapper.

1.6.2 Joint equalization

Channel equalization performance can be improved by performing joint equalization [45] of all received copies of the same packet compared with separate equalization followed by maximum-ratio-combining [46]. We present now the corresponding equalizer structure with multiple inputs.

1.6.2.1 Joint MAP equalizer

The Forward-Backward algorithm for MAP equalization can be generalized for the joint equalization of multiple transmissions [45]. All what we need is to update the transition probabilities on the trellis at each retransmission of the same packet. This expressed by the following recursion

$$\gamma_{n,T}(s,s') = \gamma_{n,T-1}(s,s') \times p(z_n^{(T)}|x_n = x, s, s')$$

where

$$p(z_n^{(T)}|x_n = x, s', s) = \frac{1}{\pi\sigma_w^2} e^{-|z_n^{(T)} - \psi^{(T)}(x,S_n)|^2/\sigma_w^2}$$

where the upper index $^{(T)}$ refers to the T-th HARQ round. Then the equalizer uses these transition probabilities in the same way as for a single transmission in order to estimate the transmitted packet.

1.6.2.2 Joint MMSE equalizer

The structure of the finite length MMSE equalizer with a priori can be generalized to the case of multiple inputs as shown in Figure 1.11.

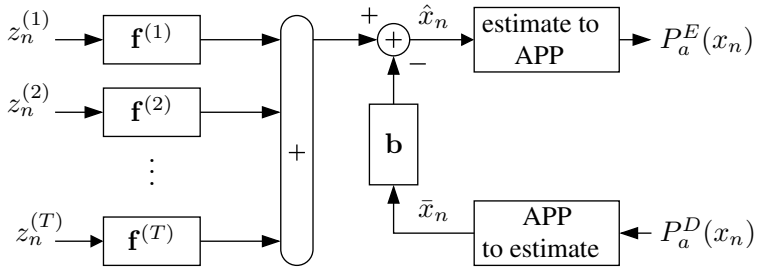

FIGURE 1.11: Time-domain joint SISO MMSE equalizer with interference canceler.

The joint SISO MMSE equalizer includes multiple forward linear filters, denoted as $\mathbf{f}^{(1)}, \cdots, \mathbf{f}^{(T)}$, and an interference canceler filter, denoted by $\mathbf{b}$. The linear estimate $\hat{x}_n$ of the transmitted symbol x_n after T transmissions is given by

$$\hat{x}_n = \sum_{t=1}^{T} (\mathbf{f}^{(t)})^H \mathbf{z}_n^{(t)} - \mathbf{b}^H \bar{\mathbf{x}}_n \tag{1.54}$$

where $\mathbf{z}_n^{(t)} = [z_{n-l_2}^{(t)}, \cdots, z_{n+l_1}^{(t)}]^\top$ are the observation samples around the estimated symbol. By grouping all received copies of the same packet in a single vector, the problem of the joint equalization of multiple identical transmissions can be turned back to the case of a single transmission by considering the equivalent single-input multiple-output (SIMO) channel model given in matrix form by

$$\mathbf{z}_{T,n} = \mathbf{H}_T \mathbf{x}_n + \mathbf{w}_{T,n}$$

where

$$\begin{aligned}
\mathbf{x}_n &= [x_{n-l_2-L+1}, \cdots, x_{n+l_1}]^\top \\
\mathbf{z}_{T,n} &= [(z_{n-l_2}^{(1)}, z_{n-l_2}^{(2)}, \cdots, z_{n-l_2}^{(T)}), \quad \cdots \quad, (z_{n+l_1}^{(1)}, z_{n+l_1}^{(2)}, \cdots, z_{n+l_1}^{(T)})]^\top \\
\mathbf{w}_{T,n} &= [(w_{n-l_2}^{(1)}, w_{n-l_2}^{(2)}, \cdots, w_{n-l_2}^{(T)}), \quad \cdots \quad, (w_{n+l_1}^{(1)}, w_{n+l_1}^{(2)}, \cdots, w_{n+l_1}^{(T)})]^\top
\end{aligned}$$

and $\mathbf{H}_T$ is the $TL_f \times (L_f + L - 1)$ equivalent channel matrix given by

$$\mathbf{H}_T = \begin{bmatrix}
\mathbf{h}_{L-1} & \cdots & \mathbf{h}_0 & \mathbf{0} & \cdots & \mathbf{0} \\
\mathbf{0} & \mathbf{h}_{L-1} & \cdots & \mathbf{h}_0 & \ddots & \vdots \\
\vdots & \ddots & \ddots & & \ddots & \mathbf{0} \\
\mathbf{0} & \cdots & \mathbf{0} & \mathbf{h}_{L-1} & \cdots & \mathbf{h}_0
\end{bmatrix}, \tag{1.55}$$

where $\mathbf{h}_i = [h_i^{(1)}, \cdots, h_i^{(T)}]^\top$.
Using this model, the joint equalization can be solved as in the case of a single input using the equivalent channel matrix. We remark that the size of this matrix increases steadily with the number of retransmissions resulting in an increased computational complexity. By contrast, we will see in the next chapter that frequency-domain joint equalization has too much lower computational complexity requirements.

1.6.3 Numerical results

In order to show the relative performance of CC-HARQ and IR-HARQ protocols over frequency-selective channels, we consider the following HARQ transmission scenario with $T_{\max} = 3$.

For the IR-HARQ scheme, we consider the rate-compatible family of codes given in the example of section 1.3.2 with initial rate $r_1 = 4/5$. The different rates in this example were carefully selected in order to have the same block length at each HARQ transmission. A packet of 960 information bits is encoded leading to 1200 coded bits at each HARQ transmission. For CC-HARQ scheme, we repeat the same punctured codeword obtained by $\mathcal{C}1$ which is used at the first transmission of the IR-HARQ scheme.

We assume BPSK modulation over a long-term static channel of length $L = 5$ with uniform power-delay profile. Figure 1.12 shows the obtained FER performance for both protocols under separate MMSE equalization and decoding and with MMSE turbo-equalization which performs a maximum of five turbo-iterations.

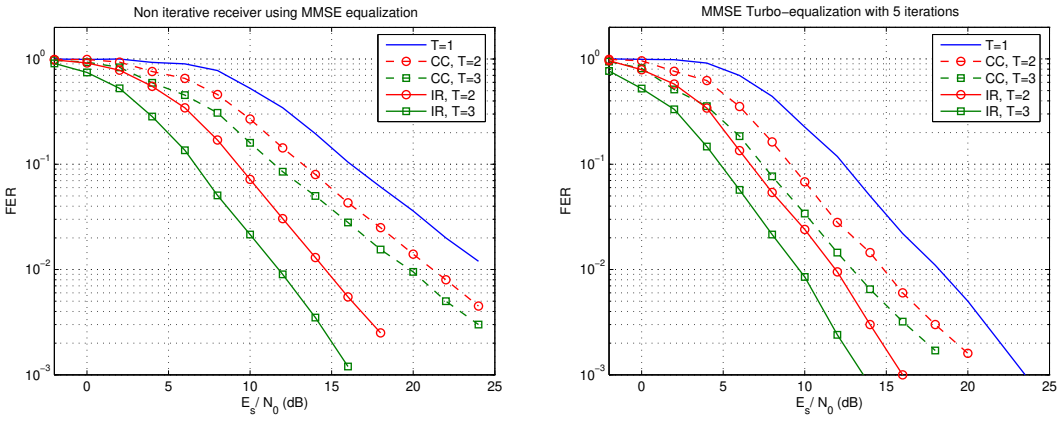

FIGURE 1.12: Performance comparison between CC-HARQ and IR-HARQ over long-term static channel with $L = 5$ and $T_{\max} = 3$.

The FER performance over short-term static channel model are depicted on Figure 1.13. We can observe from Figures 1.12 and 1.13 that depending on the channel model and the receiver structure, the relative gains of IR over CC are different.

First, we note that IR significantly outperforms CC over long term static channel especially a non-iterative receiver. This can be justified by a higher coding gain, in

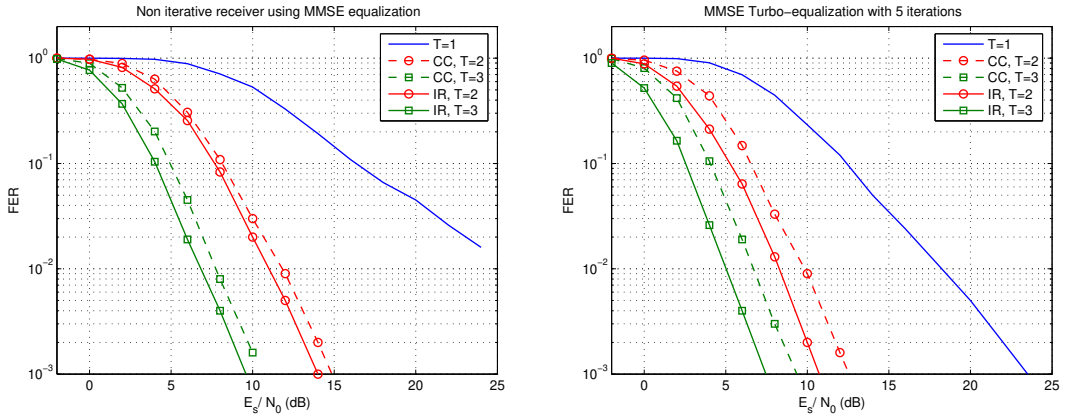

FIGURE 1.13: Performance comparison between CC-HARQ and IR-HARQ over short-term static channel with $L = 5$ and $T_{\max} = 3$.

addition to signal diversity in IR HARQ scheme. The achieved gain with IR is less important for short term static channel especially for a non-iterative receiver because in the latter case the CC has better detection performance thanks to the joint equalization with uncorrelated channels in comparison with joint decoding at the bit level. This compensates a part of the coding gain advantage of the IR.

1.7 Conclusions

We have presented in this chapter an overview over the existing HARQ protocols which are used to ensure data reliability for data packet communication systems over wireless channels. On one hand, IR-HARQ protocols provide better performance than CC-HARQ protocols due to the superior coding gain at the expense of constrained code design and increased complexity. The obtained gain is particularly important for slow time-varying channels and decrease with lower initial coding rate. This gain is less impressive for rapidly time-varying frequency-selective channels. On the other hand, CC-HARQ protocols are more simple and offer more flexibility for practical implementation.

We aim to improve the performance of CC-HARQ protocols while keeping their advantages. To this end, we start by investigating the theoretical performance of the transmission scheme over frequency-selective channels assuming an optimal maximum-likelihood receiver in order to determine the effect of different system parameters on the system performance. This is the subject of the next chapter.

Chapter 2

Maximum-Likelihood Detection and Decoding

In this chapter, we study the performance of the bit-interleaved coded modulation (BICM) scheme over frequency-selective channels using maximum likelihood (ML) sequence detection and decoding with perfect channel state information (CSI) at the receiver. We aim to determine the performance limits for the BICM scheme over frequency-selective channels with an optimal receiver. This allows us to evaluate how much the performance of a sub-optimal receiver, in particular a turbo-equalizer, are far from the optimal performance. In addition, we hope getting some insights into the improvement of the transmission scheme in the context of Chase combining HARQ retransmission scheme in order to reduce the performance gap with incremental redundancy HARQ scheme.

2.1 Introduction

The performance of maximum likelihood sequence estimation was first analyzed by Forney in [11, 47] for uncoded transmission over static frequency-selective channels. Upper and lower bounds were derived based on the Euclidean distance spectrum at the output of the noiseless frequency-selective channel. The Euclidean distance weight enumerators are evaluated using a trellis-based approach to calculate the transfer function of the channel. However, for a multipath-fading channel, where the channel is time-variant, trellis-based approaches can not be applied because the transfer function depends on the particular channel realization.

For bit-interleaved coded transmission, the system performance are usually investigated under the *uniform interleaving* assumption which was initially introduced by Benedetto in [15, 48] for the study of the performance of serially concatenated codes. This approach has been applied to BICM transmission over a frequency-selective channel by considering the frequency-selective channel as a rate-1 trellis encoder in concatena-

tion with the channel code. For example, in [49, 50], the authors have applied this approach for the simple case of partial response channels.

We derive an upper bound on the FER performance based on the union bound and the uniform interleaving assumption. The uniform interleaving assumption leads, in general, to loose bounds on the bit error rate (BER) performance. However, for FER performance, the obtained bounds are more tight as it will be seen in this chapter. The main problem which arises from in the evaluation of the union bound is the computation of the Euclidean distance distribution at the output of the noiseless frequency-selective channel. We present in this chapter a novel approach for the evaluation of the output Euclidean distance distribution. We start by developing a general framework for the evaluation of the output Euclidean distance as a function of the deterministic autocorrelation functions of the error sequence and channel response. Based on this framework, we then investigate the statistical properties of the output Euclidean distance distribution instead of exact enumeration techniques. We apply this framework on static and time-varying frequency-selective channels yielding to satisfactory performance bounds especially for time-varying channels. In both cases, an approximation of the output Euclidean distance distribution is used for the evaluation of an upper bound on the FER performance. We consider in this study convolutional channel coding. However, the proposed bound can be applied to any type of binary channel codes with known distance spectrum.

More important than the upper bounds, is the better understanding of the effect of different system parameters, such as interleaving, symbol mapping, and channel model, on the Euclidean distance. We generalize this study for CC-HARQ scheme which introduces for two transmit diversity techniques that will be presented in Chapter 3 and Chapter 4, respectively. The proofs of lemmas and propositions announced in this chapter are given in the Appendix.

2.2 Error probability analysis

In a classical BICM transmission scheme as it has been presented in Chapter 1, let $\mathbf{c} = [c_0, \cdots, c_{N_b-1}]^\top$ be the transmitted interleaved binary codeword, and $\mathbf{x} = [x_0, \cdots, x_{N_s-1}]^\top$ be the corresponding modulated sequence. The received signal $\mathbf{z} = [z_0, \cdots, z_{N_s-1}]^\top$ is given by

$$\mathbf{z} = \mathbf{h} * \mathbf{x} + \mathbf{w} \tag{2.1}$$

where $*$ denotes the discrete linear convolution, and $\mathbf{w} = [w_0, \cdots, w_{N_s-1}]^\top$ is the noise vector. In an equivalent manner, the received sequence sample are given by the channel convolution

$$z_n = \sum_{i=0}^{L-1} h_i x_{n-i} + w_n, \quad n = 0, \cdots, N_s - 1 \tag{2.2}$$

The average received SNR is defined by $\rho = \frac{E_s}{\sigma_w^2}$.

Given the channel response $\mathbf{h}$, the maximum likelihood receiver estimates the transmitted sequence $\mathbf{x}$ by the sequence $\hat{\mathbf{x}}$ taken from the ensemble of all possible interleaved and modulated codewords, denoted by $\mathcal{X}$, that solves the following minimization problem

$$\hat{\mathbf{x}} = \arg\min_{\mathbf{x}\in\mathcal{X}} ||\mathbf{z} - \mathbf{h} * \mathbf{x}||^2. \tag{2.3}$$

The estimated sequence $\hat{\mathbf{x}}$ is then demodulated to obtain the estimated interleaved codeword $\hat{\mathbf{c}}$ for the transmitted interleaved codeword $\mathbf{c}$.

For a large number of transmitted information bits per packet K_b, the minimization problem (2.3) can not be solved numerically in practice due to the high cardinality of $\mathcal{X}$ which contains 2^K different sequences. In order to evaluate the performance of the ML receiver analytically, we resort to the union bound technique which is based on the evaluation of the pairwise error probability and the output distance spectrum.

2.2.1 Pairwise error probability

The ML pairwise error probability (PEP) between two different sequences $\mathbf{x}$ and $\hat{\mathbf{x}}$ from $\mathcal{X}$ is the probability that the ML receiver commits an error by selecting $\hat{\mathbf{x}}$ as an estimate of the transmitted sequence $\mathbf{x}$. We denoted this probability as $P_2(\mathbf{x}, \hat{\mathbf{x}})$, which is given in [11] by

$$P_2(\mathbf{x}, \hat{\mathbf{x}}) = Q\left(\sqrt{d_E^2(\mathbf{x}, \hat{\mathbf{x}})\rho/2}\right), \tag{2.4}$$

where $Q(x) = \frac{1}{\sqrt{2\pi}} \int_x^{+\infty} e^{-t^2/2} dt$, ρ is the average received SNR, and $d_E^2(\mathbf{x}, \hat{\mathbf{x}})$ is the output squared Euclidean distance (OSED) between $\mathbf{x}$ and $\hat{\mathbf{x}}$ at the output of the noiseless channel and given by

$$\begin{aligned} d_E^2(\mathbf{x}, \hat{\mathbf{x}}) &\triangleq \|\mathbf{h} * \hat{\mathbf{x}} - \mathbf{h} * \mathbf{x}\|^2 = \|\mathbf{h} * (\hat{\mathbf{x}} - \mathbf{x})\|^2 && (2.5)\\ &= \|\mathbf{h} * \mathbf{e}\|^2 && (2.6)\\ &= \sum_{n=0}^{N_s-1} \left| \sum_{i=0}^{L-1} h_i e_{n-i} \right|^2, && (2.7) \end{aligned}$$

where we have defined the error sequence $\mathbf{e} \triangleq \hat{\mathbf{x}} - \mathbf{x}$. We remark that the OSED does not depend directly on the $\mathbf{x}$ and $\hat{\mathbf{x}}$. It only depends on the error sequence $\mathbf{e}$ between them. Therefore, the OSED is denoted in the following as a function of the error sequence $d_E^2(\mathbf{e})$.

In the following, we use the following notations:

- $\Delta = d_E^2(\mathbf{x}, \hat{\mathbf{x}}) = d_E^2(\mathbf{e})$ is the OSED between two modulated sequences $\mathbf{x}$ and $\hat{\mathbf{x}}$. When considering Δ as a random variable, we denote by δ the value of this random variable.
- $\boldsymbol{\epsilon} = \mathbf{c} \oplus \hat{\mathbf{c}}$ is the corresponding binary error codeword.

- $d = d_H(\boldsymbol{\epsilon})$ or equivalently $d = d_H(\mathbf{e})$ is the input Hamming weight of the binary error codeword $\boldsymbol{\epsilon}$ which corresponds to $\mathbf{e}$.

In the next section, we give the general expression for the union bound on the FER performance of the BICM transmission system over a frequency-selective channel.

2.2.2 Union bound

The average error probability over all possible transmitted sequences is upper bounder by the union bound as,

$$P_e(\rho) \triangleq \Pr(\mathbf{e} \neq 0) \leq P_{\text{sub}}(\rho) \tag{2.8}$$

where $P_{\text{sub}}(\rho)$ is given by

$$P_{\text{sub}}(\rho) = \frac{1}{2^K} \sum_{\mathbf{x}\in\mathcal{X}} \sum_{\hat{\mathbf{x}}\in\mathcal{X}:\hat{\mathbf{x}}\neq\mathbf{x}} P_2(\mathbf{x}, \hat{\mathbf{x}}) \tag{2.9}$$

$$= \frac{1}{2^K} \sum_{\mathbf{x}\in\mathcal{X}} \sum_{\hat{\mathbf{x}}\in\mathcal{X}:\hat{\mathbf{x}}\neq\mathbf{x}} Q\left(\sqrt{d_E^2(\mathbf{x}, \hat{\mathbf{x}})\rho/2}\right) \tag{2.10}$$

$$\tag{2.11}$$

assuming that all transmitted sequences are equally likely. By regrouping all terms in the second sum resulting from sequences $\hat{\mathbf{x}}$ at the same Euclidean distance from $\mathbf{x}$, and performing the summation with respect to the values δ of $\Delta = d_E^2(\mathbf{x}, \hat{\mathbf{x}})$, we get

$$P_{\text{sub}}(\rho) = \frac{1}{2^K} \sum_{\mathbf{x}\in\mathcal{X}} \sum_{\delta>0} A_x^{\text{ch}}(\delta) Q\left(\sqrt{\delta\rho/2}\right) \tag{2.12}$$

where $A_x^{\text{ch}}(\delta)$ denotes the number of sequences $\hat{\mathbf{x}}$ at OSED δ from $\mathbf{x}$. By changing the order of summation, we can rewrite (2.12) in a more compact form as

$$P_{\text{sub}}(\rho) = \sum_{\delta>0} \frac{1}{2^K} \sum_{\mathbf{x}\in\mathcal{X}} A_x^{\text{ch}}(\delta) Q\left(\sqrt{\delta\rho/2}\right) \tag{2.13}$$

$$= \sum_{\delta>0} A^{\text{ch}}(\delta) Q\left(\sqrt{\delta\rho/2}\right) \tag{2.14}$$

where $A^{\text{ch}}(\delta)$ is the weight enumerator at the output of the noiseless channel defined by

$$A^{\text{ch}}(\delta) \triangleq \frac{1}{2^K} \sum_{\mathbf{x}\in\mathcal{X}} A_x^{\text{ch}}(\delta) \tag{2.15}$$

which is the average of $A_x^{\text{ch}}(\delta)$ over all sequences $\mathbf{x} \in \mathcal{X}$.

The evaluation of the channel output enumerator $A^{\text{ch}}(\delta)$ is not a simple task in general because of the dependence of $A_x^{\text{ch}}(\delta)$ on the transmitted sequence. Consequently, we can not take a particular sequence, such as the all-zero sequence for example, as a

TABLE 2.1: Example of error sequences with BPSK mapping.

$\mathbf{x}$	+1	+1	+1	-1	+1	+1	-1	-1
$\hat{\mathbf{x}}$	-1	+1	-1	-1	-1	+1	+1	-1
$\boldsymbol{\epsilon}$	1	0	1	0	1	0	1	0
$\mathbf{e}$	-2	0	-2	0	-2	0	+2	0

reference for the study of system performance as it is the case for binary error correcting codes. Actually, the same binary error word $\boldsymbol{\epsilon}$ may correspond to different error sequences $\mathbf{e}$ depending on the transmitted sequence $\mathbf{x}$. Hence, different Euclidean distances at the output of a frequency-selective channel. We illustrate this by the example given in Table 2.1 using BPSK mapping. for a BPSK mapping scheme, the non-zero elements e_n of the error sequence take their values from the ensemble $\{-2, +2\}$ depending on the transmitted symbols x_n in such a way that $\mathbf{x} + \mathbf{e}$ is a valid sequence from $\mathcal{X}$. For example, if the transmitted symbol is '+1', the corresponding error elements can only take the value '-2' giving an estimated symbol '-1'. This means that the error elements are not independent.

Let $\mathcal{E}(\mathcal{X})$ be the ensemble of all possible error sequences between the elements of $\mathcal{X}$, i.e.

$$\mathcal{E}(\mathcal{X}) \triangleq \{\mathbf{e} = \hat{\mathbf{x}} - \mathbf{x} : \mathbf{x}, \hat{\mathbf{x}} \in \mathcal{X}\} \tag{2.16}$$

The cardinality of $\mathcal{E}(\mathcal{X})$ is $|\mathcal{E}(\mathcal{X})| = 2^K \times 2^K = 2^{2K}$ sequences (not necessarily distinct). In order to take account for the coded nature of the elements of $\mathcal{X}$, the term $A_x^{\text{ch}}(\delta)$ can be decomposed with respect to the Hamming weight d of the corresponding binary error words as

$$A_x^{\text{ch}}(\delta) = \sum_{d \geq d_{\min}} A_x^{\text{ch}}(d, \delta) \tag{2.17}$$

where $d_{\min}$ is the free distance of the code and $A_x^{\text{ch}}(d, \delta)$ denote the number of error sequences $\mathbf{e} \in \mathcal{E}(\mathcal{X})$ of Hamming weight d leading to a sequence $\hat{\mathbf{x}}$ at OSED δ from $\mathbf{x}$. For a given transmitted sequence $\mathbf{x}$, the number of possible error sequences $\mathbf{e}$ of Hamming weight d is given by the Hamming weight enumerator $A^{\text{c}}(d)$ of the binary channel code. The linear property of binary codes ensures that $A^{\text{c}}(d)$ is independent of $\mathbf{x}$. Therefore, we can write (2.17) as

$$A_x^{\text{ch}}(\delta) = \sum_{d \geq d_{\min}} A^{\text{c}}(d) \frac{A_d^{\text{ch}}(\delta, \mathbf{x})}{A^{\text{c}}(d)} \tag{2.18}$$

$$= \sum_{d \geq d_{\min}} A^{\text{c}}(d) \Pr(\Delta = \delta | \mathbf{x}, d) \tag{2.19}$$

where

$$\Pr(\Delta = \delta | \mathbf{x}, d) = \frac{A_d^{\text{ch}}(\delta, \mathbf{x})}{A^{\text{c}}(d)} \tag{2.20}$$

is the conditional probability of error sequences $\mathbf{e} \in \mathcal{E}(\mathcal{X})$ with an OSED δ, having $\mathbf{x}$ and d. Mathematically,

$$\Pr(\Delta = \delta|\mathbf{x}, d) = \Pr(\mathbf{e} \in \mathcal{E}(\mathcal{X}) : d_E^2(\mathbf{e}) = \delta|\mathbf{x}, d_H(\mathbf{e}) = d) \tag{2.21}$$

Let $\mathcal{E}_d(\mathbf{x})$ be the sub-ensemble of $\mathcal{E}(\mathcal{X})$ which can be committed on $\mathbf{x}$ with Hamming weight d. The cardinality of $\mathcal{E}_d(\mathbf{x})$ is $|\mathcal{E}_d(\mathbf{x})| = A^{\mathrm{c}}(d)$. The evaluation of $\Pr(\Delta|\mathbf{x}, d)$ is intractable in the general context because the probability space $\mathcal{E}_d(\mathbf{x})$ depends upon the mapping scheme, and the positions of error bits which, in turns, depend upon the error event patterns of the channel code and the used interleaver.

To overcome this problem, we resort to two simplifying assumptions:

A1: Uniform interleaver: We assume that the interleaver is a *uniform interleaver* of length N_b defined as a probabilistic device which maps a given input word of weight d into all $\binom{N_b}{d}$ distinct permutations of it with equal probability $1/\binom{N_b}{d}$.

The uniform interleaver may be thought of as the average over the ensemble of all deterministic length-N_b interleavers, assuming a uniform distribution. This is not of major concern for the evaluation of the upper bound, because it can be found, with a high probability, an interleaver which performs better than the average. The use of this device has proven to be very valuable in analyzing the average ML performance of parallel and serial concatenated coding architectures.

This assumption allows to compute $\Pr(\Delta|\mathbf{x}, d)$ over an extended ensemble which corresponds to all binary error patterns of Hamming weight d. The extended ensemble is denoted by $\mathcal{E}'_d(\mathbf{x})$ and contains $\binom{N_b}{d}$ elements instead of $A^{(c)}(d)$ for $\mathcal{E}_d(\mathbf{x})$. Thus,

$$\Pr(\Delta = \delta|\mathbf{x}, d) = \frac{A_d^{\mathrm{ch}}(\delta)}{\binom{N_b}{d}} \tag{2.22}$$

where $A_d^{\mathrm{ch}}(\delta)$ is the number of error sequence in $\mathcal{E}'_d(\mathbf{x})$ with an OSED δ.

Even though, an additional assumption is need in order remove the dependence on the transmitted sequence $\mathbf{x}$ in the computation of the conditional probability. This is the second simplifying assumption.

A2: Conditional independence of error symbols: We assume that the non-zero error elements e_n of $\mathbf{e}$ are zero mean random variables which are mutually independent and identically distributed conditionally to the Hamming weight. Non-zero error elements take their values from the ensemble $\varepsilon = \{e_n = \hat{x}_n - x_n : x_n, \hat{x}_n \in \mathcal{S}, x_n \neq \hat{x}_n\}$ which has $2^Q(2^Q - 1)$ elements.

While the first assumption A1 overcome the constaint imposed by the deterministic interleaver, the second assumption A2, in turns, removes any constraint resulting from the code structure except its weight distribution.

By substituting (2.19) in (2.15) and invoking that $A^{\mathrm{c}}(d)$ is independent of $\mathbf{x}$, we obtain

$$A^{\mathrm{ch}}(\delta) = \frac{1}{2^K} \sum_{\mathbf{x}\in\mathcal{X}} \sum_{d\geq d_{\min}} A^{\mathrm{c}}(d) \Pr(\Delta = \delta|\mathbf{x}, d) \tag{2.23}$$

$$= \sum_{d\geq d_{\min}} A^{\mathrm{c}}(d) \frac{1}{2^K} \sum_{\mathbf{x}\in\mathcal{X}} \Pr(\Delta = \delta|\mathbf{x}, d) \tag{2.24}$$

$$= \sum_{d\geq d_{\min}} A^{\mathrm{c}}(d) \Pr(\Delta = \delta|d) \tag{2.25}$$

Then, the problem of finding the output Euclidean distance enumerator $A^{\mathrm{ch}}(\delta)$ reduces to finding the conditional probability

$$\Pr(\Delta = \delta|d) = \Pr(\mathbf{e} \in \mathcal{E}_d : d_E^2(\mathbf{e}) = \delta) \tag{2.26}$$

Under the assumptions A1 and A2, the conditional probability $\Pr(\Delta|d)$ is calculated over the extended space $\mathcal{E}_d$ which contains all possible error sequences of Hamming weight d even if there is no pair of sequences $\mathbf{x}$ and $\hat{\mathbf{x}}$ from the codebook $\mathcal{X}$ giving this error sequence.

The rational behind the assumption A2 is that the conditional probability $\Pr(\Delta|d)$ remains approximately the same when it is computed over a larger space $\mathcal{E}_d$ instead of $\mathcal{E}_d(\mathcal{X})$ by considering that the elements of $\mathcal{E}_d(\mathcal{X})$ are randomly distributed over $\mathcal{E}_d$ due to the random interleaving assumption. Statistically speaking, $\mathcal{E}_d(\mathcal{X})$ is a representative subset of $\mathcal{E}_d$. This assumption seems to be more accurate for low value of d or a high-rate channel code for which the cardinality ratio between the extended space to the original space $|\mathcal{E}_d|/|\mathcal{E}_d(\mathcal{X})|$ is not too high.

Finally, by substitution (2.25) in (2.14), we obtain the expression of the upper bound

$$\boxed{P_{\mathrm{sub}}(\rho) = \sum_{\delta>0} \left(\sum_{d\geq d_{\min}} A^{\mathrm{c}}(d) \Pr(\Delta = \delta|d) \right) Q\left(\sqrt{\delta\rho/2}\right)} \tag{2.27}$$

In the following, we give some remarks about the evaluation of the code weight enumerator $A^{\mathrm{c}}(d)$ before moving in Section 2.3 to the main problem which is the determination of the conditional probability $\Pr(\Delta|d)$ over the extended space of error sequences $\mathcal{E}_d$.

2.2.3 Code weight enumerator

The evaluation of the channel code weight enumerator depends on the channel code type and the packet length N_b. Therefore, we present the evaluation of this term for trellis based codes such convolutional and turbo-codes with known output weight enumerators of error events, denoted by $a(d)$. For trellis based codes, an error event is an error path which diverges from the correct path at one trellis section and return later to the correct

path after multiple sections (see Figure 2.1). The length of the error event L_e is given by the number of trellis sections between the beginning and the end of the error event. The free distance of the code $d_{\min}$ is the minimum value of d for which $a(d) > 0$.

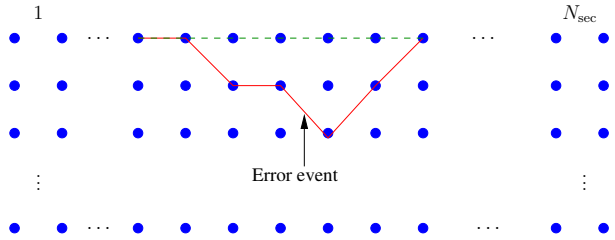

FIGURE 2.1: Error event in trellis-based codes.

An error sequence can be composed from multiple error events. Therefore, the code weight enumerator $A^c(d)$ can be computed by enumerating all possible combinations of error events which requires the knowledge of the output weight-length enumerators of error events for the considered error correcting code. This is actually a very complicated task. Since we are looking for an upper bound on the system performance, this task can be simplified as in [48] by upper bounding $A^c(d)$. The upper bound on $A^c(d)$ is obtained by considering that the length of any error event is only one section. Under this assumption, the enumeration of all possible combination of error events is given by

$$A^c(d) \leq \sum_{j=1}^{j_{max}} \binom{N_{\text{sec}}}{j} \sum_{\substack{d_1,\cdots,d_j \geq d_{\min} \\ d_1+\cdots+d_j=d}} a(d_1) \times \cdots \times a(d_j), \tag{2.28}$$

where N_{sec} is total number of sections in the trellis and $j_{max} = \lfloor d/d_{min} \rfloor$. This is actually a loose bound especially for high values of d. However, this can be improved by considering the particular code structure. For example, using a convolutional code with k input bits and n output bits at each trellis section, we have $N_{\text{sec}} = K_b/k = N_b/n$, assumed integer, and the length of an error event of weight d_k is at least $j_{\min} = \lceil d_k/n \rceil$.

2.3 Output Euclidean distance

In order to evaluate the conditional probability $\Pr(\Delta|d)$, we start by rewriting the expression of the OSED in a more compact and convenient form.

2.3.1 Formulation

The following Lemma gives the main mathematical formulation for the evaluation of the OSED in this thesis.

Lemma 1. *The OSED between two sequences at the output of noiseless frequency-selective channels of length L is given by*

$$\Delta(\mathbf{e}) = \sum_{\ell=-L+1}^{L-1} R_\ell^*(\mathbf{h}) R_\ell(\mathbf{e}) \tag{2.29}$$

where $R_\ell(\mathbf{x})$ is the periodic autocorrelation function of the sequence $\mathbf{x}$ for lag ℓ defined by

$$R_\ell(\mathbf{x}) \triangleq \sum_{n=0}^{N_s-1} x_n x_{n-\ell}^*, \tag{2.30}$$

where $R_\ell(\mathbf{h})$ is computed by zero padding of $\mathbf{h}$ up to length N_s.

Lemma 1 gives the OSED as the sum product between the autocorrelation functions of the channel and the error sequence. Due to the finite length of the channel L, only the first L autocorrelation coefficients of the error sequences are involved in the expression of the OSED.

Note: Lemma 1 is still valid for systems not using cyclic-prefix insertion by considering the aperiodic autocorrelation instead of the periodic definition.

Now, by separating the central term in the sum (2.29), we can rewrite the OSED as the sum of two variables as follows:

$$\Delta(\mathbf{e}, \mathbf{h}) = \Gamma(\mathbf{e}, \mathbf{h}) + \Lambda(\mathbf{e}, \mathbf{h}) \tag{2.31}$$

where we have explicitly shown the dependence on the channel response $\mathbf{h}$ for the sake of generality and future investigation for random channels. The two introduced variables are defined as follows

$$\Gamma(\mathbf{e}, \mathbf{h}) \triangleq R_0(\mathbf{h}) R_0(\mathbf{e}), \tag{2.32}$$

$$\Lambda(\mathbf{e}, \mathbf{h}) \triangleq 2\Re\left(\sum_{\ell=1}^{L-1} R_\ell^*(\mathbf{h}) R_\ell(\mathbf{e}) \right) \tag{2.33}$$

where $\Re(.)$ denotes the real part of a complex number. The first term Γ is the OSED over an equivalent ISI-free channel, whereas the second term Λ includes the effect of ISI on the Euclidean distance. We see that isolated error elements that are separated by more than L positions do not contribute to the interference term Λ. This actually the rational behind S-random interleavers which eliminate the effect of burst errors up to length S on the output Euclidean distance for frequency-selective channels.

In order to separate the channel gain effect from the ISI effect on the Euclidean distance, we rewrite (2.31) as the product of two **independent** random variables as follows

$$d_E^2(\mathbf{e}|\mathbf{h}) = \Gamma(\mathbf{e}, \mathbf{h}) \times \Theta(\mathbf{e}, \mathbf{h}), \tag{2.34}$$

where

$$\Theta(\mathbf{e}, \mathbf{h}) \triangleq 1 + \frac{\Lambda(\mathbf{e}, \mathbf{h})}{\Gamma(\mathbf{e}, \mathbf{h})} = 1 + 2\Re\left(\sum_{\ell=1}^{L-1} \tilde{R}_\ell^*(\mathbf{h}) \tilde{R}_\ell(\mathbf{e}) \right), \tag{2.35}$$

where $\tilde{R}_\ell(\cdot)$ denotes the normalized autocorrelation coefficients.
The independence between Γ and Θ can be seen intuitively since for a given value of the error amplitude $R_0(\mathbf{e})$, the variable $\tilde{R}_\ell(\mathbf{e})$ can take any value depending on the relative errors locations. The random variable Θ can be interpreted as an additional fading factor which quantifies the Euclidean distance fluctuations due to the selectivity of the channel. The formulation given in (2.34) is useful for the evaluation of the upper bound for time-varying channel as it will be seen later in this chapter.

Returning to the initial expression of Δ in (2.29), we see that for a given channel response, Δ is a weighted sum of related random variables $R_\ell(\mathbf{e})$. Therefore, the complete characterization of the output distance distribution over $\mathcal{E}_d$ requires the knowledge of the joint probability of the first L autocorrelation coefficients of the error sequence. Unfortunately, the joint probability density function is difficult to derive analytically in general [51]. Consequently, for instance the distribution of Δ can only be analytically assessed through an approximation. However, exact expressions for the main statistical characteristics of Δ including the mean and the variance, can be derived. These statistics are useful for the derivation of an approximated expression for the Euclidean distance distribution. Moreover, they provides a comprehensive indicator about the effect of system parameters on the Euclidean distance.

2.3.2 Main statistics of the output Euclidean distance

In order to compute the main statistics of Δ, we first need the statistics of the autocorrelation coefficients $R_\ell(\mathbf{e})$ which are announced by the following proposition.

Proposition 1 (Statistics of $R_\ell(\mathbf{e})$)**.** *Over the probability space $\mathcal{E}_d$, the mean of the random variable $R_\ell(\mathbf{e})$ is given by*

$$\mu(R_\ell(\mathbf{e})) = \begin{cases} N_s\mu_2 & \text{if } \ell = 0, \\ 0 & \text{if } 0 < \ell \leq L-1. \end{cases} \tag{2.36}$$

and the variance is given by

$$\sigma^2(R_\ell(\mathbf{e})) = \begin{cases} N_s\mu_4 + N_s(N_s-1)\varrho_2 - N_s^2\mu_2^2 & \text{if } \ell = 0, \\ N_s\varrho_2 & \text{if } 0 < \ell \leq L-1. \end{cases} \tag{2.37}$$

where

$$\mu_2 \triangleq E(|e_n|^2) = \binom{N_b}{d}^{-1} \sum_{k=1}^{Q} \binom{Q}{k}\binom{N_b-Q}{d-k} m_2(k) \tag{2.38}$$

$$\mu_4 \triangleq E(|e_n|^4) = \binom{N_b}{d}^{-1} \sum_{k=1}^{Q} \binom{Q}{k}\binom{N_b-Q}{d-k} m_4(k) \tag{2.39}$$

$$\varrho_2 \triangleq E(|e_{n_1}|^2|e_{n_2}|^2) = \binom{N_b}{d}^{-1} \sum_{\substack{k_1,k_2=1 \\ k_1+k_2\leq d}}^{Q} \binom{Q}{k_1}\binom{Q}{k_2}\binom{N_b-2Q}{d-k_1-k_2} m_2(k_1)m_2(k_2) \tag{2.40}$$

where $m_2(k) = E(|e_n|^2|d_H(e_n) = k)$ *and* $m_4(k) = E(|e_n|^4|d_H(e_n) = k)$ *are the conditional moments of error elements which can be both computed directly from the mapping scheme.*

In the following example, we evaluate these results for the case of BPSK modulation.

Example 2. For the BPSK mapping scheme $\mathcal{S} = \{-1, +1\}$ and $Q = 1$, we have $N_s = N_b$, $m_2 = 4$, and $m_4 = 16$. The expressions for μ_2, μ_4, and ϱ_2 simplify as follows

$$\mu_2 = 4\frac{d}{N_b} \tag{2.41}$$

$$\mu_4 = 16\frac{d}{N} \tag{2.42}$$

$$\varrho_2 = 16\frac{d(d-1)}{N_b(N_b-1)} \tag{2.43}$$

Substituting these values in (2.36) and (2.37), we obtain

$$\mu(R_\ell(\mathbf{e})) = \begin{cases} 4d & \text{if } \ell = 0, \\ 0 & \text{if } 0 < \ell \leq L-1. \end{cases} \tag{2.44}$$

and the variance is given by

$$\sigma^2(R_\ell(\mathbf{e})) = \begin{cases} 0 & \text{if } \ell = 0, \\ 16\frac{d(d-1)}{N_b-1} & \text{if } 0 < \ell \leq L-1. \end{cases} \tag{2.45}$$

We note that the out of phases autocorrelation coefficients ($\ell \neq 0$) of error sequences have the same mean and variance. Therefore, we can expect that they are identically distributed but, of course, not independent. Indeed, the autocorrelation $R_\ell(\mathbf{e})$ are identically distributed under uniform interleaving because for any value of $R_{\ell_1}(\mathbf{e})$, there is an interleaver π which can be applied on $\mathbf{e}$ such that $R_{\ell_2}(\pi(\mathbf{e}))$ takes the same value and this is for any for any $\ell_2 \neq \ell_1$.

An important statistical property of the autocorrelation coefficients of the error sequence which derives from the uniform interleaving and the independence between error sequences assumptions is the pairwise decorrelation which simplifies the derivation of the statistics of the OSED. This is shown by the following proposition

Proposition 2 (Decorrelation of $R_\ell(\mathbf{e})$)**.** *The ensemble of random variables* $\{R_\ell(\mathbf{e}) : \ell = 0, \cdots, L-1\}$ *are pairwise uncorrelated; i.e.* $E(R_{\ell_1}(\mathbf{e})R^*_{\ell_2}(\mathbf{e})) = 0$ *for* $\ell_1 \neq \ell_2$.

Now we are ready to announce the main statistics of the OSED which follows immediately from the results of Propositions 1 and 2.

Proposition 3 (Statistics of Δ)**.** *For a given channel response* $\mathbf{h}$*, the main statistics of the OSED are given by*

$$\mu(\Delta) = R_0(\mathbf{h})\mu(R_0(\mathbf{e})) \tag{2.46}$$

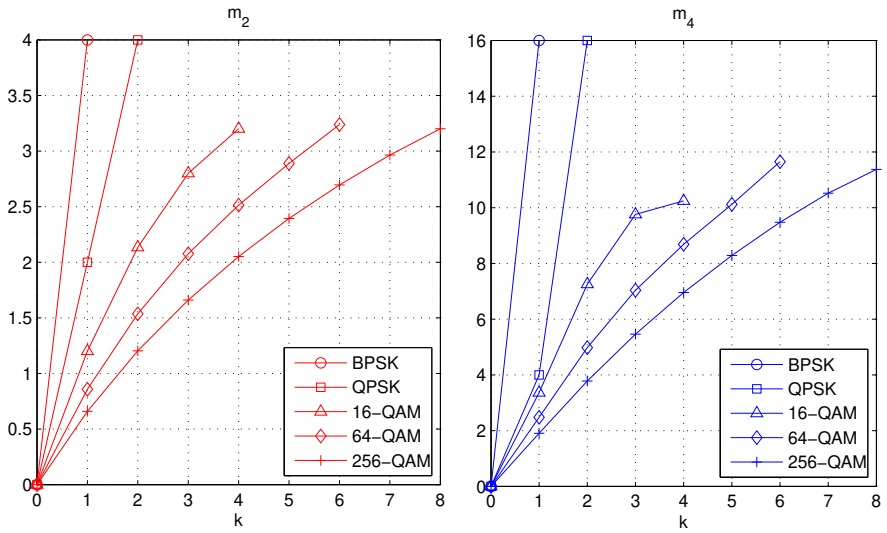

FIGURE 2.2: Error sequence statistics m_2 and m_4 for different modulation schemes with Gray mapping.

$$\sigma^2(\Delta) = |R_0(\mathbf{h})|^2\sigma^2(R_0(\mathbf{e})) + \kappa\sum_{\ell=1}^{L-1}|R_\ell(\mathbf{h})|^2\sigma^2(R_\ell(\mathbf{e})) \tag{2.47}$$

where $\kappa = 2$ *for complex symmetrical modulation (real and imaginary parts have the same statistics), and* $\kappa = 4$ *for real modulation and real channel response* $\mathbf{h}$*. The values of* $\mu(R_0(\mathbf{e}))$ *and* $\sigma^2(R_\ell(\mathbf{e}))$ *are given by Proposition 1.*

Example 3. Again, for BPSK modulation, the evaluation of the mean and the variance of the OSED using the results of Proposition 1 and Proposition 3 leads to

$$\mu(\Delta) = 4dR_0(\mathbf{h}) = 4d||\mathbf{h}||^2 \tag{2.48}$$

$$\sigma^2(\Delta) = 64\frac{d(d-1)}{N_b-1}\sum_{\ell=1}^{L-1}|R_\ell(\mathbf{h})|^2 \tag{2.49}$$

We remark that the variance of Δ is proportional to $1/N_b$ which explains the interleaving role in the reduction of the Euclidean distance fluctuation over a frequency selective channel. For a fixed value of d, the variance $\sigma^2(\Delta)$ tends to zero when N_b tends to the infinity. This explains the convergence of the ML performance to the AWGN case as it was already shown in [52] under an iterative detection and decoding approach.

The term $\sum_{\ell=1}^{L-1}|R_\ell(\mathbf{h})|^2$ gives the effect of the frequency selectivity on the fluctuation of the Euclidean distance. It can be expressed in the frequency-domain using Parseval's

theorem as

$$\sum_{\ell=1}^{L-1} |R_\ell(\mathbf{h})|^2 = \frac{1}{N_s} \sum_{n=0}^{N_s-1} (|\underline{h}_n|^2 - \mu(|\underline{h}_n|^2))^2 \tag{2.50}$$

where $\underline{h}_n = \sum_{k=0}^{N_s-1} h_k e^{-\frac{2\pi i}{N_s} kn}$ is the DFT of the channel response over N_s points, and $\mu(|\underline{h}_n|^2) = \frac{1}{N_s} \sum_{n=0}^{N_s-1} |\underline{h}_n|^2$. This the mean squared fluctuations of the squared channel response around the mean value in the frequency-domain. Obviously, for a flat channel, it is equal to zero.

After the determination of the main statistics of Δ, we look for the definition domain for the values of Δ and in particular the minimum output Euclidean distance. For simplicity, we assume in the following of this chapter a BPSK modulation with real channel response.

2.3.3 Minimum output Euclidean distance

Since the autocorrelation coefficients $R_\ell(\mathbf{e})$ take discrete values depending on the used modulation and the packet length N_s, the OSED takes also discrete values because the OSED is a linear function of the error autocorrelation coefficients. The minimum output Euclidean distance is a performance parameter which determines the asymptotic system performance for high SNR. For a given channel response, the minimum distance can be found by from the transfer function of the channel which determine the output weight distribution as in [11, 53]. Here, we propose an alternative approach based on the minimization of the determinant of the autocorrelation matrix of the error sequence assuming large sequence length N_s.

Let $\mathbf{R}_e = (R_0, \cdots, R_{L-1})$ denotes the L-uple vector formed by the first L autocorrelation coefficients. It is shown in [54] that attainable autocorrelation values for large block size lay within a convex region, denoted by V_R, which can be determined by noticing that the autocorrelation matrix M_L defined by

$$M_L = \begin{bmatrix} R_0 & R_1 & \cdots & R_{L-1} \\ R_1^* & R_0 & \ddots & \vdots \\ \vdots & \ddots & \ddots & R_1 \\ R_{L-1}^* & \cdots & R_1^* & R_0 \end{bmatrix}. \tag{2.51}$$

is a positive-definite matrix, i.e. $\det(M_L) > 0$. Mathematically, V_R is defined by

$$V_R \triangleq \{\mathbf{R}_e \in \mathbb{R}^L : \det(M_L) > 0\}. \tag{2.52}$$

For finite block length N_s, the region V_R is reduced as shown in [55].

The minimum free Euclidean distance at the output of the channel can be found by solving a minimization problem under constraints. Minimizing the OSED over valid autocorrelation values (V_R) gives the minimum Euclidean distance δ_{min}. Because the

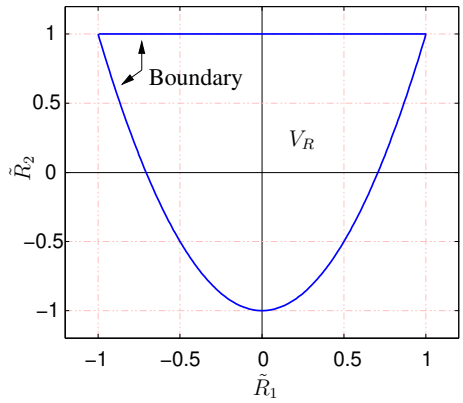

FIGURE 2.3: The region V_R of attainable values for R_1 and R_2.

Euclidean distance is a linear function of the autocorrelation coefficients, the minimum will be achieved at some point on the boundary region of valid autocorrelation values. The convexity of V_R ensure the convergence of the minimization algorithm to the actual minimum free distance of the channel.

We show this by an example. The channel response of the Proakis-B channel is $\mathbf{h} = (0.408, 0.817, 0.408)$ of length $L = 3$. The autocorrelation coefficients for positive lags are $R_0(\mathbf{h}) = 1$, $R_1(\mathbf{h}) = 0.666$ and $R_2(\mathbf{h}) = 0.166$. Then, the output Euclidean distance an be evaluated from (2.29) as,

$$\Delta = R_0 + 1.33R_1 + 0.33R_2. \tag{2.53}$$

The determinant of the autocorrelation matrix, expressed in terms of the normalized autocorrelation coefficients $\tilde{R}_\ell$, and it is given by

$$\det(M_3) = R_0^3(1 - \tilde{R}_2)(1 + \tilde{R}_2 - 2\tilde{R}_1^2). \tag{2.54}$$

The boundary region can be found by solving $\det(M_3) = 0$ which yields to following solution

$$\tilde{R}_2 = 2\tilde{R}_1^2 - 1, \quad \text{or} \quad \tilde{R}_2 = 1. \tag{2.55}$$

Figure 2.3 shows the corresponding boundary region.
Minimizing the Euclidean distance in (2.53) over all valid autocorrelation values with the constraints in (2.55) leads to the following solution

$$R_1 = -4(d-1) \text{ and } R_2 = 4(d-2) \tag{2.56}$$

for which we have $\delta_{min} = 2.66$ for any value of d. This minimum value is attained by any error sequence with consecutive error elements of alternating signs. This value determines the error floor on the FER performance in the system.

2.4 Performance over a static channel

As mentioned before, the determination of the Euclidean distance distribution requires the knowledge of the joint probability of autocorrelation coefficients. Let $P_d(\mathbf{R_e})$ be this joint probability of the autocorrelation vector $\mathbf{R_e}$ conditionally to the error Hamming weight d. Then, the conditional probability for the OSED can be calculated as

$$\Pr(\Delta = \delta | d) = \sum_{\mathbf{R_e} \in V_R : d_E^2 = \delta} P_d(\mathbf{R_e}) \tag{2.57}$$

Since the joint probability is difficult to be calculated, we resort to bounding techniques on the joint probability. The joint probability $P_d(\mathbf{R_e})$ can be upper bounded by Fréchet bound [56] given by the minimum of all marginal probabilities of auto-correlation coefficients.

$$P_d(\mathbf{R_e}) \leq \min\{\Pr(R_0), \cdots, \Pr(R_{L-1})\}, \tag{2.58}$$

for $\mathbf{R_e} \in V_R$ and zero otherwise. This bound is the best known bound on the joint probability if no other information is available about the joint probability.

The following proposition gives the marginal distribution for BPSK modulation.

Proposition 4. *For BPSK modulation, the marginal probability mass function (pmf) of the autocorrelation coefficients of the error sequences of Hamming weight d is given by*

$$\Pr(R_\ell(\mathbf{e}) = 4k) = \frac{1}{\binom{N_b-1}{d}} \sum_{s=|k|}^{d-1} 2^{-s} \binom{d-1}{s} \binom{N_b - d}{d-s} \binom{s}{\frac{s-k}{2}}. \tag{2.59}$$

For simple ISI channels with only two non-zero tap coefficients, as it is the case for some partial response channels, $\mathbf{h} = (h_0, 0, \cdots, 0, h_{L-1})$ for some $L > 1$ only a single autocorrelation R_{L-1} will be implied in the evaluation of the Euclidean distance. In this case, the corresponding marginal probability mass function, denoted by $\Pr(R_{L-1})$, determines the output Euclidean distance distribution of the channel. With this, we find the same results given in [49, 57] for the distance distribution of 2-taps channels with slight difference related to the cyclic prefix insertion.

By substituting the upper bound (2.58) in (2.57), we obtain an upper bound on the Euclidean distance distribution. Using the result on the expression of the union bound in from (2.27) we obtain the upper bound on the FER performance. In Figure 2.4, we show the computed upper bound for the Proakis-B channel. On the same figure, we traced the lower bound on code FER performance over AWGN channel given by

$$P_{\text{inf}}(\rho) = Q\left(\sqrt{d_{\min}\rho/2}\right) \tag{2.60}$$

which is also a lower bound on the coded system over any ISI channel. We compare obtained bounds to the simulated performance using a MAP turbo-equalizer with 5 turbo-iterations. The gap between the two bounds at medium SNR is about 1 dB, and

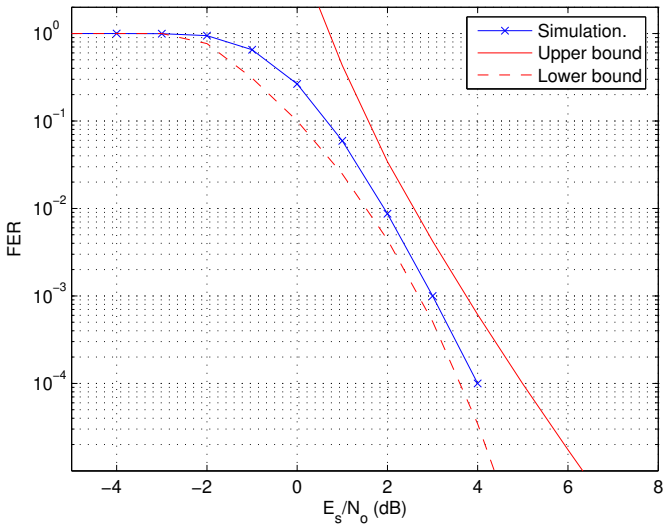

FIGURE 2.4: Bounds on FER performance for Proakis-B channel.

the upper bound diverges for at high SNR values. This is actually due to the loose bound on the joint probability. Further investigations for additional information about joint probability may result in a tighter upper bound. This remain an open problem for future research.

2.5 Performance over a time-varying channel

In this section, we consider the case of data transmission over a time-varying channel with uniform power-delay profile where the channel change independently from one transmission to the next. We aim to evaluate the upper bound on average FER performance over all possible channel realizations assuming BPSK modulation and a real channel response.

In order to determine the average Euclidean distance distribution, we consider the expression (2.34) for the OSED. Since the OSED is the product of two independent random variables Γ and Θ, we determine the distribution of Δ by finding the distribution of each variable. For BPSK modulation, we have $\Gamma = 4d||\mathbf{h}||^2$. The squared channel gain $||\mathbf{h}||^2$ follows a Gamma distribution with shape parameter $\alpha = L/2$ and scale parameter $\beta = 2/L$. Its probability density function (pdf) is given by

$$f_\Gamma(\gamma) = \frac{1}{\beta^\alpha \Gamma(\alpha)} \gamma^{\alpha-1} e^{-\gamma/\beta}, \tag{2.61}$$

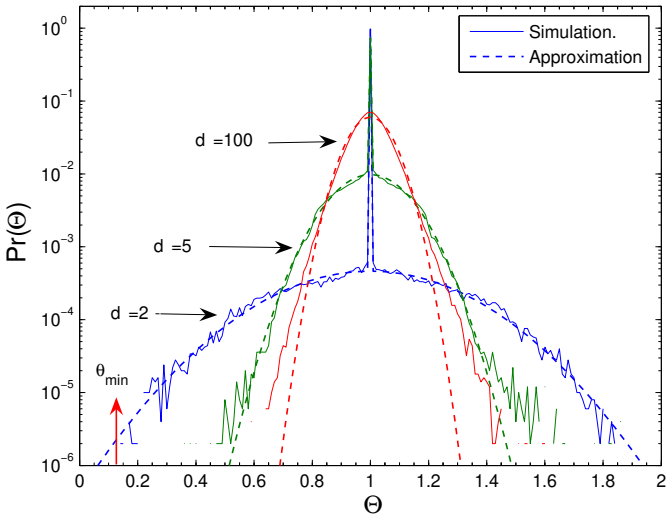

FIGURE 2.5: Distribution of the interference random variable Θ for $L = 5$, $N_b = 256$, and different values for d.

with mean and variance given by

$$\mu(R_0(\mathbf{h})) = \alpha\beta = 1, \quad \sigma^2(R_0(\mathbf{h})) = \alpha\beta^2 = \frac{2}{L}. \tag{2.62}$$

Now, the problem is the determination of the distribution of Θ which can be only assessed through an approximation. The first step in investigating the distribution of Θ is to determine its support. For normalized channel gain ($||\mathbf{h}||^2 = 1$), it is shown in [58] that the OSED is lower bounded by a certain minimum value $\delta_{\min}$ which depends on the channel length whatever was the channel response. This gives a lower bound on the interference variable $\Theta > \theta_{min} = \delta_{\min}/4d$.

Additional information about the shape of the distribution of Θ can be obtained by noticing that $\Theta = 1$ for all error sequences with isolated error elements separated by at least L positions regardless of the channel response, that is because $R_\ell(\mathbf{e})$ ($\ell > 0$) are identically zeros for these sequences. The probability of such sequences, denoted by P_z, forms a lower bound on the conditional probability $\Pr(\Theta = 1|d)$. We obtain by combinatorial enumerations the value of P_z is given by

$$\Pr(\Theta = 1|d) \geq P_z = \binom{N_b - (d-1)(L-1)}{d} \Big/ \binom{N_b}{d}. \tag{2.63}$$

which is a decreasing function of d. Numerically, for $N_b = 256$ and $L = 5$ we find $p_z = 0.97, 0.72, 0.21$ for $d = 2, 5, 10$, respectively.

We approximate the distribution of the remaining error sequences by a truncated Gaussian distribution for $\Theta > \theta_{\min}$ with the variance $\sigma^2_{ISI} = \sigma^2(\Theta)/(1 - P_z)$. Finally,

we deduce the conditional pdf of Θ:

$$f_\Theta(\theta) = P_0 \frac{1-P_z}{\sqrt{2\pi\sigma_{ISI}^2}} e^{-(\theta-1)^2/(2\sigma_{ISI}^2)} + P_z g(\theta-1),$$

where P_0 is a normalization factor due to the Gaussian truncation, and $g(x)$ is defined as $g(x) = 1$ for $x = 0$, and $g(x) = 0$ otherwise. Figure 2.5 shows the curve $f_\Theta(\theta)d\theta$ for $d\theta = 0.01$ compared with the simulated pdf over 10^6 error sequences and random channels with $L = 5$ for different values of d. From [58] (Table I), we have $\delta_{\min} = 0.2679$ for an error sequence of weight $d = 2$, which yields to $\theta_{\min} = 0.134$. We observe that our approximation is very close to the actual distribution for low values of d. For high error weights, the tail of the actual distribution decreases more slowly than the Gaussian tail and presents a slight asymmetry around the average. Using this approximation, we can now evaluate the upper bound on FER given in (2.27).

The upper bound can be rewritten using the new variables θ and γ as follows,

$$P_{sub}(\rho) = \int_\gamma \int_\theta \sum_d A^c(d) Q\left(\sqrt{2d\gamma\theta\rho}\right) f_\theta(\theta) f_\gamma(\gamma) d\theta d\gamma. \tag{2.64}$$

Because of the convexity of error function $Q(.)$, performing summation over d and limiting the obtained error probability by 1 before integration over channel statistics leads to a tight upper bound as noted by Malkamaki and Leib in [59]. Therefore, we evaluate the upper bound in two steps. First, we evaluate the average error probability over interference statistics for a fixed fading level as function of the instantaneous SNR $\rho' \triangleq \gamma\rho$,

$$P_{ISI}(\rho') = \int_0^\infty \left(\sum_d A^c(d) \frac{f_\Theta(t/d)}{d} \right) Q\left(\sqrt{2\rho' t}\right) dt, \tag{2.65}$$

where the change of variable $t = d\theta$ was used. Then we average obtained error probability over fading statistics after limiting error probability by 1 as follows

$$P_{sub}(\rho) = \int_0^\infty \min\left\{1, P_{ISI}(\rho')\right\} \frac{f_\gamma(\rho'/\rho)}{\rho} d\rho'.$$

Figure 2.6 shows the obtained upper bound for a rate 1/2 recursive, systematic convolutional (RSC) code with generator polynomial $(1, 5/7)_8$ in octal notation. The frame length is $N_b = 1204$ and the channel length is $L = 5$. Simulation results were obtained using a MAP turbo-equalizer after 5 iterations. The lower bound on FER shown in the same figure is the corresponding lower bound for a fading channel without ISI. We remark the obtained upper bound is within only 1 dB from the lower bound over all SNR range.

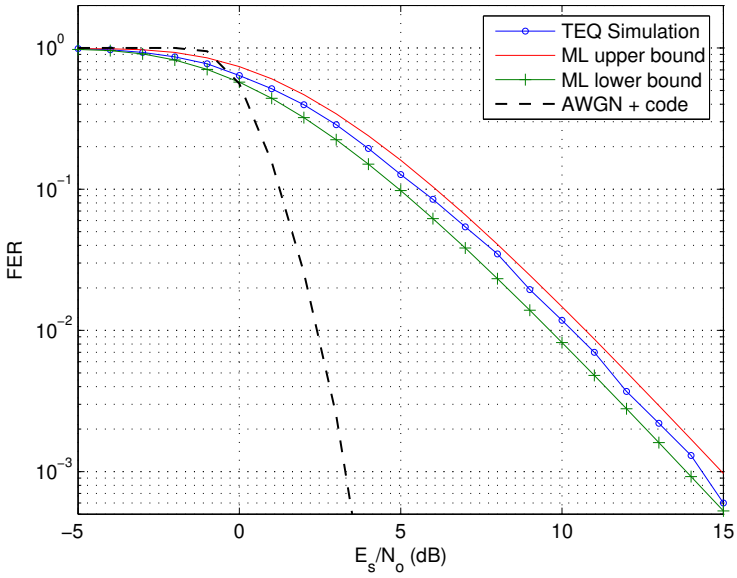

FIGURE 2.6: Upper and lower bounds on FER performance over random frequency-selective channel with $L = 5$, and $N_b = 1024$.

2.6 Euclidean distance for multiple HARQ transmissions

For multiple HARQ transmissions of the same packet, the OSED is accumulated. After the T-th HARQ transmission, the total OSED, denoted by Δ_T, is given by

$$\Delta_T = \sum_{t=1}^{T} \Delta^{(t)} = \sum_{t=1}^{T} \sum_{\ell=-L+1}^{L-1} R_\ell^*(\mathbf{h}^{(t)}) R_\ell(\mathbf{e}) \tag{2.66}$$

By interchanging the summation order, we get

$$\Delta_T = \sum_{\ell=-L+1}^{L-1} R_\ell(\mathbf{e}) \left(\sum_{t=1}^{T} R_\ell^*(\mathbf{h}^{(t)}) \right) = \sum_{\ell=-L+1}^{L-1} R_\ell(\mathbf{e}) \Omega_{T,\ell} \tag{2.67}$$

where we have defined

$$\Omega_{T,\ell} \triangleq \sum_{t=1}^{T} R_\ell^*(\mathbf{h}^{(t)}) \tag{2.68}$$

which gives the accumulated channel autocorrelations over T transmissions. This can be expressed, as in the case of a single transmission, as the sum of two variables

$$\Delta_T = \Gamma_T + \Lambda_T \tag{2.69}$$

where

$$\Gamma_T = R_0(\mathbf{e}) \Omega_{T,0} \tag{2.70}$$

$$\Lambda_T = 2\Re\left(\sum_{\ell=1}^{L-1} R_\ell(\mathbf{e})\Omega_{T,\ell}\right) \tag{2.71}$$

The obtained results for single transmission can be applied here by considering the equivalent channel autocorrelation $\Omega_{T,\ell}$ which reflects the channel diversity on the Euclidean distance. For the long-term static channel model where the channel change independently between transmissions, the relative impact of the interference term Λ_T in comparison with the gain term Γ_T becomes smaller while T increases due to the destructive effect of the summation over independent channel realization. For the long-term static channel model where $\mathbf{h}^{(T)} = \mathbf{h}^{(1)} \triangleq \mathbf{h}$, for $1 < T < T_{\max}$, we obtain

$$\Delta_T = T \times \Delta^{(1)} \tag{2.72}$$

which reflects the accumulated SNR gain but the relative impact of the interference remains the same as for a single transmission. Since the error sequence and the channel have a symmetrical effects on the Euclidean distance, this suggests introducing some transmit-diversity among subsequent HARQ transmissions in order to improve the system performance for slowly time-varying channels. Chapter 3 introduce a simple diversity scheme which compensate for the absence of channel diversity.

2.7 Conclusions

We presented in this chapter a new approach to evaluate the output Euclidean distance for a general frequency-selective channel. We have determined the main statistical characteristics of the output Euclidean distance including the mean and the variance. We investigated the system performance by the evaluation of the union bound based on the approximation of the Euclidean distance distribution at the output of the channel for static and random channels. For random channels, the average distance distribution can be well approximated by a truncated Gaussian distribution. The extension of this study to the CC-HARQ retransmissions is straightforward by considering the equivalent channel autocorrelation.

The complete characterization of the joint probability of the autocorrelation coefficients is still an open problem which need more investigation for better performance bound for static frequency-selective channels.

The results presented in this chapter have led to the following publications:

1. A. Assimi, C. Poulliat, and I. Fijalkow, "Distance distribution for turbo-equalized systems over static frequency-selective channels," in *IEEE Int. Conf. Acoust. Speech Signal Process. (ICASSP)*, Las Vegas, USA, March 2008, pp. 2949–2952.

2. A. Assimi, C. Poulliat, and I. Fijalkow, "Performance analysis of turbo-equalized systems over frequency-selective block-fading channels," in *Eur. Signal Process. Conf.(EUSIPCO)*, Lausanne, Switzerland, August 2008.

3. A. Assimi, C. Poulliat, and I. Fijalkow, "ARQ-hybride avec turbo-égalisation sur les canaux sélectifs en fréquence à évanouissements par bloc," in *Groupe de recherche et d'études du traitement du signal et des images (GRETSI)*, Troyes, France, September 2007, pp. 1145–1148.

In the next chapter, we propose a retransmission diversity scheme in order to improve HARQ performance for long-term static frequency-selective channels based on the Euclidean distance analysis developed in this chapter.

Chapter 3

Phase-Precoding Transmit Diversity

In this chapter, we present a simple and effective precoding technique to mitigate inter-symbol interference from multiple transmissions of the same packet in HARQ protocols over slowly time-varying frequency-selective channels. This technique can be used to compensate for poor channel diversity by modifying the signal form at each HARQ retransmission in such way that the channel appears to the receiver as time-variant which enhances the system performance.

3.1 Introduction

In order to combat the negative effects of the ISI on the performance of the communication system, advanced signal processing techniques have been introduced. When channel state information (CSI) is available at the transmitter, precoding (pre-equalization) techniques [60, 61] can be used in order to transform the ISI channel into an ISI-free channel. While in the absence of CSI at the transmitter, equalization techniques are usually used at the receiver to mitigate ISI from the received signal.

In the context of Chase combining HARQ protocol, channel equalization performance can be improved by performing joint equalization of all received copies of the same packet [45] compared with separate equalization followed by maximum-ratio-combining. When no channel diversity is available, as in long-term static channels for example, only an accumulated signal to noise ratio (SNR) gain can be expected after joint equalization. However, system performance can be improved by introducing some transmission diversity among subsequent HARQ transmissions. For example, a mapping diversity scheme was proposed in [62] to increase the Euclidean distance separation between transmitted packets. The drawback of this method is to be limited to high order modulations. Moreover, the optimized mapping depends on many parameters including the actual SNR and the variance of the log-likelihood ratios of the previously decoded packets. These parameters must be fed back to the transmitter resulting in an increased load on the feedback channel and additional memory requirements to store the optimized map-

pings for quantized values of these parameters. Another transmission diversity scheme is proposed in [63] using a different linear filter-based precoder for each transmission assuming that CSI is known by the transmitter.

In this chapter, we present a novel diversity scheme based on phase-precoding to combat the ISI in Chase combining HARQ protocols by changing the phases of the transmitted symbols at each HARQ transmission. An important key feature of this technique is that no CSI knowledge is assumed at the transmitter. We derive a performance criterion on the selection of precoding phases for an optimal maximum likelihood (ML) receiver. However, for a sub-optimal receiver, the obtained precoding gain in system performance is even more impressive. To exploit the introduced phase-precoding diversity, we present a low complexity joint soft-input soft-output (SISO) equalizer based on linear filtering under MMSE criterion. The SISO MMSE equalizer can be used in an iterative turbo-equalization scheme in order to approaches the performance of the optimal maximum likelihood receiver. However, we show that the performance gain due to the proposed phase-precoding diversity is even better for a linear receiver with separate equalization and decoding.

The main advantages of the proposed precoding technique are summarized by the following points:

- No CSI is required at the transmitter;
- It can be applied for any modulation order;
- It can be applied for coded or non-coded systems;
- It preserves power characteristics of the modulated signal;
- It provides a substantial performance gain without significant additional complexity.

This chapter is organized as follows. In Section 3.2, we introduce the system model and the proposed phase-precoding technique. In Section 3.3, we carry out an Euclidean distance analysis in order to define a suitable performance criterion for the selection of the precoding phases, and we present the proposed solution. In Section 3.5, we present the receiver structure using low complexity MMSE equalization that exploits the introduced phase-precoding diversity. In Section 3.6, we give some simulation results showing the efficiency of the proposed precoding technique.

3.2 Phase-precoded HARQ System

We consider the model of the communication system with retransmission diversity shown in Figure 3.1.

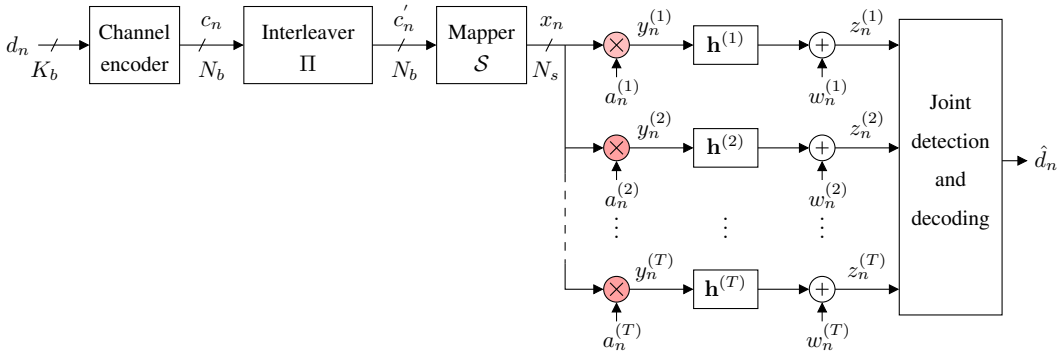

FIGURE 3.1: Phase-precoded HARQ system model.

A packet of K_b information bits $\mathbf{d} = (d_1 \cdots d_{K_b})$ are encoded by a rate-K_b/N_b error correction code to obtain a codeword $\mathbf{c} = (c_1 \cdots c_{N_b})$ of N_b coded bits. After a pseudo-random interleaver Π, the encoded bits are mapped into a sequence of symbols $\mathbf{x} = (x_1 \cdots x_{N_s})$ $(QN_s = N_b)$ using a complex modulation alphabet $\mathcal{S}$ of size $|\mathcal{S}| = 2^Q$ symbols with average power E_s assuming that all symbols are transmitted with equal probability. In each HARQ transmission, the same modulated symbol x_n is multiplied by a complex-valued precoding coefficient of unit amplitude $a_n^{(t)} = e^{j\phi_n^{(t)}}$ to obtain the precoded symbol $y_n^{(t)} = a_n^{(t)} x_n$, where t is the index of the HARQ transmission. The precoded symbols $y_n^{(t)}$ are then transmitted through a frequency-selective channel modeled by its equivalent complex-valued discrete-time finite impulse response of length L, denoted by $\mathbf{h}^{(t)} = (h_0^{(t)} \cdots h_{L-1}^{(t)})$ and assumed constant during each transmission but it may slightly vary from one HARQ transmission to the next.

The received sequence samples $z_n^{(t)}$ corresponding to the t-th HARQ transmission are modeled as

$$z_n^{(t)} = \sum_{i=0}^{L-1} h_i^{(t)} y_{n-i}^{(t)} + w_n^{(t)}, \; n = 0, \cdots, N_s - 1,$$

where $w_n^{(t)}$ is a complex Gaussian noise with variance $\sigma_w^2/2$ per real dimension. At the receiver, we consider a joint detection and decoding scheme assuming perfect CSI. At the current HARQ round T, the receiver estimates the transmitted packet from all received precoded versions of the modulated sequence $\mathbf{x}$. If the packet is still in error after a maximum number $T_{\max}$ of allowable transmissions, an error is declared and the packet is dropped out from the transmission buffer.

The first question we address is how to select the precoding coefficients $a_n^{(t)}$ in order to reduce the effect of the ISI on the frame error rate (FER) performance assuming that the channel does not change between subsequent HARQ transmissions. This is the subject of Section 3.3.

3.3 Euclidean distance analysis

In order to find out the best precoding coefficients, we carry out an Euclidean distance analysis assuming a joint ML receiver. From this analysis, we derive a performance criterion suitable for the choice of the precoding coefficients.

Let $\mathbf{x}$ and $\hat{\mathbf{x}}$ be the transmitted and the estimated sequence, respectively. Let $\mathbf{y}^{(t)}$ and $\hat{\mathbf{y}}^{(t)}$ be the corresponding precoded sequences at the t-th transmission. We define the following useful error sequences $\mathbf{e} \triangleq \hat{\mathbf{x}} - \mathbf{x}$ and $\tilde{\mathbf{e}}^{(t)} \triangleq \hat{\mathbf{y}}^{(t)} - \mathbf{y}^{(t)}$. After T HARQ transmissions, the Euclidean distance separation between $\mathbf{x}$ and $\hat{\mathbf{x}}$ at the output of noiseless ISI channel is evaluated as follows

$$\Delta_T = \sum_{t=1}^{T} \Delta^{(t)} = \sum_{t=1}^{T} \sum_{n=0}^{N_s-1} \left| \sum_{i=0}^{L-1} h_i^{(t)} \tilde{e}_{n-i}^{(t)} \right|^2 , \tag{3.1}$$

with $\tilde{e}_n^{(t)} = \hat{y}_n^{(t)} - y_n^{(t)} = a_n^{(t)} e_n$. We can rewrite d_E^2 as the sum of two terms as follows

$$\Delta_T = \Gamma_T + \Lambda_T, \tag{3.2}$$

with

$$\Gamma_T \triangleq \sum_{t=1}^{T} R_0^*(\mathbf{h}^{(t)}) R_0(\tilde{\mathbf{e}}^{(t)}), \tag{3.3}$$

$$\Lambda_T \triangleq 2\Re \left(\sum_{t=1}^{T} \sum_{\ell=1}^{L-1} R_\ell^*(\mathbf{h}^{(t)}) R_\ell(\tilde{\mathbf{e}}^{(t)}) \right), \tag{3.4}$$

Providing that $|a_n^{(t)}| = 1$, we have $R_0(\tilde{\mathbf{e}}^{(t)}) = R_0(\mathbf{e})$ which means that phase-precoding does not change the squared amplitude of the error sequence. Hence the variable Γ_T is invariant by phase-precoding. Consequently, phase-precoding does not change system performance over ISI-free channels. By contrast, the interference term Λ_T depends on the precoding coefficients through the autocorrelation function of the precoded error sequence $R_\ell(\tilde{\mathbf{e}}^{(t)})$. In order to minimize the effects of the ISI on the FER performance, we intend to minimize the interference variable Λ_T with respect to the precoding coefficients in the mean squared error sense. In other words, we minimize the variance of Λ_T for all error sequences leading to a fixed Euclidean distance over an ISI-free channel. To simplify our analysis, we consider the case of long-term quasi-static channels and we generalize our results to slowly time-varying channels through numerical simulations.

3.3.1 Performance criterion

In this section we derive a performance criterion for the selection of precoding coefficients. The performance criterion is based on the minimization of the variance of the output squared Euclidean distance.

In long-term quasi-static channel model, the channel does not change between subsequent HARQ transmissions of the same packet ($\mathbf{h}^{(1)} = \cdots = \mathbf{h}^{(T)} \triangleq \mathbf{h}$), but may change from packet to packet [32]. In this case, equation (3.4) reduces to

$$\Lambda_T = 2\Re\left(\sum_{\ell=1}^{L-1} R_\ell^*(\mathbf{h})\Sigma_{T,\ell}\right), \tag{3.5}$$

with

$$\Sigma_{T,\ell} \triangleq \sum_{t=1}^{T} R_\ell(\tilde{\mathbf{e}}^{(t)}) = \sum_{n=0}^{N_s-1} C_T(n,\ell) e_n^* e_{n+\ell}, \tag{3.6}$$

where

$$C_T(n,\ell) \triangleq \mathbf{a}_{T,n}^H \mathbf{a}_{T,n+\ell} = \sum_{t=1}^{T} (a_n^{(t)})^* a_{n+\ell}^{(t)}, \tag{3.7}$$

which is the cross-correlation between the precoding vectors $\mathbf{a}_n^{(T)}$ and $\mathbf{a}_{n+\ell}^{(T)}$ where $\mathbf{a}_n^{(T)} \triangleq [a_n^{(1)} \cdots a_n^{(T)}]^T$ denotes the vector obtained by regrouping the precoding coefficients of the same symbol x_n during the first T transmissions.

The main idea behind the proposed phase-precoding is to exploit the time diversity in order to separate different interfering paths by orthogonalization of adjacent symbols (within the channel memory L). The interference between L adjacent symbols can be assimilated to the interference between L users in a multiple access system. We can separate different symbols by allocating to each symbol a different orthogonal spreading code in the retransmission dimension. For complete interference mitigation, the code length (here the number of transmissions T) must be at least equal to L. In this particular case, a simple matched filter receiver can efficiently separate different paths without the need for equalization. However, allocating shorter spreading codes would reduce the interference level seen by each symbol. From the Euclidean distance point of view, two valid transmitted sequences having a low Euclidean distance in one transmission are remapped in the next transmission into two sequences with a high Euclidean distance, and vice-versa, in such a way that the overall Euclidean distance after combining is close to its value for an equivalent ISI-free channel. Mathematically, this is expressed by reduced variations of the interference term Λ_T in the Euclidean distance.

3.3.2 Cost function

We derive here an objective function on the precoding solution based on an upper bound on the variance of the interference variable Λ_T.

To continue our analysis, let $\mathcal{E}_\gamma$ be the ensemble of all error sequences $\mathbf{e}$ between pairs of non-precoded packets separated by a given squared Euclidean distance $\gamma = ||\mathbf{e}||^2$. We assume that the components of the error sequence e_n are modeled as complex-valued i.i.d. random variables with zero mean. This assumption is obviously verified for non-coded systems. For coded systems, the i.i.d. property is approximately verified

thanks to the uniform interleaver. Under this assumption, the interference term Λ_T is considered as a random variable over $\mathcal{E}_\gamma$ with zero mean. In order to determine an objective criterion on the choice of the precoding coefficients, we derive an upper bound on the variance of Λ_T. Then, we minimize the obtained upper bound with respect to the precoding coefficients. The squared value of Λ_T is upper bounded, using the inequality $\Re(x)^2 \leq |x|^2$, as

$$\Lambda_T^2 \leq 4 \left| \sum_{\ell=1}^{L-1} R_\ell^*(\mathbf{h}) \Sigma_{T,\ell} \right|^2 , \tag{3.8}$$

with equality for a real modulation alphabet and a real channel response. Under the i.i.d. assumption for error components, it can be easily shown from (3.6) that the random variables $\{\Sigma_{T,\ell} : \ell = 1, \cdots, L-1\}$ are pairwise uncorrelated. By developing the squared sum on the right-hand side of (3.8) and taking the expectation of both sides over $\mathcal{E}_\gamma$ we obtain

$$E(\Lambda_T^2) \leq 4 \sum_{\ell=1}^{L-1} |R_\ell(\mathbf{h})|^2 E(|\Sigma_{T,\ell}|^2), \tag{3.9}$$

where the expectation $E(|\Sigma_{T,\ell}|^2)$ can be evaluated from (3.6) as

$$E(|\Sigma_{T,\ell}|^2) = \sum_{n=0}^{N_s-1} |C_T(n,\ell)|^2 E(|e_n^* e_{n+\ell}|^2). \tag{3.10}$$

Note that the expectation $E(|e_n^* e_{n+\ell}|^2)$ is the variance of the product of two i.i.d. random variables with zero mean. Let σ_e^2 denotes the common variance of e_n. Consequently, we have $E(|e_n^* e_{n+\ell}|^2) = \sigma_e^4$ which is independent of n and ℓ, and therefore can be moved out of the sum in (3.10) as follows

$$E(|\Sigma_{T,\ell}|^2) = \sigma_e^4 \Psi_{T,\ell}(\mathbf{A}), \tag{3.11}$$

where $\mathbf{A}$ denotes the $T_{\max} \times N_s$ precoding matrix whose n-th column is the precoding vector $\mathbf{a}_{T_{\max},n}$, and

$$\Psi_{T,\ell}(\mathbf{A}) \triangleq \sum_{n=0}^{N_s-1} |C_T(n,\ell)|^2, \tag{3.12}$$

is the total squared cross-correlations between all precoding vectors separated by ℓ positions. By substituting (3.11) in (3.9), we obtain

$$E(\Lambda_T^2) \leq 4\sigma_e^4 \sum_{\ell=1}^{L-1} |R_\ell(\mathbf{h})|^2 \Psi_{T,\ell}(\mathbf{A}), \tag{3.13}$$

which is a weighted sum of the auto-correlation function of the channel indicating that the precoding vectors must be locally uncorrelated within the channel memory L, especially for lags with high channel auto-correlation. Since no CSI is assumed in this work,

we separate the effect of the precoding matrix by applying Cauchy-Schwartz inequality on the right-hand side of (3.13) to obtain an upper bound on the variance of Λ_T as

$$E(\Lambda_T^2) \leq 4\sigma_e^4 \left(\sum_{\ell=1}^{L-1} |R_\ell(\mathbf{h})|^4 \right)^{1/2} \left(\sum_{\ell=1}^{L-1} \Psi_{T,\ell}^2(\mathbf{A}) \right)^{1/2}. \tag{3.14}$$

That is only the last term in the upper bound (3.14) which depends on the precoding coefficients. Therefore, the minimization of the upper bound with respect to precoding coefficients is equivalent to the minimization of the following cost function

$$J_T(\mathbf{A}) = \left(\sum_{\ell=1}^{L-1} \Psi_{T,\ell}^2(\mathbf{A}) \right)^{1/2}. \tag{3.15}$$

Since the cost function is based on an upper bound on the variance of Λ_T, an optimal solution that minimizes the cost function does not necessarily minimize the variance for a given channel response. However, a variance reduction can be expected regardless of the channel realization. In the next section, we present some possible sub-optimal solutions for phase-precoding.

3.4 Precoding solution

Minimizing the cost function for a given value of T is a difficult multidimensional optimization problem due to the inter-dependency between the total cross-correlation variables $\Psi_{T,\ell}$. However, some general properties of the optimal solution are found by inspecting the minimum achievable value for the cost function. In fact, applying Cauchy-Schwartz inequality for sums of squares of real numbers $\left(\sum_{i=1}^N b_i\right)^2 \leq N \sum_{i=1}^N b_i^2$ on the expression of the cost function in (3.15) gives

$$J_T(\mathbf{A}) \geq \frac{1}{\sqrt{L-1}} \sum_{\ell=1}^{L-1} \Psi_{T,\ell}(\mathbf{A}) \triangleq \frac{S_T(\mathbf{A})}{\sqrt{L-1}}, \tag{3.16}$$

with equality *if and only if* $\Psi_{T,1}(\mathbf{A}) = \cdots = \Psi_{T,L-1}(\mathbf{A})$. Consequently, an ideal solution is a precoding matrix $\mathbf{A}$ which jointly verifies the two following properties:

1. Minimal total cross-correlation $S_T(\mathbf{A})$: This property ensures a maximum precoding gain in average for channels with uniform power-delay profile.
2. Uniform distribution for $\Psi_{T,\ell}(\mathbf{A})$ over lags: This property ensures that some precoding gain can be obtained for any particular channel realization.

Another difficulty arises from the fact that an optimal precoding solution which simultaneously minimizes the cost function for all $T \leq T_{\max}$ may not exist. In this case,

some minimization strategy has to be considered. For a particular choice of precoding coefficients, we consider the normalized value of the cost function by its value for the non-precoded system, denoted by G_T, as an *indicator factor* of the goodness of this choice. Hence

$$G_T(\mathbf{A}) \triangleq J_T(\mathbf{A})/J_T(\mathbf{1}), \tag{3.17}$$

where $\mathbf{1}$ is the $T_{\max} \times N_s$ matrix with all its elements are 1. The indicator factor takes its values in the interval $[0, 1]$. A smaller value of G_T indicates a better precoding solution.

By the following, we present two sub-optimal solutions, namely *random precoding* and *periodic precoding*. The random precoding solution satisfies the uniform cross-correlation distribution property, whereas the periodic precoding solution minimizes total cross-correlation $S_T(\mathbf{A})$.

3.4.1 Random precoding solution

For this solution, we select the precoding coefficients randomly from a finite alphabet $\mathcal{A} = \{e^{2j\pi k/K} : k = 0, \cdots, K-1\}$ consisting of K (for $K \geq 2$) complex numbers uniformly distributed over the unit circle. For large N_s, the value of $\Psi_{T,\ell}$ defined in (3.12) can be approximated as

$$\Psi_{T,\ell} \approx N_s E(|C_T(n,\ell)|^2) = N_s T,$$

where the expectation is taken over all possible random selections of the precoding vectors. It follows from (3.15) that

$$J_T(\mathbf{A}) \approx \sum_{\ell=1}^{L-1} N_s^2 T^2 = \sqrt{L-1} N_s T.$$

By substituting this value in (3.17), and providing that $J_T(\mathbf{1}) = \sqrt{L-1} N_s T^2$, we obtain an approximated value for the indicator factor given by

$$G_T(\mathbf{A}) = J_T(\mathbf{A})/J_T(\mathbf{1}) \approx \frac{\sqrt{L-1} N_s T}{\sqrt{L-1} N_s T^2} = \frac{1}{T},$$

indicating that the cost function for random precoding is T times lower than the non-precoded system. Next, we present a more structured precoding solution based on the minimization of S_T leading to better performance and lower implementation complexity.

3.4.2 Periodic precoding solution

To simplify the optimization problem and for equalization complexity reasons as it will be seen later in Section 3.5, we restrict ourselves to periodic precoding patterns of period $P \leq L$. Initially, let $P = L$. We construct the precoding matrix by selecting a set of L precoding vectors $\{\mathbf{v}_1, \cdots, \mathbf{v}_L\}$ of dimension $T_{\max}$. These vectors are periodically assigned to transmitted symbols, i.e. we assign to the symbol x_n the precoding

vector $\mathbf{v}_i$ where $i = n \bmod L$. We denote by $\mathbf{V}_L$ the $T_{\max} \times L$ matrix whose columns are the precoding vectors $\mathbf{v}_i$. For convenience, we assume the packet length N_s is an integer multiple of L. The precoding matrix $\mathbf{A}_L$ is obtained by N_s/L repetition of the generating matrix $\mathbf{V}_L$. In this case S_T can be written in a simpler form as

$$\begin{aligned} S_T(\mathbf{A}_L) &= \sum_{\ell=1}^{L-1} \sum_{n=0}^{N_s-1} |\mathbf{a}_{T,n}^H \mathbf{a}_{T,n+\ell}|^2 \\ &= \frac{N_s}{L} \sum_{i=1}^{L} \sum_{\substack{j=1 \\ j\neq i}}^{L} |\mathbf{v}_{T,i}^H \mathbf{v}_{T,j}|^2 \\ &= \frac{N_s}{L} \left(\mathrm{TSC}_T(\mathbf{V}_L) - LF^2\right) \end{aligned} \tag{3.18}$$

where $\mathrm{TSC}_T(\mathbf{V}_L)$ denotes the *total squared correlation* (TSC) of the set $\mathbf{V}_L$ taking only into the account the first T components of each vector and defined by

$$\mathrm{TSC}_T(\mathbf{V}_L) \triangleq \sum_{i=1}^{L} \sum_{j=1}^{L} |\mathbf{v}_{T,i}^H \mathbf{v}_{T,j}|^2, \tag{3.19}$$

which is extensively studied in the literature in the context of code division multiple access systems (see [64] and references therein). It is known that the TSC for a complex-valued set is lower bounded by Welch's bound [65] given by

$$\mathrm{TSC}_T(\mathbf{V}_L) \geq \begin{cases} LF^2 & \text{for} \quad T \geq L \\ L^2 F & \text{for} \quad T \leq L \end{cases} \tag{3.20}$$

This yields to a lower bound for S_T given by

$$S_T(\mathbf{A}_L) \geq \begin{cases} 0 & \text{for} \quad T \geq L \\ N_s T(L-T) & \text{for} \quad T \leq L \end{cases} \tag{3.21}$$

Combining (3.16), (3.17), and (3.21) leads to a lower bound for G_T under the periodic constraint as follows

$$G_T(\mathbf{A}_L) = \frac{J_T(\mathbf{A}_L)}{J_T(\mathbf{1})} \geq \frac{S_T(\mathbf{A})/\sqrt{L-1}}{J_T(\mathbf{1})} \geq \begin{cases} 0 & \text{for} \quad T \geq L \\ \frac{L-T}{(L-1)T} & \text{for} \quad T \leq L \end{cases} \tag{3.22}$$

We see that the indicator factor G_T is an increasing function with L, and for large values of L compared to T, the indicator factor tends to the value $1/T$ obtained with the random precoding solution.

3.4.2.1 Precoding period

We discuss here the dependence of the precoding period P on the channel length L and the consequence of choosing of a short period P.

In the case of a long channel, we show that limiting the period P to any integer divider of L will not change the value of the lower bound as long as $P \geq T_{\max}$. Let $L = mP + q$ for some positive integers m and q. Let $\mathbf{A}_P$ be the precoding matrix of period P and $\mathbf{V}_P$ be the corresponding generating matrix. We can evaluate S_T as

$$S_T(\mathbf{A}_P) = \underbrace{\sum_{\ell=1}^{mP-1} \sum_{n=0}^{N_s-1} |\mathbf{a}_{T,n}^H \mathbf{a}_{T,n+\ell}|^2}_{T_1} + \underbrace{\sum_{\ell=mP}^{L-1} \sum_{n=0}^{N_s-1} |\mathbf{a}_{T,n}^H \mathbf{a}_{T,n+\ell}|^2}_{T_2}$$

It can be shown in a similar manner to (18) that the first term T_1 can be expressed as

$$T_1 = \frac{N_s}{mP} \left(m^2 \mathrm{TSC}_T(\mathbf{V}_P) - mPT^2 \right)$$

When P is an integer divider of L (i.e. $q = 0$), the second term T_2 is zero and the achievable lower bound for $S_T(\mathbf{A}_P)$ is the same as for $S_T(\mathbf{A}_L)$ if $P \geq T$, because in this case, $m^2 \mathrm{TSC}_T(\mathbf{V}_P)$ and $\mathrm{TSC}_T(\mathbf{V}_L)$ have the same lower bound $m^2P^2F = L^2F$. When $q > 0$, we do not have an explicit lower bound on T_2, but its relative impact on the lower bound of $S_T(\mathbf{A}_P)$ is small when m is large. This explains that the system performance become less sensitive to the precoding period for a long channel response. In this case the precoding period can be taken equal to the maximum number of HARQ transmissions $T_{\max}$. In conclusion, for a known channel length, the precoding period can be chosen as the smallest value $P = L/m \geq T_{\max}$ without increasing S_T, and for unknown channel length, we can take $P = T_{\max}$ with some increase of S_T that vanishes with increasing values of L. The price to pay for reducing the precoding period is a non-uniform distribution of $\Psi_{T,\ell}$ (property 2) because $\Psi_{T,\ell}$ takes the same value as for a non precoded system for any value of ℓ which is multiple of P. In the worst case where all channel delays are multiple of P, no precoding gain can be expected. However, the probability of a such channel realization depends on the channel statistics and it is very small in general. In the case of a short channel length such that $L < P$, the precoding gain tends to zero when L tends to 1 which is natural because the channel becomes less frequency-selective. Therefore, P must be chosen as small as possible in order to take account for short channel realizations.

3.4.2.2 Proposed solution

Finding a set $\mathbf{V}_P$ which simultaneously meets Welch's bound in (3.20) with equality (WBE) for all T depends on the system parameters P, $T_{\max}$, and the precoding alphabet. For this purpose, we start by rewriting the TSC in (3.19) in a more convenient form. Let $\mathbf{u}_1, \cdots, \mathbf{u}_{T_{\max}}$ denote the rows of the precoding matrix $\mathbf{V}_P$. It follows from the row-column equivalence property of the TSC [66] that

$$\mathrm{TSC}_T(\mathbf{V}_P) = \sum_{i=1}^{T} \sum_{j=1}^{T} |\mathbf{u}_i \mathbf{u}_j^H|^2. \tag{3.23}$$

From this equivalence relationship, it was proved in [66] that the necessary and sufficient condition for a set to be WBE that the lines or the columns of the set are orthogonal. The advantage of using a WBE set is that the interference power is uniform across all received symbols. We distinguish two cases:

Case $P \geq T_{\max}$ This is usually the case because $T_{\max} \leq 4$ in most practical systems. The set $\mathbf{V}_P$ is a WBE set for all $T \leq T_{\max}$ if all vectors $\mathbf{u}_1, \cdots, \mathbf{u}_{T_{\max}}$ are orthogonal. These vectors could be taken for example from discrete Fourier transform (DFT) matrix of order P or more simply from Hadamard Matrix with bipolar alphabet of order P (when it exists).

Case $P < T_{\max}$ In this case, it is not possible to have a WBE set for all $T \leq T_{\max}$ because adding any $m < P$ vectors to a WBE set results in a set which has no longer the WBE property [64]. Therefore, some optimization strategy has to be considered. We consider in priority the minimization of the cost function at the early retransmissions. This enhances the throughput efficiency of the system. In fact, a WBE is still possible, at least for any $T \leq P$, by choosing $\mathbf{u}_1, \cdots, \mathbf{u}_P$ from orthogonal bases in $\mathbb{C}^P$. For $T > P$, we complete this set by periodical repetition of the previous vectors up to $T_{\max}$. Note that for $T \geq P$, the lower bound on G_T is zero. The proposed solution achieves this bound for any value of T which is integer multiple of P because we have a complete orthogonality between the column vectors. For these particular values of T, the interference is completely canceled.

Fourier-based solution: For example, in the case of $P > T_{\max}$, and as previously mentioned, the generating matrix $\mathbf{V}_P$ can be obtained by selecting $T_{\max}$ rows from the Fourier transform matrix of order P,

$$\mathbf{V}_P = \begin{bmatrix} 1 & e^{j\frac{2\pi}{P}p_1} & \cdots & e^{j\frac{2\pi}{P}(P-1)p_1} \\ 1 & e^{j\frac{2\pi}{P}p_2} & \cdots & e^{j\frac{2\pi}{P}(P-1)p_2} \\ \vdots & \vdots & \vdots & \vdots \\ 1 & e^{j\frac{2\pi}{P}p_{T_{\max}}} & \cdots & e^{j\frac{2\pi}{P}(P-1)p_{T_{\max}}} \end{bmatrix}, \tag{3.24}$$

where the $p_i \in [0, P-1]$ are the indexes of the selected rows. In this case, the phase-precoding of the t-th transmission is equivalent to a simple frequency shift of p_t/P. Of course, an arbitrary selection of rows leads to a WBE set, but the best selection is that which gives the most uniform distribution for $\Psi_{T,\ell}(\mathbf{V}_P)$. A very useful property of this structured solution is that the product between any two vectors depends only on the shift between them

$$\mathbf{v}_{T,i}^H \mathbf{v}_{T,i+\ell} = \sum_{t=1}^{T} e^{j2\pi p_t \ell/P}, \tag{3.25}$$

where the shift ℓ is taken modulo P. As it will been seen later, this property allows reducing the complexity of the receiver. Consequently, the total correlation can be

computed as

$$\Psi_{T,\ell}(\mathbf{V}_P) = N_s \left| \sum_{t=1}^{T} e^{j2\pi p_t \ell/P} \right|^2 , \ \ell = 1, \cdots, P-1 \tag{3.26}$$

which simplifies the evaluation of the cost function. An exhaustive search is performed to find an optimal selection of the DFT lines' indices $\{p_1, \cdots, p_{T_{\max}}\}$ that minimizes the cost function J_T simultaneously for $T = 2, \cdots, T_{\max}$. For example, we find for $T_{\max} = 4$ that a possible solution (which is not unique) is $\{0, 1, 2, 3\}$ for $P = 4$, $\{0, 2, 3, 1\}$ for $P = 5$, and $\{0, 3, 2, 6\}$ for $P = 8$.

Hadamard-based solution: In the previous analysis, we did not impose any constraint on the precoding phases. It is sometimes preferable for practical reasons to choose the precoding phases from a limited alphabet. We show in the following that the precoding alphabet has small impact on the precoding gain. The simplest form of phase-precoding is when the precoding alphabet is constrained to have bipolar values (± 1). For bipolar vectors, Welch's bound is only tight for vectors whose number is multiple of 4 and loose otherwise. In that case, we can use Hadamard matrix for the construction of the precoding matrix in the same manner as Fourier Matrix. In the frequency-domain this is equivalent to the superposition of two symmetrically shifted versions of the signal. In general, a tight bound on the TSC for bipolar vectors is given by Karystinos in [67] and can be used in order to find the corresponding lower bound on the reduction factor G_T. For example, for $P = L = 5$ and $T_{\max} = 4$, a direct application of Karystinos's lower bound to our case ([67] Table II, case $P \equiv 1 \bmod 2$) leads to

$$\mathrm{TSC}_T(\mathbf{V}_P) \geq P^2 F + (T-1)T,$$

and the lower bound on G_T becomes

$$G_T(\mathbf{A}_P) \geq \frac{P-T}{(P-1)T} + \frac{T-1}{P(P-1)T},$$

where the second term gives the relative increase of G_T compared to its value for a WBE set. Numerically, we obtain for a WBE set $G_T \geq 0.3750$, 0.1667, and 0.0625 for T =2, 3, and 4, respectively. Whereas, for a bipolar set meeting Karystinos's bound, we obtain $G_T \geq 0.4$, 0.2, and 0.1 for T =2, 3, and 4, respectively. We propose the following precoding generator matrix whose lines are quasi-orthogonal,

$$\mathbf{V}_5 = \begin{bmatrix} +1 & +1 & +1 & +1 & +1 \\ +1 & -1 & +1 & -1 & -1 \\ +1 & +1 & -1 & -1 & +1 \\ +1 & -1 & -1 & +1 & +1 \end{bmatrix}. \tag{3.27}$$

We can verify that the bipolar set $\mathbf{V}_5$ achieves Karystinos's lower bound as shown in Table 3.1 where we can see that the uniform distribution of $\Psi_{T,\ell}$ is only verified for $T = 4$. In this case the effective value of G_T meets its lower bound.

TABLE 3.1: Performance parameters of the precoding matrix $\mathbf{A}$ constructed from the bipolar set $\mathbf{V}_5$.

T ▼	$\Psi_{T,\ell}(\mathbf{A})/\Psi_{T,\ell}(\mathbf{1})$				$S_T(\mathbf{A})/S_T(\mathbf{1})$ ▼	G_T ▼
	$\ell=1$	$\ell=2$	$\ell=3$	$\ell=4$		
1	1.0	1.0	1.0	1.0	1.0	1.0
2	0.2	0.6	0.6	0.2	0.4	0.45
3	0.29	0.11	0.11	0.29	0.2	0.22
4	0.1	0.1	0.1	0.1	0.1	0.1

To show the effect of phase-precoding on the Euclidean distance spectrum, we have simulated the normalized squared Euclidean distance distribution $d_E^2/\Gamma_T = 1 + \Lambda_T/\Gamma_T$ for input error sequences with a fixed Hamming weight w. We assume that the non-zero error elements are uniformly distributed over the packet. We consider multiple HARQ transmissions over the Proakis-C ISI channel [22] of length $L = 5$ whose the impulse response is $\mathbf{h} = (0.227, 0.460, 0.688, 0.460, 0.227)$ using binary phase shift keying (BPSK) modulation and the precoding set $\mathbf{V}_5$ defined in (3.27) . Figure 3.2 shows simulation results over 10^4 packets with $N_b = 600$ and $w = 10$ for T =1, 2, 3, and 4. We remark spectrum thinning phenomena with relative variance reductions of 0.32, 0.23, and 0.10 for T =2, 3, and 4, respectively.

In order to exploits the introduced transmission diversity, all received copies of the same packet must be jointly processed by the receiver. To this end, we present in Section 3.5 the receiver structure for an iterative detection and decoding approach. The separate detection and decoding approach follows immediately as a particular case.

3.5 Receiver structure

At the receiver, we consider a joint turbo-equalizer as it is presented in 1.6.2.2 of Chapter 1. For low complexity requirements, we focus on MMSE-based equalization. We present two different schemes for the joint detector that differ in the way of performing the combining of the various received packets. The first performs joint-equalization, while the second performs LLR combining after separate equalization.

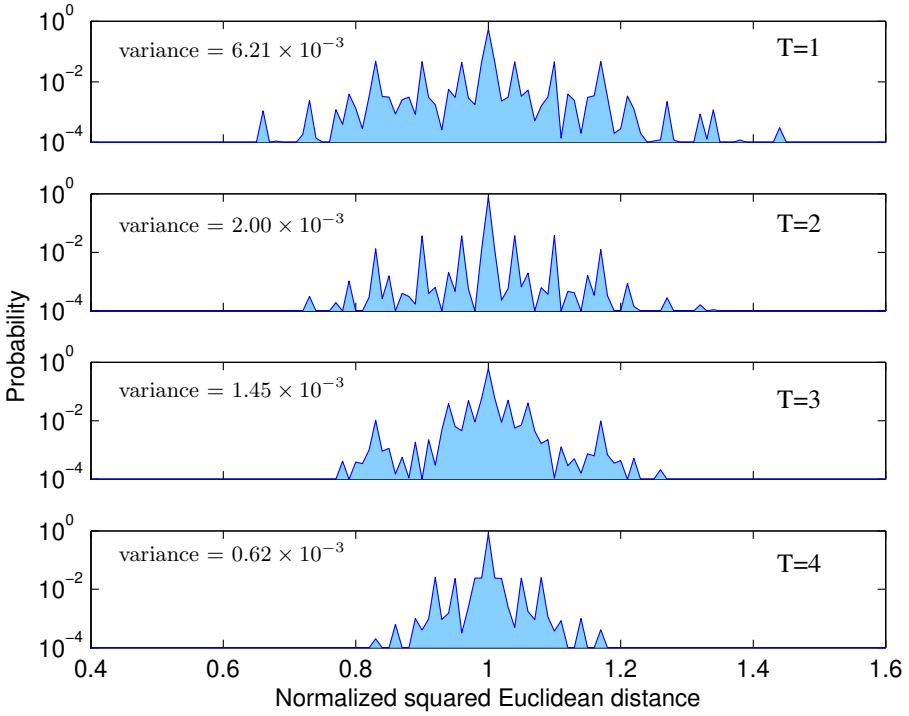

FIGURE 3.2: Normalized squared Euclidean distance distribution at the output of the Proakis-C ISI channel for input error sequences of length $N_b = 600$ of Hamming weight $w = 10$ using BPSK modulation and bipolar precoding alphabet for T =1,2,3 and 4.

3.5.1 Joint MMSE equalization

For each received sequence, the receiver performs the inverse precoding operation to obtain

$$\begin{aligned}\tilde{z}_n^{(t)} &= (a_n^{(t)})^* z_n^{(t)} \\ &= \sum_{i=0}^{L-1} (a_n^{(t)})^* h_i^{(t)} a_{n-i}^{(t)} x_{n-i} + (a_n^{(t)})^* w_n^{(t)} \\ &= \sum_{i=0}^{L-1} \tilde{h}_{n,i}^{(t)} x_{n-i} + \tilde{w}_n^{(t)}.\end{aligned}$$

By considering the phase-precoding as part of the ISI channel, the equivalent ISI channel becomes time-variant whose impulse response during the t-th transmission of the symbol x_n is given by

$$\tilde{h}_{n,i}^{(t)} \triangleq (a_n^{(t)})^* a_{n-i}^{(t)} h_i^{(t)}. \tag{3.28}$$

We generalize the finite length MMSE equalizer with *a priori* proposed in [40] to the case of precoded system. The joint SISO MMSE equalizer includes multiple forward

linear filters $\mathbf{f}_n^{(t)}$ and an interference canceller filter $\mathbf{b}_n$. The linear estimate $\hat{x}_n$ of the transmitted symbol x_n after T transmissions is given by

$$\hat{x}_n = \sum_{t=1}^{T} (\mathbf{f}_n^{(t)})^H \mathbf{z}_n^{(t)} - \mathbf{b}_n^H \bar{\mathbf{x}}_n, \tag{3.29}$$

where the superscript $(\cdot)^H$ denotes the hermitian transpose, $\mathbf{z}_n^{(t)} = [z_{n-l_2}^{(t)} \ \cdots \ z_{n+l_1}^{(t)}]^\top$ are the required observations samples around the estimated symbol. The forward filters $\mathbf{f}_n^{(t)}$ are implemented using $L_f = l_1 + l_2 + 1$ taps, where the parameters l_1 and l_2 specify the length of the non-causal and the causal part of the estimator filter, respectively. Note that we allow the filter coefficients to vary with n because of the variant-time equivalent channel model defined in (3.28), and not because we are looking for a time varying solution.

The problem of the joint equalization can be turned back to the case of a single transmission by considering the equivalent single-input multiple-output (SIMO) channel model given in matrix form by

$$\tilde{\mathbf{z}}_n = \tilde{\mathbf{H}}_n \mathbf{x}_n + \tilde{\mathbf{w}}_n,$$

where

$$\begin{aligned}
\mathbf{x}_n &= [x_{n-l_2-L+1} \ \cdots \ x_{n+l_1}]^\top, \\
\tilde{\mathbf{z}}_n &= [\tilde{z}_{n-l_2}^{(1)} \ \cdots \ \tilde{z}_{n-l_2}^{(T)} \ \cdots \ \tilde{z}_{n+l_1}^{(1)} \ \cdots \ \tilde{z}_{n+l_1}^{(T)}]^\top, \\
\tilde{\mathbf{w}}_n &= [\tilde{w}_{n-l_2}^{(1)} \ \cdots \ \tilde{w}_{n-l_2}^{(T)} \ \cdots \ \tilde{w}_{n+l_1}^{(1)} \ \cdots \ \tilde{w}_{n+l_1}^{(T)}]^\top,
\end{aligned}$$

and $\tilde{\mathbf{H}}_n$ is the $TL_f \times (L_f + L - 1)$ equivalent channel matrix given by

$$\tilde{\mathbf{H}}_n = \begin{bmatrix}
\tilde{\mathbf{h}}_{n-l_2,L-1}^{(T)} & \cdots & \tilde{\mathbf{h}}_{n-l_2,0}^{(T)} & & \mathbf{0} \\
& \ddots & & \ddots & \\
\mathbf{0} & & \tilde{\mathbf{h}}_{n+l_1,L-1}^{(T)} & \cdots & \tilde{\mathbf{h}}_{n+l_1,0}^{(T)}
\end{bmatrix} \tag{3.30}$$

where $\tilde{\mathbf{h}}_{n,\ell}^{(T)} = [\tilde{h}_{n,\ell}^{(1)} \cdots \ \tilde{h}_{n,\ell}^{(T)}]^\top$. The joint MMSE equalizer uses this equivalent channel matrix in order to detect the transmitted symbols.

3.5.2 Separate equalization with maximum-ratio-combining

Another alternative for packet combining with lower complexity is to use a separate equalizer for each transmission followed by maximum-ratio-combiner before the channel decoder. For each transmission, a SISO MMSE equalizer, as described in Section 3.5.1, with single input is used to detect the precoded sequence $y_n^{(t)}$. Then, the inverse precoding operation is performed after the equalizer by $\hat{x}_n^{(t)} = (a_n^{(t)})^* \hat{y}_n^{(t)}$. The various estimated sequences $\hat{x}_n^{(t)}$ in all transmissions are then combined by a maximum-ratio-combiner operating at the bit level after the soft demapper [46]. At each retransmission,

the combiner simply accumulates the extrinsic LLRs $L_e(\mathbf{c}')$ which are de-interleaved and decoded. This type of combining has in general lower performance than joint equalization, but the performance loss is not very important when the residual interferences in the combined signals are uncorrelated. Thanks to the phase-precoding, the non-correlation property is approximately verified. The main advantage of this solution is to be independent of the precoding solution and its period. This resolves the problem of the dependency between the system complexity and the precoding period encountered by the joint equalizer.

It is important to note that the precoding gain results from packet combining and not from the iterative structure of the equalizer. Actually, the phase-precoding decorrelates the ISI among the different received copies in order to add destructively after combining. Consequently, the role of the proposed phase-precoding is to help the equalizer in its task by removing a part of the ISI. This enhances the overall performance for a non-iterative detection approach. Using a powerful detection scheme as a turbo-equalizer could be sufficient alone without the help the phase-precoding in order to remove the interference, but this may require many turbo-iterations. In this case the use of the phase-precoding technique reduces the number of turbo-iterations which are required by the turbo-equalizer to converge.

3.5.3 Complexity issues

We discuss now the required additional complexity due to the phase-precoding in comparison with the non-precoded system. In the case of the JE scheme, the complexity of the MMSE equalizer itself per transmission is mainly dominated by the inversion of the matrix $(\sigma_w^2\mathbf{I}+v^2\tilde{\mathbf{H}}_n\tilde{\mathbf{H}}_n^H)$ which grows linearly with the number of HARQ transmissions. Since the phase-precoding transforms the ISI channel into a time-variant channel, one matrix inversion is required for each symbol in the frame. Therefore, the complexity of the receiver is highly increased. This is true in general for a non-structured phase-precoding solution like a random phase-precoding. By contrast, for a periodic precoding solution with period P, the required number of matrix inversions is reduced to only P inversions. As we have seen in section 3.4.2 that the period value can be chosen as small as $\min(L, T_{\max})$, this significantly reduces the additional complexity. In addition, by using the periodic precoding solution based on the DFT matrix, only one matrix inversion is required because the equivalent channel is actually invariant with n. This results from the particular structure of the precoding coefficients where

$$\tilde{h}_{n,i}^{(t)} = (a_n^{(t)})^* a_{n-i}^{(t)} h_i^{(t)} = e^{-j2\pi\frac{i}{P}p_t} h_i^{(t)}. \tag{3.31}$$

In the case of the SE-MRC scheme, the additional complexity is reduced to complex multiplications at the receiver for any phase-precoding solution. Moreover, with a bipolar precoding, the precoding operation and its inverse reduce to simple sign inversion operations.

Finally, in the case of a long channel response, the complexity of the time-domain MMSE equalizer [68] becomes very high due to the large dimension of the channel

matrix. It would be interesting to perform the equalization in the frequency-domain with a cyclic-prefix insertion at the transmitter. In this case, the DFT-based precoding turns into a simple cyclic shift in the frequency-domain as shown in the next sub-section.

3.5.4 Simple frequency-domain implementation

In the frequency-domain, the DFT based solution is equivalent to a simple circular frequency shift. Therefore, the implementation of this solution in the frequency-domain reduces to a simple frequency shift which practically has no significant additional complexity. The receiver structure is shown in Fig. 3.3. For each received frame $\mathbf{y}^{(f)}$, the

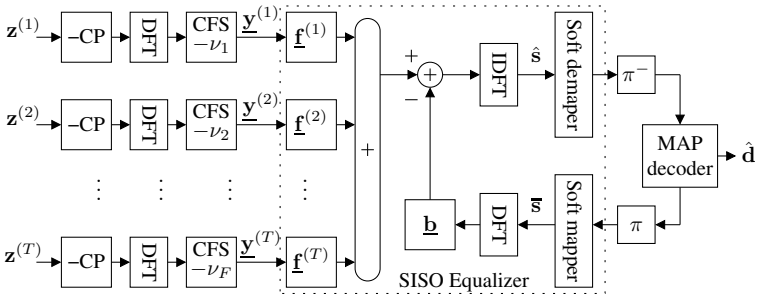

FIGURE 3.3: Receiver structure for the DFT-based PPD solution.

CP is first removed and then a DFT is applied in order to perform equalization in the frequency domain. In the following, the DFT of a signal vector $\mathbf{x}$ is denoted by $\underline{\mathbf{x}}$. Thanks to the cyclic prefix insertion, the time domain convolution becomes a simple multiplication in the frequency domain. The received frame can be written as

$$\underline{\mathbf{z}}^{(t)}[n] = \underline{\mathbf{h}}^{(t)}[n]\underline{\mathbf{x}}^{(t)}[n] + \underline{\mathbf{w}}^{(t)}[n]. \tag{3.32}$$

The inverse frequency shift is performed on $\underline{\mathbf{z}}^{(t)}$ to obtain $\underline{\mathbf{y}}^{(t)}$. Since $\underline{\mathbf{x}}^{(f)}[n] = \underline{\mathbf{x}}[n+n_t]$ where n_t is the index which corresponds to the frequency shift $\nu^{(t)} = n_t/N_s$ and $n+n_t$ is computed modulo N_s, we can write $\underline{\mathbf{y}}^{(f)}$ as

$$\begin{aligned}\underline{\mathbf{y}}^{(t)}[n] &= \underline{\mathbf{z}}^{(t)}[n-n_t] \\ &= \underline{\mathbf{h}}^{(t)}[n-n_t]\underline{\mathbf{x}}[n] + \underline{\mathbf{w}}^{(t)}[n-n_t] \\ &= \tilde{\underline{\mathbf{h}}}^{(t)}[n]\underline{\mathbf{x}}[n] + \underline{\tilde{\mathbf{w}}}^{(t)}[n].\end{aligned} \tag{3.33}$$

The signals $\underline{\mathbf{y}}^{(t)}$ for $t = 1, \cdots, T$ are then processed by a joint turbo-equalizer using the equivalent channels $\tilde{\underline{\mathbf{h}}}^{(t)}$. The linear estimate $\hat{\mathbf{x}}$ of $\mathbf{x}$ after T transmissions is given in the frequency-domain by

$$\hat{\underline{\mathbf{x}}} = \sum_{t=1}^{T} \underline{\mathbf{f}}^{(t)}\underline{\mathbf{z}}^{(t)} - \underline{\mathbf{b}}\,\bar{\underline{\mathbf{x}}} \tag{3.34}$$

As in [69, 70] and using the equivalent SIMO model, the derivation of the MMSE filters are given by

$$\underline{\mathbf{f}}^{(f)} = \frac{(\underline{\tilde{\mathbf{h}}}^{(t)})^*}{\sigma_w^2 + vH_T^2} \tag{3.35}$$

$$\underline{\mathbf{b}} = \sum_{t=1}^{T} \underline{\mathbf{f}}^{(t)} \underline{\tilde{\mathbf{h}}}^{(t)} - \mu \tag{3.36}$$

where $H_T^2 = \sum_{t=1}^{T} |\underline{\tilde{\mathbf{h}}}^{(t)}|^2$ is the squared compound channel.

With regard to the system complexity, we need only N_s additional complex multiplications at the transmitter and a simple vector shift operation at the receiver. In addition, the complexity of the joint MMSE equalizer in the frequency-domain is almost the same as for an MMSE equalizer with a single input. To show that, we note that the numerator of each forward filter $\underline{\mathbf{f}}^{(t)}$ is the matched filter to the channel which does not change across turbo-iterations. Hence, it is performed once per transmission. The denominator is common between all forward filters and the division can be performed after summation of the matched filters output. Consequently, for each new reception, the accumulated sum of the matched filters is updated and so the squared compound channel. Other operations are the same as for an equalizer with a single input.

3.6 Numerical results

In order to illustrate the effectiveness of the proposed phase-precoding diversity for HARQ transmissions, we present in the following some simulation results using different system configurations. In the presented simulations, we use a rate-1/2 recursive systematic convolutional code whose generator polynomial is $(1, 21/37)$ in octal notations. A maximum of $T_{\max} = 4$ HARQ transmissions is assumed. We evaluate the system performance by Monte-Carlo simulations versus the average SNR defined as $E_s/N_0 = E_s/\sigma_w^2$. Simulations were performed over a maximum of 10^4 packets.

In order to compare the performance of the precoded system to the performance of the non-precoded system under the two proposed detection schemes without turbo-iteration, we first consider a communication system using BPSK modulation over the Proakis-C channel, which is a highly frequency-selective static channel. Since both of the channel response and the modulation alphabet are real, we use the Hadamard-based precoding solution of period $P = L = 5$. This prohibits the exploitation of the imaginary dimension. The MMSE equalizer is implemented using linear filters of length $L_f = 15$ ($l_1 = 9$, $l_2 = 5$). Figure 3.4 shows the corresponding FER performance.

For the first transmission, the FER performance of the precoded system are the same as for the non-precoded system because phase-precoding does not offer any advantage for a single transmission. For the following retransmissions, a noticeable gain can be observed for both combining schemes. Moreover, the performance of the precoded

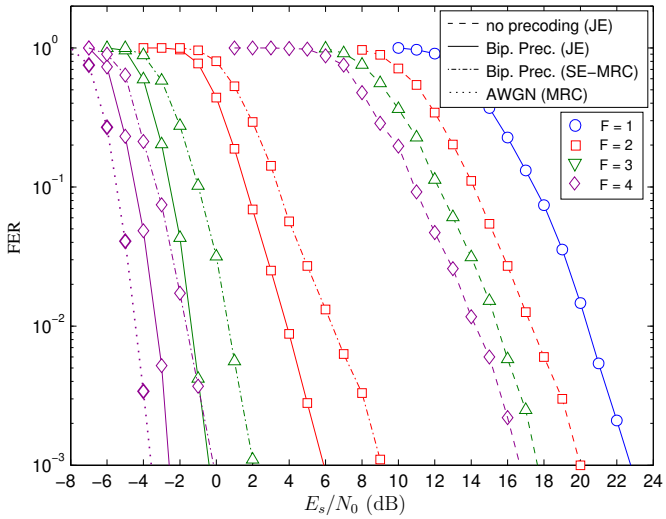

FIGURE 3.4: FER performance of the precoded HARQ system over the Proakis-C frequency-selective channel using BPSK modulation and joint MMSE equalization without turbo-iteration.

system for $T = 4$ are close to the system performance over AWGN channel. This indicates that ISI is efficiently removed from the last retransmission resulting in a better dropping rate in the HARQ protocol. We can see clearly that the performance loss of the SE-MRC combining scheme in comparison with the JE scheme is small when compared to the precoding gain.

Now, we consider the transmission system using QPSK modulation with Gray mapping over a random frequency-selective channel with uniform power-delay profile. The channel changes independently from one packet to the next, but stays correlated between successive HARQ retransmissions of the same packet. The correlation coefficient α between two subsequent HARQ transmissions is given according to Jakes' model [35] by $\alpha = J_0(2\pi f_d \tau)$, where $J_0(\cdot)$ is the zero-order Bessel function of the first kind, f_d denotes the maximum Doppler frequency, and τ is the time delay between two subsequent HARQ transmissions. In our simulations, the channel is normalized to unit energy as in [45, 62] in order to evaluate the effect of ISI on system performance independently of the fading distribution. However, a realistic simulations without normalization are given at the end of this section.

Figure 3.5 compares between a DFT-precoding solution of period $P = L$ and a random precoding solution for $f_d = 0$ ($\alpha = 1$). As predicted by our analysis, we can see that the advantage of the DFT precoding with the increasing number of retransmissions. We have found that the performance of the bipolar precoding (not shown on the figure) are only 0.2 dB behind the performance of the DFT precoding reflecting the small effect of the precoding alphabet. By comparing the slope of the FER curve between the

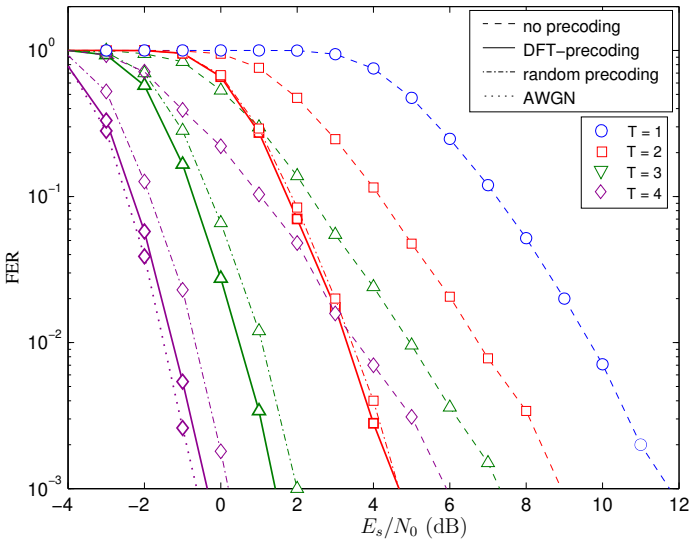

FIGURE 3.5: FER performance of the precoded HARQ system over long-term quasi-static frequency-selective channel ($\alpha = 1$) using QPSK modulation. The receiver was implemented using the joint equalization scheme without turbo-iteration.

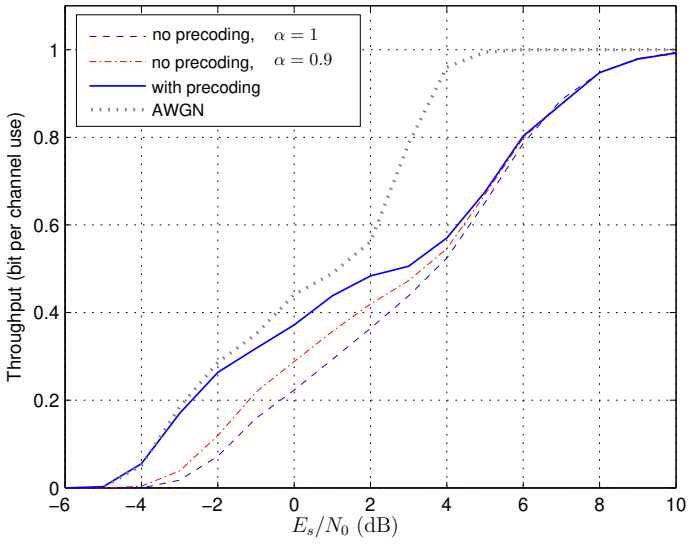

FIGURE 3.6: Throughput of precoded HARQ system over correlated frequency-selective channels for various values of channel correlation coefficient α using the DFT-based precoding solution of period $P = 4$ and QPSK modulation.

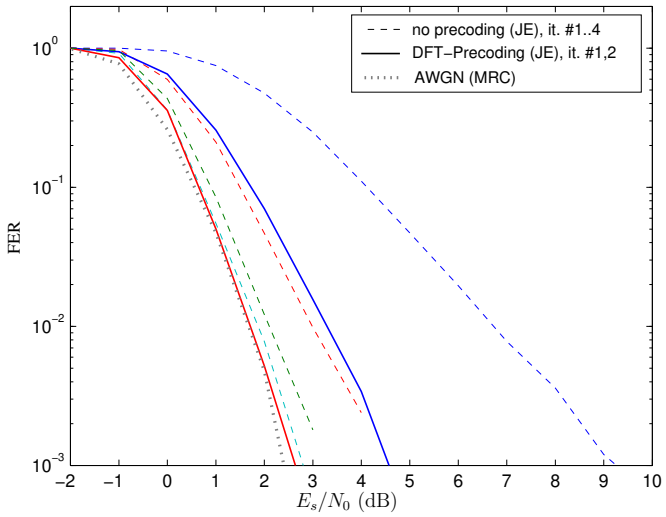

FIGURE 3.7: Convergence behavior of the MMSE turbo-equalizer for the precoded HARQ system over a long-term quasi-static frequency-selective channel using the DFT-based precoding solution of period $P = 4$ and QPSK modulation.

precoded and the non-precoded scheme, we observe a diversity gain due to the precoding technique.

Figure 3.6 shows the corresponding data throughput of the HARQ system for $f_d\tau = 0$ and $f_d\tau = 0.1$ ($\alpha = 0.9$). We have found by simulation that the throughput of the precoded system stays practically unchanged for all values of α. We note that the throughput performance for low to medium SNR values are the same as for AWGN channel. For high SNR values the throughput is essentially dominated by the FER of the first transmission, hence there is no significant improvement in comparison with non-precoded system.

In addition to the performance gain, the proposed phase-precoding technique improve the convergence behavior when turbo-equalization scheme is used. Fig 3.7 shows the FER at each turbo-iteration for the case of two HARQ transmissions ($T = 2$). We note that the convergence of the turbo-equalizer for the precoded system is faster than for the non-precoded system thanks to the reduced interference power. The non-precoded system needs more than four turbo-iterations to converge, while only two turbo-iterations are required when using phase-precoding.

Finally, we consider a more realistic channel model based on the the 3GPP Spatial Channel Model Extended (SCME). For each transmitted packet, a random channel realization is generated and used for all HARQ transmissions of the packet. Note that we do not normalize the channel in this case for a more realistic gain evaluation. Other simulation parameters are taken from the 3GPP LTE (Long-Term-Evolution)

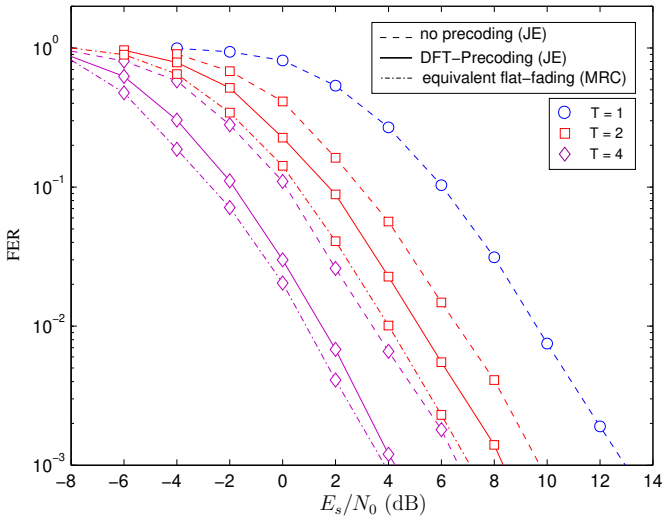

FIGURE 3.8: Phase-precoding performance over the SCME channel model using the DFT-based precoding solution with period $P = 4$.

standard [8, 28, 19]. The transmission speed is $Fs = 7.68$ MSPS, $N_s = 512$ and the maximum channel delay spread is $L_{\max} = 128$ symbols. Since the channel length is unknown we choose the precoding period $P = T_{\max}$. Due to the long channel memory, the equalizer was implemented in the frequency-domain thanks to cyclic prefix insertion at the transmitter. Fig 3.8, shows the obtained results where about 2 dB of gain is obtained by phase-precoding at the fourth transmission.

3.7 Conclusions

We presented in this chapter an efficient phase-precoding technique to mitigate inter-symbol interference from multiple HARQ transmissions over slowly time-varying frequency-selective channels. The introduced phase-precoding technique can be viewed as a transmission diversity technique to combat the channel selectivity in the frequency-domain. A general framework was introduced assuming no CSI is available at the transmitter to find a performance criterion on the precoding coefficients. We proposed an efficient periodic precoding solution leading to a significant gain in FER performance without any significant increase in receiver complexity. The effect of the precoding period and the precoding alphabet and on the precoding gain were investigated. When a turbo-equalization scheme is used at the receiver, the proposed technique allows a faster convergence resulting in a reduced overall complexity. Finally, for a specific channel model with known auto-correlation statistics, phase-precoding technique can further be optimized to enhance system performance.

The results presented in this chapter have led to the following publications:

1. A. Assimi, C. Poulliat, and I. Fijalkow, "Phase-precoding without CSI for packet retransmissions over frequency-selective channels," *Accepted to IEEE Trans. Commun.*, 2009.

2. A. Assimi, C. Poulliat, I. Fijalkow, and D. Declercq, "Periodic Hadamard phase precoding for HARQ systems over intersymbol interference channels,"(*Invited paper*) in *Int. Symp. on Spread Spectrum Techniques and Applications (ISSSTA)*, Bologna, Italy, August 2008, pp. 714 –718.

3. A. Assimi, C. Poulliat, and I. Fijalkow, "Phase precoding with integrated turbo-equalization for packet retransmissions," in *IEEE Int. Symp. Pers., Indoor Mob. Radio Commun.(PIMRC)*, Cannes, France, September 2008.

4. A. Assimi, C. Poulliat, and I. Fijalkow, "On cyclic frequency diversity for single-carrier packet retransmissions," in *IEEE Int. Symp. Inf. Theory*, Seoul, Korea, June 2009.

In the next chapter, we study another transmit-diversity scheme for HARQ retransmissions and we compare its performance with the performance of the PPD diversity scheme.

Chapter 4

Bit-Interleaving Transmit-Diversity

BIT-INTERLEAVING transmit-diversity, is another diversity technique which exploits the available time-diversity in Chase combining HARQ protocols. In this chapter, we first show by Euclidean distance analysis the good potential of this diversity scheme which can be exploited by an appropriate choice of the receiver. Then we compare the performance of this diversity scheme with the performance of the phase-precoding diversity scheme which was presented in the previous chapter. Finally, we extend the use of this scheme for MIMO frequency-selective channels.

4.1 Introduction

Inspired from the turbo-coding scheme [23], the bit-interleaving diversity (BID) scheme as shown in Figure 4.1 was initially introduced in [71] for uncoded ARQ transmissions over frequency-selective channels using a different interleaver at each ARQ retransmission in order to form a parallel concatenated system. At the receiver, multiple MAP equalizers are used in iterative manner in order to detect the transmitted symbols. The same scheme was proposed in [72] by replacing the MAP equalizer with an MMSE equalizer. This scheme was enhanced later in [73] by introducing a binary precoder before the frequency-selective channel in order to transform the linear channel into a recursive channel. More recently, similar iterative equalization strategy including channel coding was proposed in [74] for turbo-equalization.

For coded systems, it was shown by Samra and Ding in [45], in the context of CC-HARQ transmissions, using a BPSK modulation and MAP equalization, that joint turbo-equalization of identically interleaved coded transmissions outperforms the bit-interleaving diversity scheme with iterative equalization.

In the first part of this chapter, we show that this is not due to the limitation of the bit-interleaving diversity scheme itself, but to the sub-optimality of the iterative equalization approach (iteration between multiple equalizers before channel decoding). To this end, we first show that the BID scheme outperforms the identical transmis-

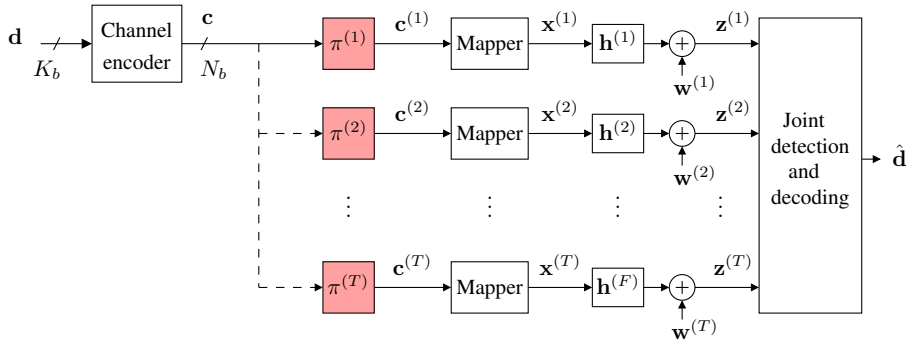

FIGURE 4.1: Bit-interleaving transmit diversity scheme for CC-HARQ systems.

sion (IT) scheme under joint maximum-likelihood (ML) detection and decoding. The advantages of the BID scheme is even more important for high order modulation. In order to exploit the potential of the BID scheme, we propose a low complexity MMSE-based turbo-equalization scheme for packet combining, including multiple and separate equalizers followed by a maximum ratio combiner. The performance of the proposed combining scheme are illustrated by EXIT charts analysis [43] and numerical simulations.

In the second part, we compare the performance of the BID scheme with the phase precoding diversity scheme. Finally, we extend the use of BID for MIMO frequency-selective channels where the interleaver can be optimized for better performance.

4.2 Euclidean distance analysis

We start by showing the advantages of the BID scheme in comparison with the IT scheme when using a maximum-likelihood receiver. To this end, we show the effect of using different random interleavers for multiple HARQ transmissions on the statistics of the squared output Euclidean distance.

Let $\mathbf{x}^{(t)}$ be the interleaved and modulated transmitted sequence at the t-th HARQ round. Let $\mathbf{e}^{(t)}$ be the corresponding error sequence, i.e. $\mathbf{e}^{(t)} = \hat{\mathbf{x}}^{(t)} - \mathbf{x}^{(t)}$. We recall from Equation (2.66) that the total OSED after T HARQ rounds is given by

$$\Delta_T = \sum_{t=1}^{T} \Delta^{(t)} = \sum_{t=1}^{T} \sum_{\ell=-L+1}^{L-1} R_\ell^*(\mathbf{h}^{(t)}) R_\ell(\mathbf{e}^{(t)}) \tag{4.1}$$

which can be expressed as

$$\Delta_T = \Gamma_T + \Lambda_T \tag{4.2}$$

where

$$\Gamma_T = \sum_{t=1}^{T} R_0^*(\mathbf{h}^{(t)}) R_0(\mathbf{e}^{(t)}) \tag{4.3}$$

$$\Lambda_T = 2\Re\left(\sum_{t=1}^{T}\sum_{\ell=1}^{L-1} R_\ell^*(\mathbf{h}^{(t)})R_\ell(\mathbf{e}^{(t)})\right) \tag{4.4}$$

Remember that Γ_T gives the squared Euclidean distance for an equivalent frequency-non-selective channel, while Λ_T reflects the effect of the frequency-selective nature of the channel. The performance of the system over an equivalent flat-fading channel ($\Lambda_T = 0$) is referred to as the Matched filter bound (MFB) which can be obtained by perfect removing of intersymbol interference from the received signal.

In the following, we will compare the statistics of both Γ_T and Λ_T between the BID scheme and the IT scheme over the extended error space $\mathcal{E}_d$ (cf. Chapter 2) and all possible channel realizations. We will consider the two channel models LTSC and STSC as defined in Chapter 1.

For a time-varying channel, the channel autocorrelations $R_\ell^*(\mathbf{h}^{(t)})$ are also random variables whose statistics are required for the calculation of the statistics of the Euclidean distance.

4.2.1 Statistics of channel autocorrelation

For simplicity, we consider a multipath fading channel with uniform power-delay profile. Since the channel tap coefficients are independent, the random variables $R_\ell^*(\mathbf{h}^{(t)})$ are independent for different t and pairwise uncorrelated for different lags ℓ. The statistics of the channel autocorrelation coefficients can be calculated easily using the independence between channel tap coefficients and the fact that $R_0(\mathbf{h}^{(t)}) = ||h^{(t)}||^2$ is Gamma distributed random variable with mean 1 and variance $1/L$. This yields to the following results

$$\mu_{R_{h,\ell}} \triangleq \mu(R_\ell^*(\mathbf{h}^{(t)})) = \begin{cases} 1 & \text{if } \ell = 0 \\ 0 & \text{if } 0 < \ell \leq L-1 \end{cases} \tag{4.5}$$

$$\sigma^2_{R_{h,\ell}} \triangleq \sigma^2(R_\ell^*(\mathbf{h}^{(t)})) = \begin{cases} \frac{1}{L} & \text{if } \ell = 0 \\ \frac{L-\ell}{L^2} & \text{if } 0 < \ell \leq L-1 \end{cases} \tag{4.6}$$

In the following, the Euclidean distance statistics are given as function of $\mu_{R_{h,\ell}}$ and $\sigma^2_{R_{h,\ell}}$.

4.2.2 Statistics of autocorrelations product

Since the Euclidean distance is the sum of products between the channel autocorrelation coefficients and the error autocorrelation coefficients, we need to characterize the statistics of the product $R_\ell^*(\mathbf{h}^{(t)})R_\ell(\mathbf{e}^{(t)})$.

In order to simplify our notations, we also define the following quantities

$$\mu_{R_{e,\ell}} \triangleq \mu(R_\ell(\mathbf{e}^{(t)})) \tag{4.7}$$

$$\sigma^2_{R_{e,\ell}} \triangleq \sigma^2(R_\ell(\mathbf{e}^{(t)})) \tag{4.8}$$

Since $R_\ell^*(\mathbf{h}^{(t)})$ is independent of the error autocorrelation $R_\ell(\mathbf{e}^{(t)})$, the mean and the variance of their product can be calculated as

$$\mu(R_\ell^*(\mathbf{h}^{(t)})R_\ell(\mathbf{e}^{(t)})) = \mu_{R_{h,\ell}}\mu_{R_{e,\ell}} = \begin{cases} \mu_{R_{e,0}} & \text{if } \ell = 0, \\ 0 & \text{if } 0 < \ell \leq L-1. \end{cases} \tag{4.9}$$

$$\tag{4.10}$$

$$\sigma^2(R_\ell^*(\mathbf{h}^{(t)})R_\ell(\mathbf{e}^{(t)})) = \sigma^2_{R_{h,\ell}}\sigma^2_{R_{e,\ell}} + \mu^2_{R_{h,\ell}}\sigma^2_{R_{e,\ell}} + \sigma^2_{R_{h,\ell}}\mu^2_{R_{e,\ell}} \tag{4.11}$$

$$= \begin{cases} \sigma^2_{R_{h,0}}\mu^2_{R_{e,0}} + (\mu^2_{R_{h,0}} + \sigma^2_{R_{h,0}})\sigma^2_{e,0} & \text{if } \ell = 0, \\ \sigma^2_{R_{h,\ell}}\sigma^2_{R_{e,\ell}} & \text{if } 0 < \ell \leq L-1. \end{cases} \tag{4.12}$$

where we have used the fact that $\mu_{R_{e,\ell}} = 0$ and $\mu_{R_{h,\ell}} = 0$ for $\ell \neq 0$.

Under the uniform interleaving assumption, the choice of the interleaver does not change the statistics statistics for error autocorrelation for a single transmission. Therefore, the mean statistics for both variables remain the same for both HARQ retransmission schemes, i.e.

$$\mu(\Gamma_T) = T\mu_{R_{h,0}}\mu_{R_{e,0}} \tag{4.13}$$

$$\mu(\Lambda_T) = 0 \tag{4.14}$$

However, the variance statistics could change according to the HARQ retransmission scheme and the channel model as it will presented by the following.

4.2.3 CC-HARQ with identical transmissions

For the IT scheme, the same sequence $\mathbf{x}$ is transmitted at each HARQ round. For T transmissions, we have $\mathbf{e} = \mathbf{e}^{(1)} = \cdots = \mathbf{e}^{(T)}$ and consequently the autocorrelations of the error sequence $R_\ell(\mathbf{e}^{(t)})$ are the same for $1 \leq t \leq T_{\max}$. In this case, the expressions of Γ_T and Λ_T simplify to

$$\Gamma_T^{\mathrm{IT}} = R_0(\mathbf{e})\Omega_{T,0} \tag{4.15}$$

$$\Lambda_T^{\mathrm{IT}} = 2\Re\left(\sum_{\ell=1}^{L-1} R_\ell(\mathbf{e}^{(t)})\Omega_{T,\ell}\right) \tag{4.16}$$

where $\Omega_{T,\ell} = \sum_{t=1}^{T} R_\ell^*(\mathbf{h}^{(t)})$ which was previously defined in (2.68). We see from (4.15) and (4.16), that a simple retransmission of the same codeword offers only channel diversity expressed by an accumulative channel gain $\Omega_{T,0}$ and accumulative interference $\Omega_{T,\ell}$ which both depend on the channel statistics.

4.2.3.1 LTSC model

For this channel model, we have $\mathbf{h}^{(t)} = \mathbf{h}$ for $1 \leq t \leq T_{\max}$. The accumulated channel autocorrelation at the T-th transmission is then $\Omega_{T,\ell} = TR_\ell^*(\mathbf{h})$. From this, we deduce the statistics of the two variables Γ_T and Λ_T by using the results of Proposition 2 in Chapter 2 as given below

$$\sigma^2(\Gamma_T^{\mathrm{IT-LTSC}}) = T^2\sigma^2_{R_{h,0}}\mu^2_{R_{e,0}} + T^2(\mu^2_{R_{h,0}} + \sigma^2_{R_{h,0}})\sigma^2_{e,0} \tag{4.17}$$

$$\sigma^2(\Lambda_T^{\mathrm{IT-LTSC}}) = T^2\kappa^2 \sum_{\ell=1}^{L-1} \sigma^2_{R_{h,\ell}}\sigma^2_{R_{e,\ell}} \tag{4.18}$$

where κ is a constant depending on the used modulation (cf. Proposition 3 in Chapter 2). This is simply T^2 times the variance for a single transmission. This indicates that both the equivalent channel gain and the interference power increase by the same factor resulting in a simple SNR shift from the performance of the maximum-likelihood receiver at the first transmission.

4.2.3.2 STSC model

For this channel model, the channel changes independently from one transmission to the next. Consequently, $\mu(\Omega_{T,\ell}) = T\mu_{R_{h,\ell}}$ and $\sigma^2(\Omega_{T,\ell}) = T\sigma^2_{R_{h,\ell}}$ which leads to the following statistics for Γ_T and Λ_T:

$$\sigma^2(\Gamma_T^{\mathrm{IT-STSC}}) = T\sigma^2_{R_{h,0}}\mu^2_{R_{e,0}} + T(T\mu^2_{R_{h,0}} + \sigma^2_{R_{h,0}})\sigma^2_{e,0} \tag{4.19}$$

$$\sigma^2(\Lambda_T^{\mathrm{IT-STSC}}) = T\kappa^2 \sum_{\ell=1}^{L-1} \sigma^2_{R_{h,\ell}}\sigma^2_{R_{e,\ell}} \tag{4.20}$$

In comparison with the LTSC model, we remark a variance reduction by a factor of $1/T$ for both variables which reflects the effect of channel diversity on the Euclidean distance.

In the next subsection, we show how the BID scheme changes these statistics.

4.2.4 CC-HARQ with bit-interleaving diversity

Using independent interleavers $R_\ell(\mathbf{e}^{(t)})$ become i.i.d. random variables for different values of t. Using this assumption, we can recompute the statistics of the Euclidean distance for both channel models in a similar way to the case of identical retransmissions.

4.2.4.1 LTSC model

For this channel model, the expressions of Γ_T and Λ_T which are given respectively in (4.3) and (4.4) simplify to

$$\Gamma_T^{\text{BID}-\text{LTSC}} = R_0(\mathbf{h}) \sum_{t=1}^{T} R_0(\mathbf{e}^{(t)}) \tag{4.21}$$

$$\Lambda_T^{\text{BID}-\text{LTSC}} = 2\Re\left(\sum_{\ell=1}^{L-1} R_\ell^*(\mathbf{h}) \left(\sum_{t=1}^{T} R_\ell(\mathbf{e}^{(t)})\right)\right) \tag{4.22}$$

This leads to the following variances

$$\sigma^2(\Gamma_T^{\text{BID}-\text{LTSC}}) = T^2\sigma^2_{R_{h,0}}\mu^2_{R_{e,0}} + T(\mu^2_{R_{h,0}} + \sigma^2_{R_{h,0}})\sigma^2_{e,0} \tag{4.23}$$

$$\sigma^2(\Lambda_T^{\text{BID}-\text{LTSC}}) = T\kappa^2 \sum_{\ell=1}^{L-1} \sigma^2_{R_{h,\ell}}\sigma^2_{R_{e,\ell}} \tag{4.24}$$

In comparison with the IT scheme, we observe that the second term in (4.17) is reduced by a factor of $1/T$ resulting in a variance reduction for Γ_T when $\sigma^2_{e,0} \neq 0$. This manifests by a spectrum thinning of the distribution Γ_T about its average value. The case where $\sigma^2_{e,0} = 0$ happens for some low order modulations such as BPSK modulation and QPSK modulation with Gray mapping for which $R_0(\mathbf{e}^{(t)})$ is proportional to the Hamming weight of the error sequence whatever was the interleaving. Actually, $\sigma^2_{e,0}$ reflects the inherent modulation diversity of the used mapping scheme. The relative amount of variance reduction for Γ_T depends on the ratio between the second term to the first term in (4.17) i.e.

$$\frac{(\mu^2_{R_{h,0}} + \sigma^2_{R_{h,0}})\sigma^2_{R_{e,0}}}{\sigma^2_{R_{h,0}}\mu^2_{R_{R_{e,0}}}} = (1+L)\frac{\sigma^2_{R_{e,0}}}{\mu^2_{R_{e,0}}} \tag{4.25}$$

which, increase with the channel length L and the modulation order as shown in Figure 4.2 for a packet length $N_b = 1200$ bits and different orders of QAM modulation with Gray mapping. As an example, for $d = 10$, $L = 5$, and 16-QAM modulation, this ratio is about $6 \times 0.133 = 0.8$. This means that the second term forms 45% of the total variance.

We conclude that for the LTSC model, the performance limits of the BID scheme are better than the IT for high order modulations due to the resulting modulation diversity.

With regards to the variance of Λ_T, we observe a reduction factor of $1/T$ indicating a reduced interference power in the combined signal. This is an expected result, because the equivalent interleaving length for T transmissions (forming a single codeword obtain from a concatenated T-repetition code) in the BID scheme is T times larger than the interleaving length for the IT scheme. We conclude that the joint detection performance of the BID scheme are better under joint maximum-likelihood sequence detection.

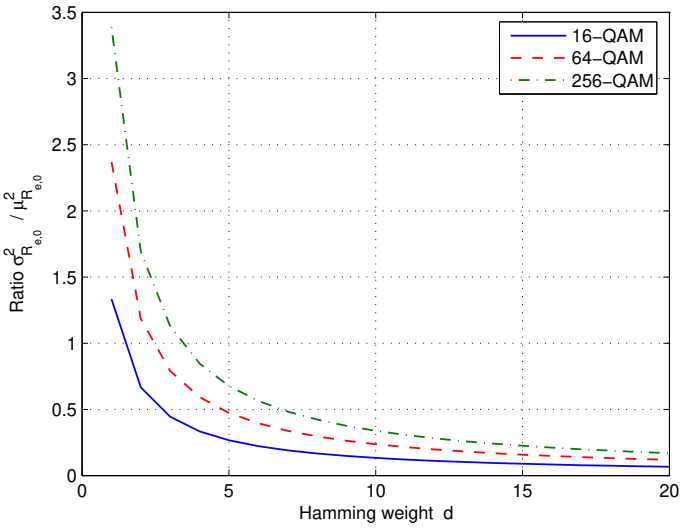

FIGURE 4.2: Ratio $\sigma^2_{R_{e,0}}/\mu^2_{R_{e,0}}$ as function of the Hamming weight of error sequence d.

4.2.4.2 STSC model

For this channel model, we obtain

$$\sigma^2(\Gamma_T^{\text{BID-STSC}}) = T\sigma^2_{R_{h,0}}\mu^2_{R_{e,0}} + T(\mu^2_{R_{h,0}} + \sigma^2_{R_{h,0}})\sigma^2_{e,0} \tag{4.26}$$

$$\sigma^2(\Lambda_T^{\text{BID-STSC}}) = T\kappa^2 \sum_{\ell=1}^{L-1} \sigma^2_{R_{h,\ell}}\sigma^2_{R_{e,\ell}} \tag{4.27}$$

In comparison with the IT scheme for the STSC model, we see a reduction in the variance of Γ_T observed in the second term of (4.19) (only if $\sigma^2_{e,0} \neq 0$) by a factor of

$$\frac{\mu^2_{R_{h,0}} + \sigma^2_{R_{h,0}}}{T\mu^2_{R_{h,0}} + \sigma^2_{R_{h,0}}} = \frac{1 + 1/L}{T + 1/L} = \frac{1 + L}{1 + LT} \tag{4.28}$$

which tends to $1/T$ for large value of L. again, this indicates the inherent modulation diversity in the BID scheme. For Λ_T, the variance remains the same as for the IT scheme.

In conclusion, the BID scheme has better performance limits than the IT scheme for high order modulations for both channel models. The interference power is only reduced for the LTSC model due the decorrelation of ISI among the different received signals.

4.3 Turbo-equalizer structure

Motivated by finding a turbo-equalizer structure which exploits the potential of the bit-interleaving diversity scheme, and to overcome the excessive complexity and the performance limitation of the iterative combining scheme, we show in this section that maximum ratio combining after separate equalization constitutes a suitable combining scheme for the BID scheme.

Figure 4.3 shows the proposed turbo-equalizer structure. For T HARQ transmissions, each transmission is equalized separately using the *a posterior* LLRs $L_a^D(\mathbf{c})$ from the channel decoder after interleaving as *a priori*. The extrinsic LLRs at the output of all equalizers are added after deinterleaving before being fed to the channel decoder. Note that we use an enhanced version of the turbo-equalizer proposed by [41] by using the full soft output channel decoder information which leads to improved soft ISI cancellation.

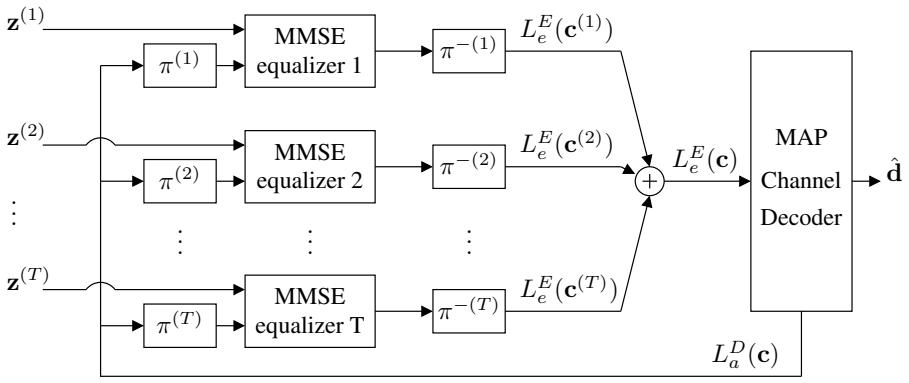

FIGURE 4.3: Turbo-equalizer structure with joint decoding for the BID scheme.

In the following, we will show by EXIT charts analysis why this combining scheme with a turbo-equalizer has a better performance than iterative equalization for the BID scheme and the joint equalization for the IT scheme.

4.3.1 EXIT charts analysis

Consider two HARQ transmissions generated by a rate-1/2 convolutional code $C_1(31, 27)_8$ and transmitted using 16-QAM modulation with gray mapping over random long-term static ISI channel.

The principle of iterative equalization is illustrated on Figure 4.4 where the interleaving operations are omitted for figure clarity. The first received signal is equalized by an equalizer, denoted by EQ1. A second equalizer, denoted by EQ2, is used to equalize the second received signal using the output of EQ1 and the decoder output as a-priori. Then, EQ1 re-performs the equalization of the first signal using the output of EQ2 and the decoder output as a-priori. Several iterations are performed between the two

equalizers until the convergence. The output of both equalizers are combined and fed to the channel decoder. This operation can repeated for several iterations.

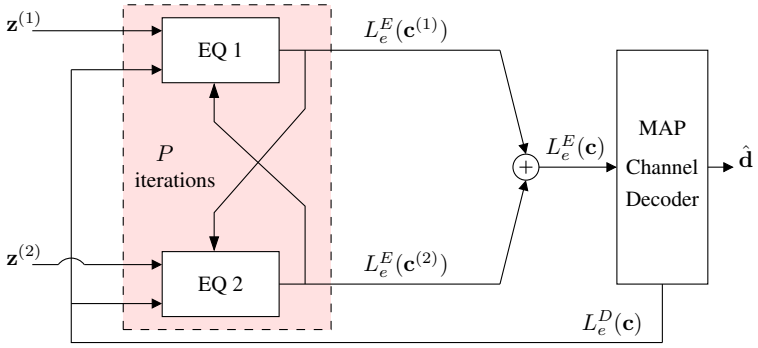

FIGURE 4.4: Principle of iterative equalization for BID scheme.

The code combining between two differently interleaved observations of the same codeword is equivalent to the decoding of a single codeword generated by a rate-1/4 code C_2 formed by the concatenation of the channel code with a rate-1/2 repetition code. On Figure 4.5, we have plotted the EXIT charts for two MMSE equalizers for SNR=2 dB. The curve $I_2 = f(I_1)$ gives the transfer function of EQ2 and the curve $I_1 = f^{-1}(I_2)$ gives the inverse transfer function of EQ1. Also, we have plotted the inverse transfer functions of the two codes $\mathcal{C}_1$ and $\mathcal{C}_2$.

Starting with no *a priori* information about the transmitted packet, the two equalizers converge to the cross-point between their transfer functions (Point 'A'). At the output of the combined code $\mathcal{C}_2$, we obtain the mutual information value I_d which corresponds to the point 'B'. Even if we iterate between the two equalizers and the decoder, we will converge always into the same point 'B'.

For the joint equalization method, we have plotted the transfer function of the joint equalizer which benefits from a retransmission energy gain leading to a higher transfer function. The convergence point of the turbo-equalizer is the intersection point between the transfer function of the joint equalizer and the channel decoder $\mathcal{C}_1$ (Point 'C'). We can see that Point 'C' has slightly higher output mutual information than Point 'B' which explains the superiority of joint equalization combining strategy in comparison with iterative equalization.

Now, we investigate the convergence behavior of the maximum ratio method without iteration between the different equalizers. As the two transmissions have the the same SNR, the two equalizers give equal output mutual information. Therefore, the average mutual information at the output of the two equalizers is the same as for the first equalizer EQ1. After many iterations between the pair (EQ1, EQ2) and the channel decoder of $\mathcal{C}_2$ we obtain the convergence point 'D' which has better reliability than 'C'. These results confirm the performance improvement provided by the BID scheme.

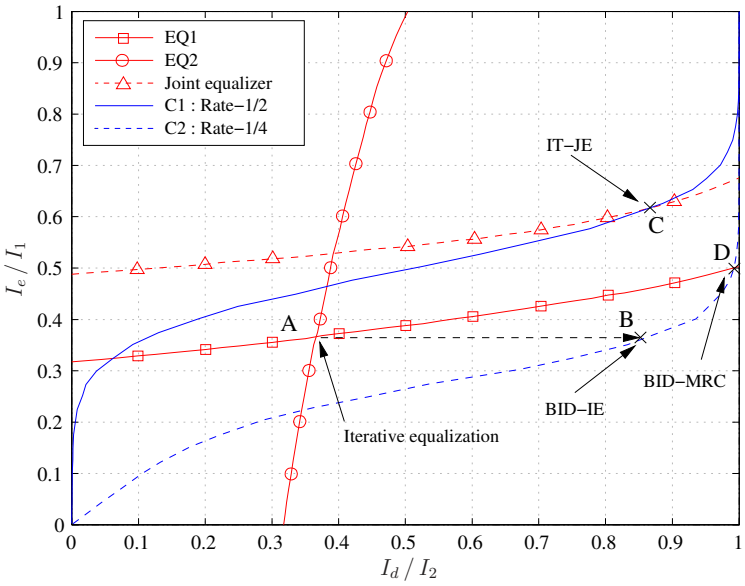

FIGURE 4.5: Convergence behavior of the joint-decoding combining method in a turbo-equalization scheme compared to both of the iterative equalization and the joint equalization combining methods.

4.3.2 Numerical results

In this section, we present some simulation results showing the performance of the BID scheme using maximum ratio combining in comparison with identical transmissions with joint equalization.

First, we consider a CC-HARQ retransmission scheme with $T_{max} = 4$ over long-term static channel of 5 taps with uniform power-delay profile. A packet of 600 information bits are encoded by a rate-1/2 convolutional code $\mathrm{CC}(31, 27)_8$ giving 1200 coded bits. After a random interleaver, each block is mapped to $M = 600$ symbols using a QPSK modulation. At the receiver, we use an MMSE equalizer using a 15-tap linear filter ($l_1 = 9$ causal taps and $l_2 = 5$ non-causal taps). We evaluate the FER versus E_s/N_0 for both BID and IT schemes over 10000 packets. Figure 4.6 shows simulation results without iteration. For comparison purposes, the MFB using perfect a-priori are also plotted on the same Figure.

Obviously, the FER performance are the same in the first transmission. We see clearly the superiority of the BID scheme in comparison with IT scheme for a non-iterative receiver. A gain of more than 2 dB at FER=10^{-3} is obtained at the second transmission. The relative gain increases with the number of retransmission. Note that the MFB for both schemes are identical.

Now, we consider the same previous setup using 16-QAM modulation with Gray mapping. Figure 4.7 shows the corresponding simulation results. We observe an impor-

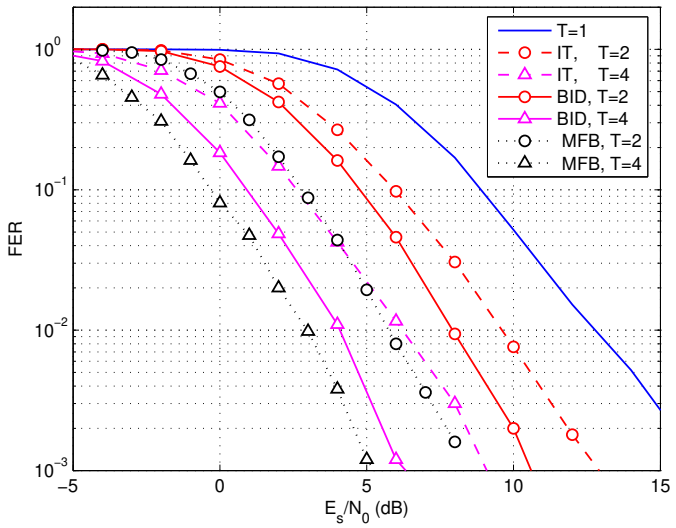

FIGURE 4.6: Performance comparison between BID and IT schemes with a non-iterative receiver using QPSK modulation over LTSC model.

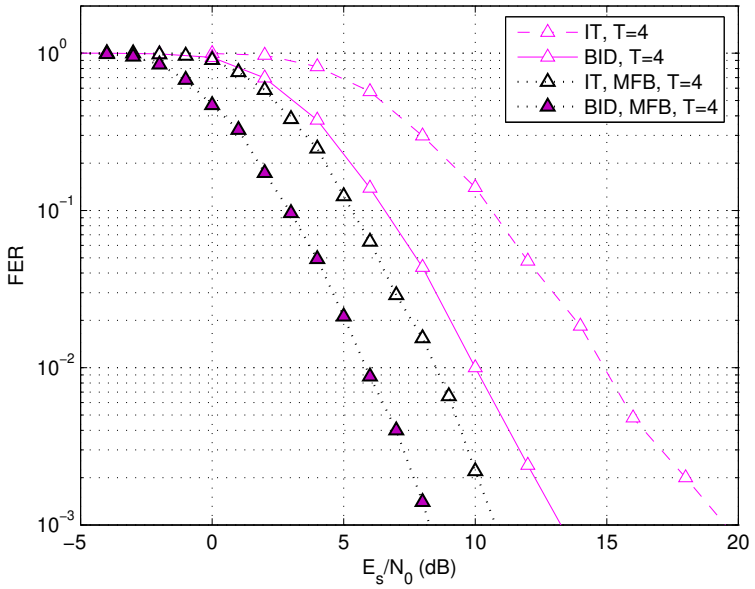

FIGURE 4.7: Performance comparison between BID and IT schemes with a non-iterative receiver using 16-QAM modulation over LTSC model.

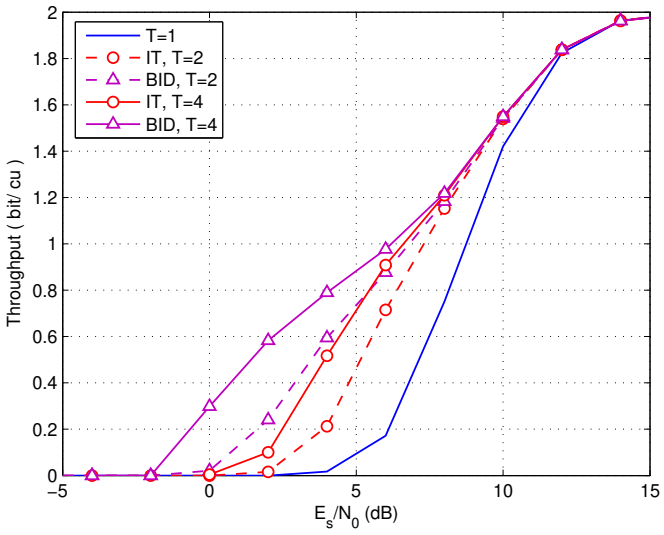

FIGURE 4.8: Throughput performance for BID and IT schemes using 16-QAM modulation over STSC model. The receiver implements an MMSE turbo-equalizer with 5 turbo-iterations.

tant gain of more than 5 dB at FER=10^{-3} in favor of the BID scheme. We observe that the MFB of the BID scheme is about 2.5 dB better than the MFB for the IT scheme due to the modulation diversity.

For the STSC model we obtain similar results and Figure 4.8 shows the obtained throughput performance. We see clearly the improvement in data throughput due to BID, especially at low and medium SNR values. for high SNR values, the throughput performance is dominated by the FER at the first transmission which is the same for all discussed transmission schemes.

4.4 Comparison with phase precoding diversity

In this section, we compare the performance of the BID scheme with those of the PPD scheme presented in the previous Chapter 3.

We know that phase precoding does not change the amplitude of the error symbol and consequently, the PPD scheme has the same performance limits as the IT scheme. Therefore, we focus here on the comparison of the statistics of the interference term Λ_T in the OSED.

4.4.1 Euclidean distance analysis

We evaluate the variance of Λ_T using the periodic phase precoding solution based on the DFT matrix which is equivalent to frequency shift of the transmitted signal.

For the LTSC model, Λ_T is given by

$$\Lambda_T^{\text{PPD-LTSC}} = 2\Re\left[\sum_{\ell=1}^{L-1} R_\ell^\star(\mathbf{h})\Xi_{T,\ell}\right], \tag{4.29}$$

where we have defined $\Xi_{T,\ell}$ as the total autocorrelation of the precoded error sequence given by

$$\Xi_{T,\ell} \triangleq \sum_{t=1}^{T} R_\ell(\mathbf{e}^{(t)}) = \sum_{n=0}^{N_s} C_{T,\ell}(n) e_n e_{n-\ell}^* \tag{4.30}$$

Using the precoding coefficients $a_n^{(t)} = e^{-j2\pi n\nu^{(t)}}$, we have

$$C_{T,\ell}(n) = \sum_{t=1}^{T} a_n^{(t)}(a_{n-\ell}^{(t)})^* = \sum_{t=1}^{T} e^{-j2\pi\ell\nu^{(t)}} \tag{4.31}$$

which is independent of n, and therefore can be moved out from the sum in (4.30) leading to

$$\Xi_{T,\ell} = C_{T,\ell} R_\ell(\mathbf{e}) \tag{4.32}$$

Consequently, the variance of $\Xi_{T,\ell}$ reduces to

$$\sigma^2(\Xi_{T,\ell}) = |C_{T,\ell}|^2 \sigma_{R_{e,\ell}}^2 \tag{4.33}$$

As it was shown in Chapter 3, by choosing frequency shifts $\nu^{(t)}$ from the set $\{k/L : k = 0, \cdots, L-1\}$, the squared cross-correlation of the precoding coefficients is also independent of ℓ and given by

$$|C_{T,\ell}|^2 = T\frac{L-T}{L-1}, \quad \forall \ell > 0,\ T < L. \tag{4.34}$$

Finally, using (4.12) and the decorrelation between different product terms of Λ_T, the variance of Λ_T can be computed as

$$\sigma^2(\Lambda_T^{\text{PPD-LTSC}}) = T\frac{L-T}{L-1}\kappa^2 \sum_{\ell=1}^{L-1} \sigma_{R_{h,\ell}}^2 \sigma_{R_{e,\ell}}^2 \tag{4.35}$$

In comparison with BID, we observe smaller variance for Λ_T by a factor of $\frac{L-T}{L-1}$. In the particular case when $T = L$, we have $\sigma^2(\Lambda_T) = 0$ which means that the interference is completely canceled by the PPD scheme. For large values of channel memory L, we have $|C_{T,\ell}|^2 \approx T$ and both diversity schemes become equivalent with regards to the ISI power.

We conclude that the BID scheme has a better performance limits than the PPD scheme for high order modulations, but the PPD scheme is more efficient in combating the interference for a short channel memory.

4.4.2 Numerical results

Simulations are performed using SCME channel model. For each transmitted packet, a random channel realization is generated and then used for all HARQ retransmissions of the packet. We assume that the maximum of HARQ transmissions is $T_{\max} = 4$. For the PPD scheme, frequency-shift parameters are $\nu^{(1)} = 0$, $\nu^{(2)} = 1/2$, $\nu^{(3)} = 1/4$, and $\nu^{(4)} = 3/4$. All used interleavers are pseudo-random interleavers. Other simulation parameters are inspired from the LTE standard [28] and listed in Tab. 4.1. Monte Carlo simulations are performed over a maximum of 5000 packets.

TABLE 4.1: Simulation parameters.

Parameter	Value
Frame length	$N = 516$ for QPSK, $N = 258$ for 16-QAM
Symbol rate	7.68 Msps
CP length	$P = 64$
Channel model	SCME urban macro scenario
Shaping filter	raised cosine with roll off 0.23
Doppler	no Doppler

We first consider a non-coded transmission system in order to show the intrinsic gain for both diversity schemes compared to the identical transmission scheme. This corresponds to the system performance before channel decoding for coded systems. Figure 4.9 shows the FER performance versus the average SNR after the last HARQ round ($T = 4$) for QPSK and 16-QAM modulations.

We can observe the superiority of the PPD scheme among all transmission schemes due to its best capability in interference mitigation. For QPSK modulation, we have SNR gain at FER=10^{-2} of about 2 dB for the BID scheme and 4 dB for the PPD scheme in comparison with the IT scheme. Note that the PPD scheme is only at 0.4 dB of the MFB which is the same for all schemes in the case of QPSK modulation. For 16-QAM modulation, the MFB for the BID scheme gives the best performance, but the better performance for the PPD scheme are due to the better performance of the joint equalization compared to the LLR combining used for the BID scheme.

It is true that the used channel has a large channel memory which may attain more than 100 symbol periods, but it has a decreasing power-delay profile with most of the interference power originating from the less delayed paths. In this sense, the effective channel memory is not very large. This explains the larger interference reduction in the case of the PPD scheme.

Now, we consider a coded system with a non-iterative receiver including separate equalization and channel decoding without turbo-iteration. The performance of the non-iterative receiver is obtained by performing one equalization step followed by one channel decoding step.

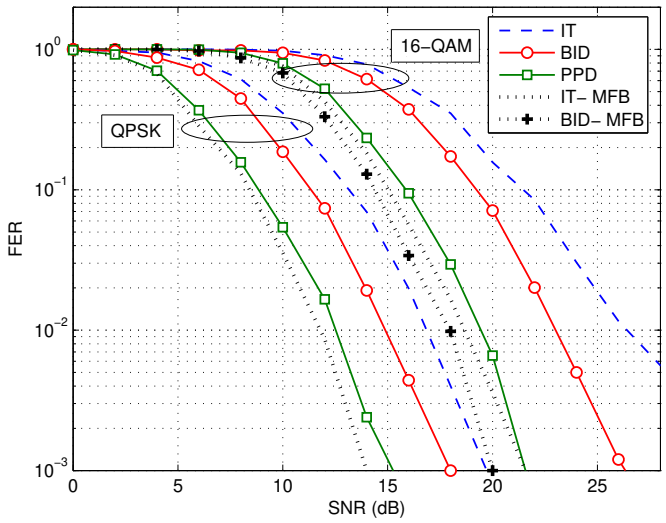

FIGURE 4.9: FER performance comparison between different transmission schemes for a non coded system using QPSK and 16-QAM modulations.

The channel code is the LTE turbo-code of rate-1/3 using two identical constituent convolutional codes $(1, 15/13)_8$ with quadratic permutation polynomial internal interleaver of length $K = 344$ taken from [28] (Table 5.1.3-3). For simplicity, no trellis termination is performed for the component codes. The receiver performs one equalization step followed by one channel decoding step. The channel decoder itself performs a maximum of five internal iterations between the two internal convolutional decoders in the turbo-decoder. Simulation results are given in Figure 4.10 for both QPSK and 16-QAM modulations.

We remark that using a powerful code, both diversity schemes have almost similar performance. We can observe that the performance of the BID scheme are still far from the corresponding MFB for 16-QAM modulation. For a higher coding rate, the performance gains of the proposed diversity schemes lay somewhere between the full rate case (rate 1/3) and the uncoded case. In order to close this gap, an iterative processing can be performed between the detector and the channel decoder.

Due to the high complexity of the iterative processing using a turbo-code, we use the LTE convolutional code of rate-1/3 whose generator polynomial is $(133, 171, 165)_8$. Here again, no trellis termination is performed for the convolutional code. Figure 4.11 shows the FER performance at the last HARQ round for separate detection and decoding, while Figure 4.12 shows the corresponding FER performance for a turbo-equalizer which performs a maximum of four turbo-iterations.

We note that for a linear receiver without turbo-iterations, the performance of both diversity schemes are almost the same. Unlike for a non coded system, using a turbo-

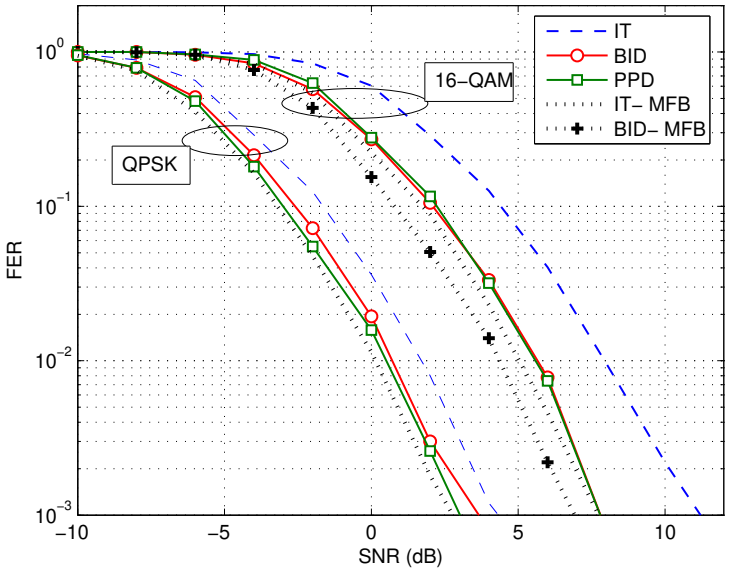

FIGURE 4.10: FER performance comparison between different transmission schemes for a coded system using a turbo-code for QPSK and 16-QAM modulations.

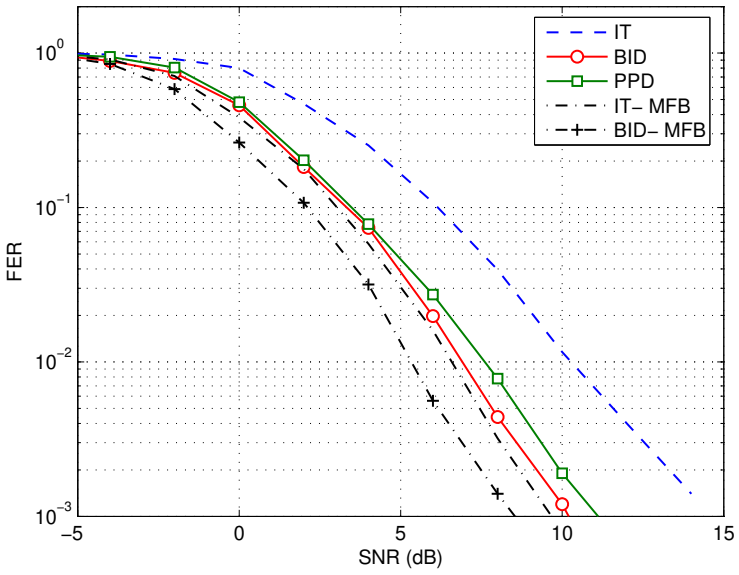

FIGURE 4.11: FER performance for different transmission schemes for a coded system with a rate-1/3 convolutional code using 16-QAM modulation and linear detection.

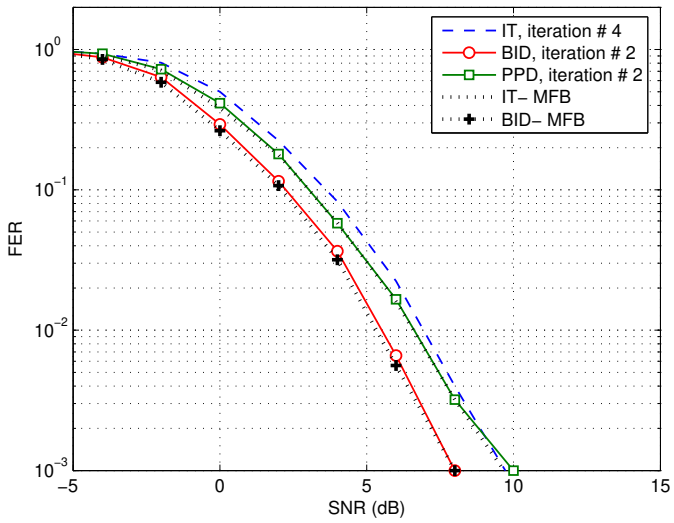

FIGURE 4.12: FER performance for different transmission schemes for a coded system with a rate-1/3 convolutional code using 16-QAM modulation and turbo-equalization.

equalizer in a coded system, the BID scheme outperforms the PPD scheme because the iterative receiver performs closely to the MFB which is better for the BID scheme.

In conclusion, the PPD is suitable for a linear receiver with separate equalization and decoding, especially for high rate channel coding. The BID scheme gives better performance with an iterative receiver at the expense of a higher system complexity.

4.5 Extension to MIMO frequency-selective channels

MIMO transmission is a powerful technique which improves the spectral efficiency by exploiting the channel diversity between the transmit and receive antennas. However, this requires more sophisticated signal processing techniques at the receiver side in order to mitigate interchannel interference (ICI) and intersymbol interference (ISI) [75]. Joint equalization for multiple HARQ transmissions over MIMO channels can be performed by the generalization of the single-antenna case as presented in [70].

In the context of CC-HARQ transmissions, antennas permutation diversity is proposed in [76, 77] in order to exploit available channel diversity between different antennas in slow time-varying channels. Each symbol is transmitted on a different antenna at each retransmission which can be viewed a special form of symbol-interleaving diversity prior to space-time multiplexing. In this section, we generalize the BID scheme to the case of MIMO multiplexing.

4.5.1 System model

We consider the same transmission system with the difference that the modulated symbols are spatially multiplexed and transmitted over $N_t \times N_r$ MIMO frequency-selective channel. The channel between the j-th transmit antenna and the i-th receive antenna is a frequency-selective channel modeled by its equivalent response of length L, denoted by $\mathbf{h}_{i,j}^{(t)} = (h_{i,j,0}^{(t)} \cdots h_{i,j,L-1}^{(t)})$. The received sequence vectors are modeled as

$$\mathbf{z}_n^{(t)} = \sum_{\ell=0}^{L-1} \mathbf{H}_\ell^{(t)} \mathbf{s}_{n-\ell}^{(t)} + \mathbf{w}_n^{(t)}, \quad n = 0, \cdots, N_s - 1$$

where $\mathbf{H}_\ell^{(t)}$ denotes the ℓ-th path $N_r \times N_t$ channel matrix, $\mathbf{w}_m^{(t)}$ is an independent additive white complex Gaussian noise $\mathbf{w}_n^{(t)} \sim \mathcal{N}(\mathbf{0}_{N_r \times 1}, \sigma_w^2 \mathbf{I}_{N_r})$, and $N_s = N_b/(QN_t)$ assumed integer.

4.5.2 Euclidean distance analysis

For a MIMO channel, the total OSED after T HARQ rounds can be found by a straightforward generalization of the single antenna case by first considering the case of N_t transmit antennas and one receive antenna, then accumulating the results over N_r receive antennas and T HARQ transmissions. This leads to

$$\Delta_T = \sum_{t=1}^{T} \sum_{i=1}^{N_r} \sum_{j=1}^{N_t} \sum_{k=1}^{N_t} \sum_{\ell=-L+1}^{L-1} R_\ell^*(\mathbf{h}_{i,j}^{(t)}, \mathbf{h}_{i,k}^{(t)}) R_\ell(\mathbf{e}_k^{(t)}, \mathbf{e}_j^{(t)}), \tag{4.36}$$

where $R_\ell(.,.)$ is the deterministic periodic cross-correlation at lag ℓ between the two parameter sequences, defined for two arbitrary complex sequences $\mathbf{x}$ and $\mathbf{y}$ of length N_s by $R_\ell(\mathbf{x}, \mathbf{y}) \triangleq \sum_{n=0}^{N_s-1} x_n y_{n-\ell}^\star$.

The performance limits of the maximum-likelihood receiver are obtained by supposing that the ICI and the ISI are completely canceled by the receiver. This can be obtained by forcing all channel cross-correlation terms in (4.36) to be zeros, i.e. $R_\ell(\mathbf{h}_{i,j}^{(t)}, \mathbf{h}_{i,k}^{(t)}) = 0$ for $k \neq j$ or $\ell \neq 0$. This yields to

$$\Gamma_T = \sum_{t=1}^{T} \sum_{j=1}^{N_t} \left(\sum_{i=1}^{N_r} ||\mathbf{h}_{i,j}^{(t)}||^2 \right) ||\mathbf{e}_j^{(t)}||^2. \tag{4.37}$$

The term Γ_T corresponds to the squared Euclidean distance for packet transmission over N_t block-fading channels with an equivalent squared channel gain for j-th channel $\sum_{i=1}^{N_r} ||\mathbf{h}_{i,j}^{(t)}||^2$ with mean denoted as $\mu_h = N_r$ and variance denoted as $\sigma_h^2 = N_r/L$. The remaining terms in the expression of Δ_T in (4.36) reflect the Euclidean distance fluctuation due to the presence of ICI and ISI. These terms are grouped in the variable

Λ_T given by

$$\Lambda_T = \sum_{t=1}^{T} \sum_{i=1}^{N_r} \sum_{j=1}^{N_t} \sum_{\substack{k=1 \\ k\neq j}}^{N_t} \sum_{\substack{\ell=-L+1 \\ \ell\neq 0}}^{L-1} R_\ell^*(\mathbf{h}_{i,j}^{(t)}, \mathbf{h}_{i,k}^{(t)}) R_\ell(\mathbf{e}_k^{(t)}, \mathbf{e}_j^{(t)}), \tag{4.38}$$

We limit our analysis to the effect of BID on the statistics of Γ_T since we know that BID would results in interference reduction for the LTSC model due to the introduced decorrelation between error sequences in subsequent HARQ transmissions.

For a given total Hamming weight d, the random variables $||\mathbf{e}_j^{(t)}||^2$ are identically distributed and independent with respect to t. However, for the same t, they are not independent for different j due the constraint over their total Hamming weight $d = \sum_{j=1}^{N_t} d_j^{(t)}$. Moreover, two different blocks $||e_i||^2$ and $||e_j||^2$ are conditionally independent giving their respective Hamming weight d_i and d_j. Taking into account these considerations, we obtain after a straightforward computation the following general expressions for the mean and the variance of Γ_T

$$\mu(\Gamma_T) = TN_t\mu_h\mu_e, \tag{4.39}$$

$$\sigma^2(\Gamma_T) = TN_t\left(a\mu_e^2 + b\sigma_e^2 + c\rho_e\right), \tag{4.40}$$

where we have defined $\mu_e \triangleq \mu(||\mathbf{e}_j||^2)$, $\sigma_e^2 \triangleq \sigma^2(||\mathbf{e}_j||^2)]$, and $\rho_e \triangleq E[(||\mathbf{e}_i||^2 - \mu_e)(||\mathbf{e}_j||^2 - \mu_e)]$ for $i \neq j$. The coefficients a, b, and c are tabulated in Table 4.2 according to the channel model and the transmission scheme.

TABLE 4.2: Parameters of the variance of Γ_T.

Channel-Scheme	a	b	c
IT-LTSC	$T\sigma_h^2$	$T(\mu_h^2 + \sigma_h^2)$	$T(N_t-1)\mu_h^2$
BID-LTSC	$T\sigma_h^2$	$\mu_h^2 + \sigma_h^2$	$(N_t-1)\mu_h^2$
IT-STSC	σ_h^2	$T\mu_h^2 + \sigma_h^2$	$T(N_t-1)\mu_h^2$
BID-STSC	σ_h^2	$\mu_h^2 + \sigma_h^2$	$(N_t-1)\mu_h^2$

We can verify that putting $N_r = 1$ and $N_t = 1$, we obtain the same expressions previously obtained for the case of single antenna. The difference with the single antenna case is the last term ρ_e which expresses the antenna diversity in the system. Moreover, the statistics of the error sequence are given at the sub-block level.

We observe that a is the same for both schemes because it is related to the channel diversity. However, the coefficients c and d are reduced by the BID scheme for both channel models. Actually, ρ_e is always negative because more errors in one block means less errors in the others. Therefore, the reduction of the multiplicity c of this term has a negative effect on the Euclidean distance. Therefore, we like to minimize this term by a special choice of the interleaver at each retransmission in order to equally distribute errors among different antennas as it will be seen in Section 4.5.3.

Another difference with the single antenna case is that σ_e^2 can not be zero even for low order modulations due to the variation of the Hamming weight d_j inside one error block. This indicates that some modulation diversity can be obtained for MIMO channels with $N_t > 1$. Indeed, the transmitted signal from multiple antennas is a combined signal which has a higher order modulation than the used constellation per antenna. Therefore, using the term "modulation diversity" for MIMO transmission is relevant whatever was the used constellation.

Note that the variables μ_e, σ_e^2 and ρ_e depend on N_t in addition to other system parameters N_b, Q, d and the mapping scheme as it has been seen for the single antenna case. They can be computed using combinatorial analysis as shown in Appendix-F. Numerical results for block error statistics with $N_t = 2$ are shown in Figure 4.13.

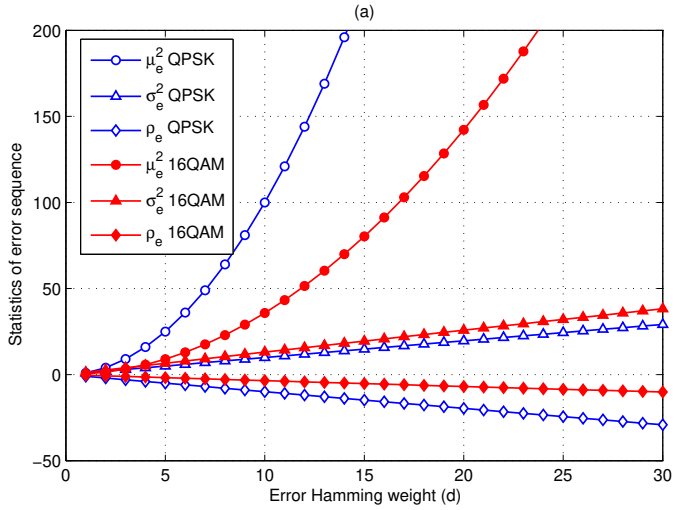

FIGURE 4.13: Block error statistics for 2×2 MIMO for $N_b = 1024$.

We observe that 16-QAM modulation has larger values of σ_e^2 and ρ_e which indicated that high order modulations take better benefits from the BID scheme. For high values of d, the first term $a\mu_e^2$ is the dominant term in the expression of the variance. Since the coefficient a is the same for both transmission schemes, they have similar variances. For low values of d, the contribution of the second and the third term becomes larger in the variance of Γ_T. Consequently, the benefit of the BID scheme is more important for channel codes with low free distance.

4.5.3 Interleaver design

The choice of the used interleavers can have some effect on the resulting diversity. Instead of using random interleavers, we propose to use more structured interleavers in order to enhance the modulation diversity and the antenna diversity.

For high order modulations, the constellation mapping can not offer the same degree of protection for all bits against error. For example, in 16-QAM modulation with Gray mapping, we can classify the modulated bits $\{b_1, b_2, b_3, b_4\}$ into two classes according their degree of protection: the first class $\mathcal{B}_1 = \{b_1, b_3\}$ is more protected than the second class $\mathcal{B}_2 = \{b_2, b_4\}$. Exchanging the transmitted bit between the two classes would offer the same degree of protection for all bits. Another diversity aspect concerns the transmitting antennas. Since the channel between different antennas are independent, we can enhance channel diversity by changing the transmission antennas for each bit at each HARQ retransmission. Based on these remarks, we construct the different interleavers using the following algorithm:

- Associate to each bit position n of the transmitted packet after interleaving a couple of parameters (a_n, l_n) indicating the transmitting antenna a_n and its protection level l_n.
- Assign to each bit c_k of the original coded packet before interleaving the ensemble of previously used antennas $\mathcal{A}_k$ and previously used protection levels $\mathcal{L}_k$. The ensembles $\mathcal{A}_k$ and $\mathcal{L}_k$ are initially empty.
- For the current transmission $t = 1, \cdots, T_{\max}$:
  - Put at the position n a randomly selected coded bit c_k such that $l_n \notin \mathcal{L}_k$ and $a_n \notin \mathcal{A}_k$.
  - Add a_n to $\mathcal{A}_k$ and l_n to $\mathcal{L}_k$ for the next transmission.

The advantage of this algorithm in comparison with antenna permutation [77] is that the group of transmitted bits over one antenna are not restricted to stay together in the next transmission. This results in an increased interleaving depth which in turns enhances turbo-equalization performance. We refer to the interleavers obtained by this construction as *combined interleavers*.

4.5.4 Numerical results

In the following simulations, we use the rate-1/2 non-recursive convolutional code $\mathrm{CC}(133, 171)_8$ for channel coding. The transmission takes place over 2×2 MIMO frequency-selective channel of length $L = 4$. We assume that the maximum number of HARQ transmissions is $T_{\max} = 3$. We evaluate the FER performance versus SNR per receive antenna defined as $\frac{E_s}{N_0} = \frac{N_t}{\sigma_w^2}$. The packet length is $N_b = 1024$. A maximum of five turbo-iterations were performed at the MMSE turbo-equalizer which was implemented in the frequency domain thanks to a cyclic prefix insertion of length $P = L$ at the transmitter. Combined interleavers obtained by the algorithm given in Section 4.5.3 have been used.

First, we consider packet transmission using QPSK modulation over the LTSC model. Simulation results are shown in Figure 4.14. We see that for the IT scheme, the obtained SNR gain is proportional to the number of transmissions. The BID scheme

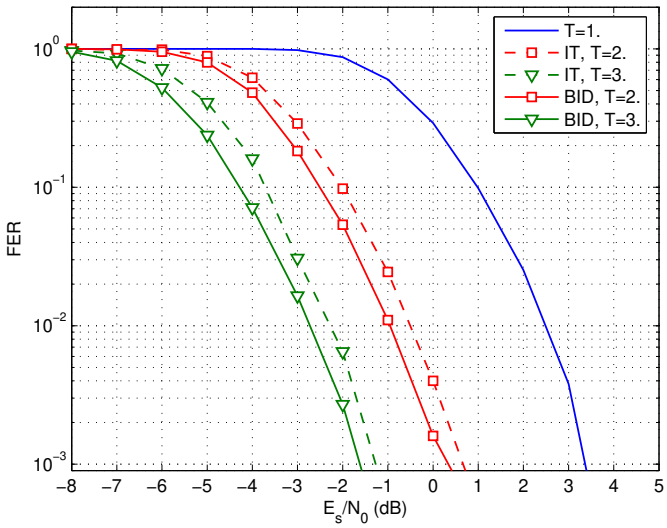

FIGURE 4.14: Performance comparison between BID and IT schemes using QPSK modulations over long-term static 2×2 MIMO channel.

provides some performance enhancement of about 0.5 dB over the IT scheme. Actually, with QPSK modulation we have less modulation diversity and the performance gap between the two scheme is mainly due to the multiplexing diversity between transmitting antennas. In addition, the convergence of the turbo-equalizer is faster for the BID scheme due to the interference reduction by error decorrelation between subsequent transmissions. Figure 4.14 shows the convergence behavior of the turbo-equalizer in this case for $T = 2$. The gain at earlier iterations is even larger which makes the BID also suitable for a non iterative receiver. Now we consider a 16-QAM modulation with Gray mapping. Simulations results for both channel models for $T = 3$ are shown in Figure 4.15. We can see that the BID scheme provides a performance gain of about 4.5 dB at FER=10^{-3} over the IT scheme at the third transmission. This the accumulative effect of the modulation diversity and the multiplexing diversity provided by the BID scheme. For the STSC case, we note a significant performance gain of about 2.5 dB at FER=10^{-3} is obtained at the third transmission which traduces the inherent modulation diversity of the BID scheme.

Finally, in order to show the advantage of the proposed combined interleavers in comparison with random interleavers, we have simulated the MFB for both schemes by providing the channel equalizers with the exact soft information about the transmitted symbols. Simulations are performed for 16-QAM modulation over the long-term static channel model and the obtained results are given in Figure 4.17. We can see a gain of 0.4 dB is obtained in this case by using combined interleavers in comparison with random interleavers.

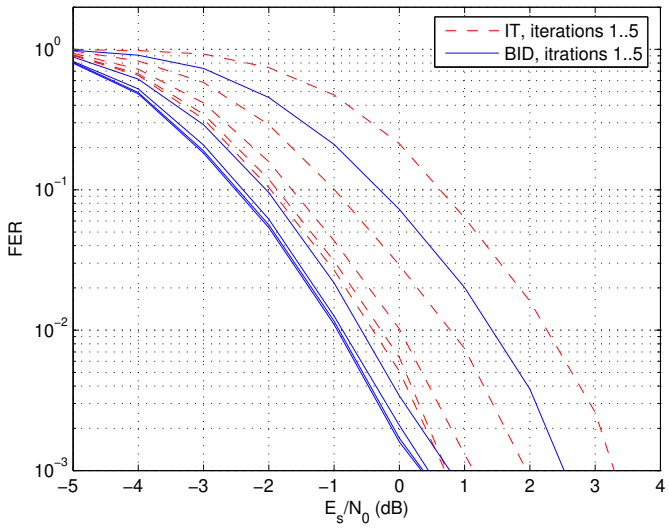

FIGURE 4.15: Convergence behavior of the turbo-equalizer for BID and IT schemes using QPSK modulation over LTSC 2×2 MIMO channel.

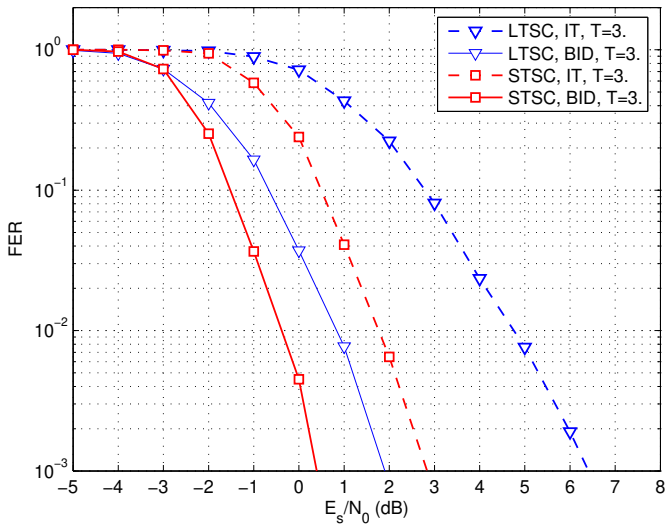

FIGURE 4.16: Performance comparison between BID and IT schemes using 16-QAM modulation for both LTSC and STSC 2×2 MIMO channel.

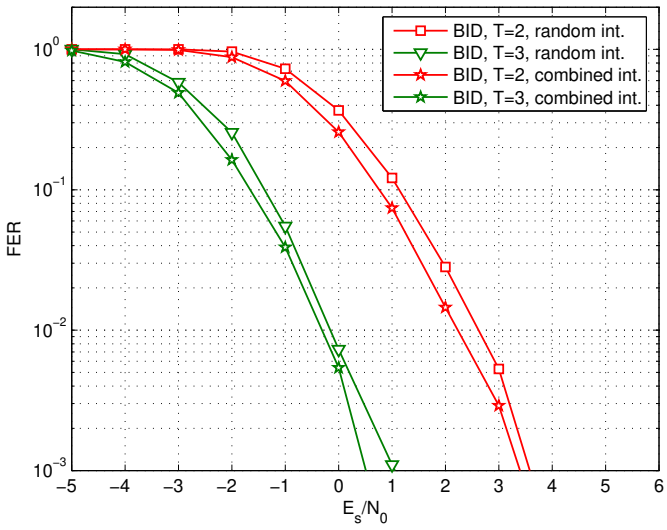

FIGURE 4.17: Comparison between the MFB for random interleaving and combined interleaving for $T = 2$ and 16-QAM mapping over long-term static 2×2 MIMO channel of length $L = 4$.

4.6 Results and discussion

In conclusion, it is possible to improve the performance of CC-HARQ protocols in order to decrease the gap with IR-HARQ protocols for frequency selective channels by using one of the proposed transmit-diversity scheme depending on the packet length, the used modulation, the receiver structure, and the communication channel model. Figures 4.18 show the performance comparison for the LTSC model between CC-HARQ with both diversity schemes and the IR-HARQ for a non-iterative receiver. Other simulation parameters are the same used in Chapter 1. Figures 4.19 show the corresponding MFB.

We see that the performance of CC-HARQ with phase-precoding diversity preforms almost the same as IR-HARQ and even better for high SNR values. This indicates that SNR gains in signal detection due to phase-precoding compensate for the precoding gain in IR-HARQ. With an iterative receiver, both diversity schemes performs almost the same for QPSK modulation, while for 16-QAM modulation, the bit-interleaving diversity scheme gives better performance than phase-precoding. However, the performance of IR-HARQ are still the best.

With regards to the STSC model, phase-precoding does not provide any significant improvement over identical retransmissions because the error sequences are already decorrelated by the effect of the varying channel. However, the gap with IR-HARQ is not too large for a non-iterative receiver. For a iterative receiver, the bit-interleaving allows some performance enhancement for 16-QAM modulation.

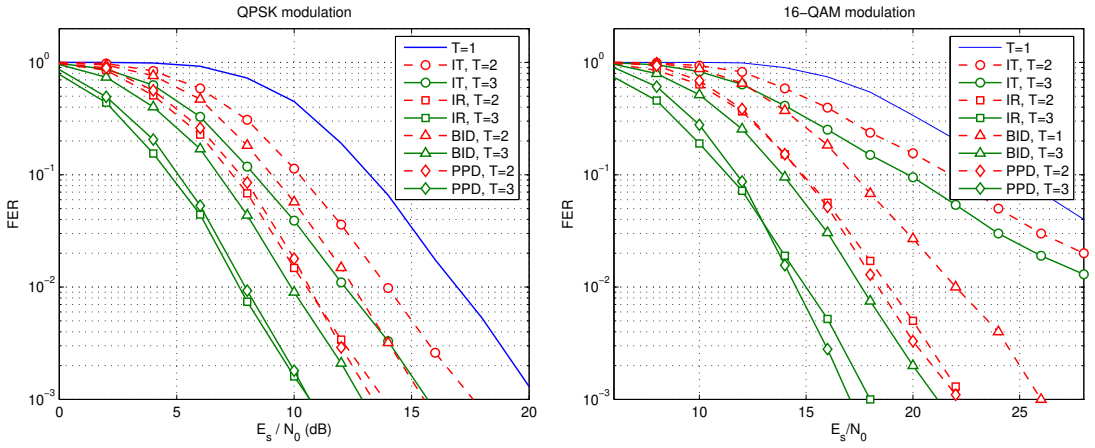

FIGURE 4.18: FER performance comparison between various retransmission schemes over LTSC with a non-iterative receiver.

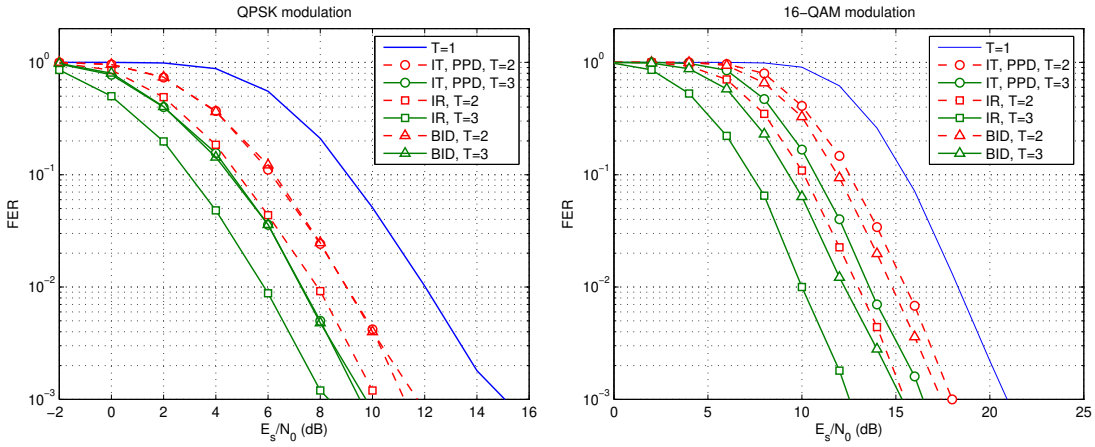

FIGURE 4.19: MFB comparison between various retransmission schemes over LTSC model.

TABLE 4.3: IR-HARQ SNR gain over CC-HARQ with transmit diversity at FER=10^{-2}.

		non-iterative receiver	iterative receiver
LTSC	QPSK	0.2 dB (PPD)	1.5 dB (PPD)
	QAM	-1 dB (PPD)	2 dB (BID)
STSC	QPSK	0.8 dB (PPD)	2 dB (PPD)
	QAM	0.5 dB (BID)	2.2 dB (BID)

we summarize the SNR gap between IR-HARQ and CC-HARQ with transmit diversity in Table 4.3. We remark that for a non iterative receiver, the performance of CC-HARQ with transmit-diversity is close to the IR-HARQ. For an iterative receiver,

IR-HARQ stays better that CC-HARQ. Note that these value are obtained for a relatively high initial rate of $r = 4/5$. The advantages of IR-HARQ decreases even more with a higher initial coding rate.

4.7 Conclusions

We have shown in this paper that the bit-interleaving diversity scheme in conjunction with joint decoding outperforms the identically interleaved scheme with joint equalization in retransmissions based HARQ protocols over frequency selective channels. We have also shown that MRC combining strategy better exploits the interleaving diversity scheme than the iterative equalization strategy with lower computational complexity. Our theoretical analysis shows that the BID scheme has better performance limits than the PPD scheme for high order modulation, but the PPD scheme is more efficient in combating the ISI for channels with short memory. The PPD is suitable for a linear receiver with separate equalization and decoding, while the BID scheme gives a better performance with an iterative receiver. These diversity schemes can be used in order to compensate for poor channel diversity in slow fading environment depending to the desired performance complexity trade-off and the system parameters including the channel coding rate, the modulation order.

The use of the BID scheme can be extended to the MIMO frequency-selective channels. An additional source of diversity which is the antenna diversity is exploited by the BID scheme. We have proposed an algorithm to construct combined interleavers in order to enhance further the bit interleaving diversity performance. Finally, One can view the BID scheme as kind of trade-off among modulation diversity, antennas permutation and phase precoding diversity schemes.

The results presented in this chapter have led to the following publications:

1. A. Assimi, C. Poulliat, and I. Fijalkow, "Diversity techniques for single-carrier packet retransmissions over frequency-selective channels," *Accepted to EURASIP Journal on Wireless Communications and Networking Special Issue on "3GPP LTE and LTE Advanced"*, 2009.

2. A. Assimi, C. Poulliat, and I. Fijalkow, "Packet combining for turbo-diversity in HARQ systems with integrated turbo-equalization," in *Int. Symp. Turbo Codes (ISTC)*, Lausanne, Switzerland, September 2008, pp. 61–66.

3. A. Assimi, C. Poulliat, and I. Fijalkow, "Bit-interleaving diversity for HARQ transmission over MIMO frequency-selective channels," in *IEEE International Workshop on Signal Processing Advances in Wireless Communications (SPAWC)*, Perugia, Italy, June 2009, pp. 310–314.

In the next chapter, we turn into a promising transmission scheme for high data throughput in rapidly time-varying channels.

Chapter 5

HARQ Protocols for Multi-Layer Transmission

We consider in this chapter into another transmission scheme called multi-layer transmission which, in conjunction with HARQ protocols, provides a promising scheme for high data throughput in rapidly time-varying channels. This chapter addresses the problem of packet combining jointly with the optimization of a HARQ protocol for multi-layer transmission in Chase combining HARQ.

5.1 Introduction

For data transmission over rapidly time-varying multipath fading channel, adaptive coding an modulation can not performed due to the unpredicted channel gain for the current transmission. In such situations where no channel state information (CSI) is available at the transmitter, multi-layer transmission is an efficient way to improve data throughput [78]. In multi-layer transmission, multiple coded packets, each of which is referred to as a *layer*, are simultaneously transmitted over the channel using a linear superposition of modulated symbols. Different transmission rates and powers can be allocated to different layers allowing different degrees of protection to the different transmitted layers. The receiver employs successive interference cancellation (SIC) in order to decode the superposed layers in the descending order of received power. With varying channel conditions, the receiver decodes layers which match the instantaneous channel gain. Therefore, partial decoding of the transmitted data in one block is possible. This is the difference with single-layer transmission where the whole transmitted data in one block can be either entirely decoded or entirely loosed. This constitutes the reason behind the layering gain.

The problem of the optimization of the transmitting rate and the transmitting power per layer has been investigated by many works in the literature under different contexts [79, 80, 81, 82]. In general, for a given power allocation scheme, there is an

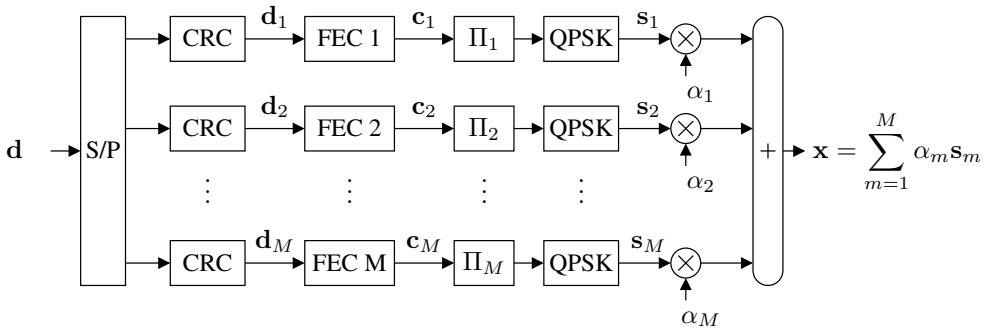

FIGURE 5.1: Transmitter scheme for multi-layer packet transmission.

optimal rate allocation solution. Inversely, for given transmission rates, there is an optimum power allocation solution. It has been shown in [83] that a small number of layers is usually sufficient to achieve most of the layering gain. Moreover, equal rate allocation is sub-optimal in general, and nearly optimal for moderate number of layers. This why, we mainly focus in this work on the case of two-layer transmission.

For HARQ error control protocols, each packet has its own CRC signature allowing layer-wise retransmission control. In incremental redundancy HARQ protocols, each received block is separately detected and multiple retransmissions are decoded by using code combining. Whereas, in Chase combining HARQ protocols, multiple blocks can be combined at the signal level for better detection performance compared to post-detection combining methods [46]. The performance of various multi-layered HARQ protocols have been investigated in [78] for broadcast channels using an infinite number of layers without power optimization. In [84], the performance of a multi-level coded QAM modulation was investigated for a frequency-selective channel.

In this chapter, we propose an adaptive retransmission protocol using CSI during the previous transmissions in order to minimize the average FER performance of the system. We first present the multi-layer transmission scheme and packet combining methods for HARQ retransmissions. Then, we establish the equivalent MIMO model for multi-layer HARQ retransmissions and the associated receiver structure. Based on this MIMO model, we optimize the linear superposition coefficients at each HARQ round for two-layer transmission.

5.2 Multi-layer transmission scheme

We consider the transmission system hown in Fig. 5.1 using multi-layer single-carrier signaling. The transmitted signal $\mathbf{x}$ is formed by a linear superposition of M modulated packets $\mathbf{s}_m$ for $m = 1, \cdots, M$. Each individual packet is referred to as a *layer*. In each layer, the information data packet $\mathbf{d}_m$, including CRC bits for error detection, is first encoded by a forward error correction code (FEC) to obtain the coded sequence $\mathbf{c}_m$ having N coded bits. Different coding rates may be used for different layers. However,

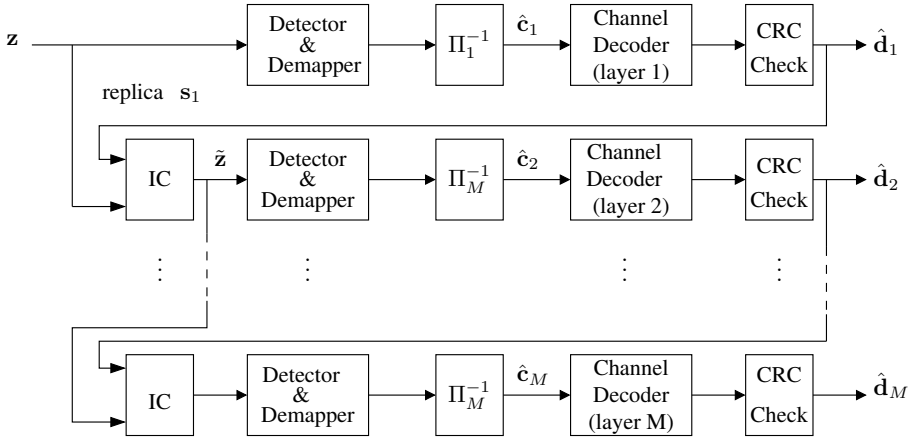

FIGURE 5.2: Successive interference cancellation receiver.

we assume in this chapter that the same code is used for all layers. This simplifies the system complexity by using the same encoder and decoder for all layer. The coded sequence is then interleaved using a random interleaver Π_m and mapped to a sequence $\mathbf{s}_m$ of N_s complex symbols using a Gray-mapped QPSK modulation. The transmitted signal $\mathbf{x}$ can be written as

$$\mathbf{x} = \sum_{m=1}^{M} \alpha_m \mathbf{s}_m, \tag{5.1}$$

with $\alpha_m = a_m \exp(j\phi_m)$ where a_m is a scaling factor and ϕ_m is a phase-shift ($\phi_m \in [0, 2\pi)$). The scaling parameter a_m determine the allocated power to each layer under the constraint of a unit average transmitted power, i.e. $\sum_{m=1}^{M} a_m^2 = 1$. Whereas, the phase-shift angles ϕ_m determine the shape of the combined constellation and consequently the characteristics of the output signal such as the peak-to-average power ratio [85].

We consider a single-input single-output transmission system through a flat fading channel. At the instant t (expressed in one block period), the received signal can be modeled as

$$\mathbf{z}^{(t)} = \sqrt{\gamma} h^{(t)} \mathbf{x}^{(t)} + \mathbf{w}^{(t)}, \tag{5.2}$$

where $h^{(t)}$ is the complex channel gain, $\mathbf{w}^{(t)}$ is the noise vector whose elements are i.i.d. complex Gaussian random variables with zero mean and unit variance, denoted by $\mathcal{CN}(0, 1)$, and $\sqrt{\gamma}$ is average transmitted power or equivalently the average received SNR. We assume that the channel gain h remains constant during the period of one block transmission and changes independently from one block to another. In addition, we assume that the receiver has a perfect CSI whereas no CSI is assumed at the transmitter which justified by the changing channel conditions from one transmission to the next.

At the receiver side, the received signal is decoded layer by layer in descending order of power as shown in Figure 5.2. Without loss of generality, let $a_1 > a_2 > \cdots > a_M$.

Then, the receiver first decodes the first layer by considering all other layers as noise,

$$\mathbf{z}^{(t)} = \sqrt{\gamma} h^{(t)} a_1^{(t)} \mathbf{s}_1^{(t)} + \underbrace{\sqrt{\gamma} h^{(t)} \sum_{m=2}^{M} a_1^{(t)} \mathbf{s}_1^{(t)} + \mathbf{w}^{(t)}}_{\text{noise}}, \tag{5.3}$$

In the case of correct decoding of s_1, the contribution of s_1 is removed from the received signal by the interference canceler (IC) leading to the signal $\tilde{\mathbf{z}}^{(t)}$ which contains the remaining $M-1$ undecoded layers, i.e.

$$\tilde{\mathbf{z}}^{(t)} = \mathbf{z}^{(t)} - \sqrt{\gamma} h^{(t)} a_1^{(t)} \mathbf{s}_1^{(t)} \tag{5.4}$$

The receiver continues with the decoding of the second layer from $\tilde{\mathbf{z}}^{(t)}$ in a similar way to the first layer. This operation continues until the decoding of all layers. In the case of decoding failure of one layer, the receiver abort the decoding process. At the end of the decoding process, the receiver returns a positive acknowledgment ACK for the successfully decoded layers, where as a negative a acknowledgment NACK for the remaining undecoded layers. In the case of successful decoding of all layers, the transmitter send new block with new M layers. Otherwise, some retransmission strategy has to be considered. The question is what the best HARQ retransmission strategy that maximizes the data throughput in the system.

5.3 HARQ protocols for multi-layer transmission

In order to ensure data reliability, we consider two retransmission strategies which have been addressed in [78] for broadcast transmission with infinite number of layers without power allocation focusing on slowly fading channels.

a) Full-layered HARQ retransmission (FL-HARQ) The transmitter responds by resending M layers consisting of the undecoded packets and new packets instead of the correctly received packets. In this HARQ strategy, each layer is treated as an independent virtual channel with an independent HARQ process associated to that layer. The maximum number of allowable retransmissions $T_{\max}$ is defined per packet.

b) Partially-layered HARQ retransmission (PL-HARQ) The transmitter responds by resending only the erroneous packets with modified linear coefficients. The number of retransmitted layers is equal to the number of erroneous packets. In this strategy, no additional packets are transmitted until the complete decoding of all packets in the previous block. The maximum number of allowable retransmissions $T_{\max}$ is defined per block of M packets.

For packet decoding using successive interference cancellation, MRC is usually used before the decoding of each layer. Since the equivalent noise (other undetected layers

and noise) in multiple layered HARQ transmissions are not independent, MRC is not an optimal combining method. Our objective is to determine a better combining method layered transmissions which takes into account the correlated nature of the equivalent noise. To this end, we establish an equivalent MIMO model suitable for layered HARQ transmissions as shown in the next section.

5.4 MIMO model for multi-layer retransmissions

One can see the multi-layer transmission of M layers as a multiple-input single-output (MISO) transmission system with M transmitting antennas with correlated channels. Each transmitting antenna corresponds to one layer. Thus

$$\mathbf{z}^{(t)} = \sqrt{\gamma} \sum_{m=1}^{M} \tilde{h}_m^{(t)} \mathbf{s}_m^{(t)} + \mathbf{w}^{(t)} \tag{5.5}$$

where $\tilde{h}_m^{(t)} = \alpha_m^{(t)} h^{(t)}$ is the equivalent channel for the m-th layer by considering the linear coefficients $\alpha_m^{(t)}$ as a part of the MISO channel. The received blocks is initially stored in a buffer with the $T_{\max}$ previously received signals after removing the contributions of already decoded layers. Thus, the buffer size is $T_{\max} + 1$ blocks. This choice for the buffer size is related to the packet combining method which will be presented later in this chapter in order to estimate a given packet from all previously received signal containing that packet.

At the instant t, the buffered signals are referred to by the variables $\tilde{\mathbf{z}}^{(t-i)}$ for $i = 0, \cdots, T_{\max}$. After each successful decoding of one layer, the buffered signal are updated by canceling the contribution of that layer from all buffered signals as in (5.4). The received block at the instant t contains a maximum of M layers consisting of a combination of retransmitted and/or new packets. Let $T_{m,t}$ be the number of transmissions of the m-th layer at the instant t. Naturally, for new transmitted layers, we have $T_{m,t} = 0$ and for retransmitted layers $\mathbf{s}_m^{(t)} = \mathbf{s}_m^{(t-1)} = \cdots = \mathbf{s}_m^{(t-T_{m,t})}$. The interference canceler performs the following task

$$\tilde{\mathbf{z}}^{(t-i)} = \tilde{\mathbf{z}}^{(t-i)} - \sqrt{\gamma} \tilde{h}_m^{(t-i)} \mathbf{s}_m^{(t)}, \quad i = 0, \cdots, T_{m,t}. \tag{5.6}$$

In this way, the buffered blocks contain undecoded layers only.

Our objective is to determine the relation between the buffered signals and the undecoded layers. For better understanding, we start by a simple example with two layers $M = 2$ and a maximum number of retransmission $T_{\max} = 1$. The general case is presented later in this section.

Example 4. Initially, at the instant $t = 1$, the received signal is

$$\mathbf{z}^{(1)} = \tilde{h}_1^{(1)} \mathbf{s}_1^{(1)} + \tilde{h}_2^{(1)} \mathbf{s}_2^{(1)} + \mathbf{w}^{(1)}$$

which is stored in the buffer as $\tilde{\mathbf{z}}^{(1)}$. Assuming that the first layer was correctly decoded, so $\tilde{\mathbf{z}}^{(1)}$ is updated as follows

$$\tilde{\mathbf{z}}^{1} = \tilde{\mathbf{z}}^{1} - \tilde{h}_1^{(1)}\mathbf{s}_1^{(1)} = \tilde{h}_1^{(2)}\mathbf{s}_1^{(2)} + \mathbf{w}^{(1)}. \tag{5.7}$$

The transmitter responds by sending a new packet on the first layer and the same packet on the second layer. The corresponding received signal is

$$\tilde{\mathbf{z}}^{(2)} = \mathbf{z}^{(2)} = \tilde{h}_1^{(2)}\mathbf{s}_1^{(2)} + \tilde{h}_2^{(2)}\mathbf{s}_2^{(2)} + \mathbf{w}^{(2)}, \tag{5.8}$$

with $\mathbf{s}_2^{(2)} = \mathbf{s}_2^{(1)}$. By combining (5.7) and (5.8), the two buffered signals can be viewed as the output of a 2×2 MIMO channel expressed as

$$\begin{bmatrix} \tilde{z}_n^{(2)} \\ \tilde{z}_n^{(1)} \end{bmatrix} = \begin{bmatrix} \tilde{h}_1^{(2)} & \tilde{h}_2^{(2)} \\ 0 & \tilde{h}_2^{(1)} \end{bmatrix} \begin{bmatrix} s_{1,n}^{(2)} \\ s_{2,n}^{(2)} \end{bmatrix} + \begin{bmatrix} w_n^{(2)} \\ w_n^{(1)} \end{bmatrix}.$$

For other cases, similar results are obtained with the corresponding equivalent MIMO channel response as illustrated in Fig. 5.3.

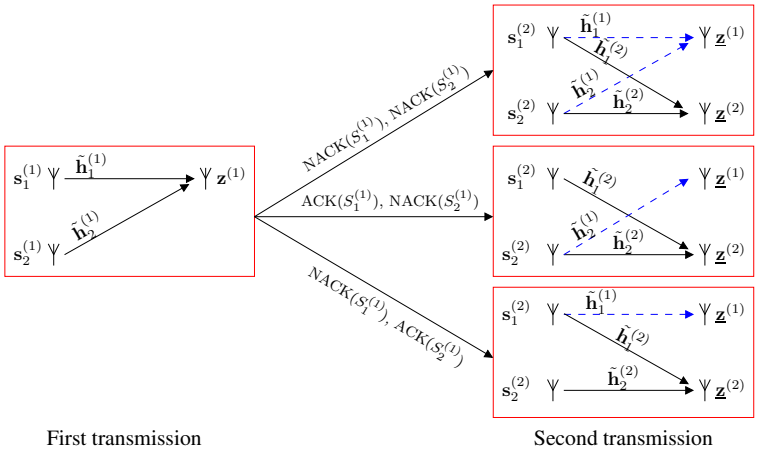

FIGURE 5.3: Equivalent MIMO channel model for two layers retransmission.

In the general case, we distinguish between three types of undecoded packets:

- New transmitted packets: for which $T_{m,t} = 0$. Their number is denoted by M_n.
- Retransmitted packets: packets which have not yet reached the maximum number of retransmissions $0 < T_{m,t} \leq T_{\max}$. Their number is denoted by M_r.
- Dropped packets: packets which have expired the maximum number of retransmissions. Their number is denoted by M_d.

The ensemble of new and retransmitted packets are referred to as *active layers* as opposite to dropped layers which are already declared in error to the upper network layer. Therefore, the current transmission contains active layers only. We denote by $M_a = M_n + M_r$ the number of active layers at the current instant. Note that for both FL-HARQ protocols, we have $M_a = M$, while for PL-HARQ protocols, we have $M_n = 0$ and $M_a \leq M$. We also denote by $M_u = M_n + M_r + M_d$ the total number of undecoded packets.

We regroup the undecoded packets in the same matrix $\mathbf{S}_t$ of size $M_u \times N_s$ as follows. The first M_r lines include the retransmitted packets. The next M_n lines include the new packets. The last M_d lines include the dropped packets. The equivalent MIMO model between the undecoded packets and the buffered signals can be written as

$$\mathbf{z}_n = \sqrt{\gamma}\mathbf{H}_t\mathbf{s}_n + \mathbf{w}_n \tag{5.9}$$

for $n = 0, \cdots, N_s - 1$, where

- $\mathbf{z}_n = [\tilde{z}_n^{(t)}, \cdots, \tilde{z}_n^{(t-T_{\max})}]^\top$,
- $\mathbf{w}_n = [w_n^{(t)}, \cdots, w_n^{(t-T_{\max})}]^\top$,
- $\mathbf{s}_n$ is the n-th column of $\mathbf{S}$,
- $\mathbf{H}_t$ is the $(T_{\max}+1) \times M_u$ equivalent channel response for the undecoded packets defined by their elements as

$$[\mathbf{H}_t]_{i,j} = \varepsilon_{i,j}\tilde{h}_{m_j}^{(t-i)}, \quad 0 \leq i \leq T_{\max},\ 1 \leq j \leq M_u \tag{5.10}$$

  where m_j is the index of layer which was used to transmit the j-th packet in $\mathbf{S}_t$, and $\varepsilon_{i,j} = 1$ if an the buffered signal $\tilde{\mathbf{z}}^{(t-i)}$ contains the j-th undecoded packet, and $\varepsilon_{i,j} = 0$ otherwise.

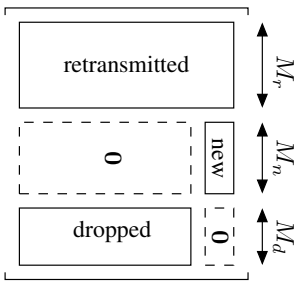

FIGURE 5.4: The equivalent MIMO matrix for multi-layer retransmission.

Figure 5.4 shows the form of the equivalent channel matrix. We illustrate the MIMO model by taking the following example.

TABLE 5.1: An example of a retransmission scenario under SFP and AFL HARQ strategies with $M = 3$ and $F_{\max} = 2$.

Time	Transmitted packets	Decoding results A=ACK, N=NACK
1	$\mathbf{d}_1, \mathbf{d}_2, \mathbf{d}_3$	A N N
2	$\mathbf{d}_4, \mathbf{d}_2, \mathbf{d}_3$	A A N
3	$\mathbf{d}_5, \mathbf{d}_6, \mathbf{d}_3$	N N N
4	$\mathbf{d}_5, \mathbf{d}_6, \mathbf{d}_7$	? ? ?

Example 5. Consider the retransmission scenario shown in Table 5.1 with $M = 3$ and $F_{\max} = 2$. At the fourth transmission, the undecoded packets are $\{\mathbf{d}_5, \mathbf{d}_6, \mathbf{d}_8\}$ which are transmitted on the layers $\{1, 2, 3\}$, respectively. We have only one dropped packet $\{\mathbf{d}_3\}$ which was transmitted on the layer $\{3\}$. In this case we have $M_a = 3$ and $M_d = 1$ and the corresponding equivalent MIMO channel model is given by

$$\begin{bmatrix} \tilde{z}_n^{(4)} \\ \tilde{z}_n^{(3)} \\ \tilde{z}_n^{(2)} \end{bmatrix} = \sqrt{\gamma} \begin{bmatrix} \tilde{h}_1^{(4)} & \tilde{h}_2^{(4)} & \tilde{h}_4^{(4)} & 0 \\ \tilde{h}_1^{(3)} & \tilde{h}_2^{(3)} & 0 & \tilde{h}_3^{(3)} \\ 0 & 0 & 0 & \tilde{h}_3^{(2)} \end{bmatrix} \begin{bmatrix} s_{1,n}^{(4)} \\ s_{2,n}^{(4)} \\ s_{3,n}^{(4)} \\ s_{3,n}^{(2)} \end{bmatrix} + \begin{bmatrix} w_n^{(4)} \\ w_n^{(3)} \\ w_n^{(2)} \end{bmatrix} \tag{5.11}$$

where $\mathbf{s}_1^{(4)}$, $\mathbf{s}_2^{(4)}$, $\mathbf{s}_3^{(4)}$, and $\mathbf{s}_3^{(2)}$ correspond to $\mathbf{d}_5$, $\mathbf{d}_6$, $\mathbf{d}_7$, and $\mathbf{d}_3$ respectively.

Now, having determined the equivalent MIMO channel model for multiple HARQ layered transmissions, we can apply classical detection methods for MIMO transmission in order to jointly decode the undecoded packets like in V-BLAST architecture with successive decoding [86].

We present in the next section the classical MRC combining method and the MMSE MIMO detection. These two methods are treated as special cases of the general class of linear detection methods. In order to simplify our notations, the time index t is omitted, and the index of the buffered signals are indexed in such a way that the most recent received block has the time index (1) and the oldest signal in the buffer has the time index ($T_{\max}$).

5.5 Packet combining

The receiver structure is shown in Fig. 5.5. From the buffered signals, the SIC receiver starts with the combining and the decoding of the layer which has the best chance to be decoded correctly. In the case of successful decoding, a replica of the interleaved and modulated packet is generated in order to remove its contribution from the buffered

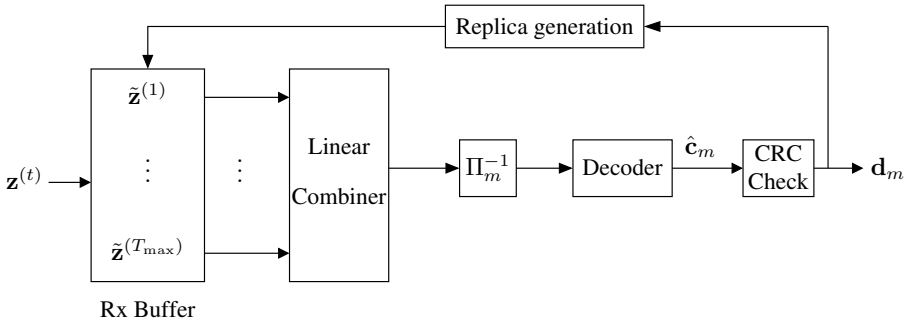

FIGURE 5.5: Receiver structure for packet combining of multi-layer HARQ transmissions using successive interference cancellation and joint equalization.

signals. Then, the receiver determine again the best layer from the remaining undecoded layers. The successive decoding continues in this manner until the decoding of all packets or a decoding failure has been occurred.

With a linear combiner, the estimated symbols are given by

$$\hat{s}_{m,n} = \mathbf{f}_m^H \tilde{\mathbf{z}}_n, \quad 0 < n \leq N_s - 1,\ 1 \leq m \leq M \tag{5.12}$$

where $\mathbf{f}_m = [f_{m,0}, \cdots, f_{m,T_{\max}}]^\top$ are the linear weighting coefficients which can be determined according to the detection criterion.
Alternatively, $\hat{s}_{m,n}$ can be written as

$$\hat{s}_{m,n} = \sqrt{\gamma}\mathbf{f}_m^H \mathbf{h}_m s_{m,n} + \sqrt{\gamma}\sum_{j \neq m}^{M_u} \mathbf{f}_m^H \mathbf{h}_j s_{j,n} + \mathbf{f}_m^H \mathbf{w}_n \tag{5.13}$$

$$= \mu_m s_{m,n} + \eta_{m,n} \tag{5.14}$$

where $\mathbf{h}_i$ is the i-th column of the equivalent MIMO channel matrix and μ_m is the equivalent channel gain for the m-th layer given by

$$\mu_m = \sqrt{\gamma}\mathbf{f}_m^H \mathbf{h}_m \tag{5.15}$$

and $\eta_{m,n}$ is the equivalent noise with zero mean and variance given by

$$\sigma_\eta^2 = \mathbf{f}_m^H(\mathbf{I} + \gamma \mathbf{H}\mathbf{H}^H)\mathbf{f}_m - \gamma(\mathbf{f}_m^H \mathbf{h}_m)^2 \tag{5.16}$$

Consequently, the SINR at the output of the linear combiner is calculated by treating all other layers as noise leading to

$$\xi_m = \frac{\mu_m^2}{\sigma_\eta^2} = \frac{\gamma(\mathbf{f}_m^H \mathbf{h}_m)^2}{\mathbf{f}_m^H(\mathbf{I} + \gamma \mathbf{H}\mathbf{H}^H)\mathbf{f}_m - \gamma(\mathbf{f}_m^H \mathbf{h}_m)^2} \tag{5.17}$$

It is natural to assume that the layer which has the best chance to be decoded first is layer which maximizes ξ_m. We denote the index of the chosen layer by $m^\star$ which is defined as

$$m^\star = \underset{1 \leq m \leq M_u}{\arg\max}(\xi_m) \tag{5.18}$$

The SIC receiver starts with the decoding of the packet $m^{\star}$. In the case of successful decoding, the decoded packet is removed from the buffered signal. The new equivalent channel matrix is reconstructed by removing the corresponding column from $\mathbf{H}$ and the detection process continues with the next packet in the same way as for the first packet.

We present now the combining solution under MRC and MMSE detection criteria.

5.5.1 Maximum ratio combining

The i-th received signal in the buffer can be rewritten as

$$\tilde{z}_n^{(i)} = \underbrace{\sqrt{\gamma}\tilde{h}_m^{(i)} s_{m,n}}_{\text{signal}} + \underbrace{\sqrt{\gamma}\sum_{j=1,j\neq m}^{M_u} \tilde{h}_j^{(i)} s_{j,n} + w_n^{(i)}}_{\text{equivalent noise}} \tag{5.19}$$

The MRC coefficients are given according to Equation (1.3) in Chapter 1 by

$$f_{m,i} = \frac{\sqrt{\gamma}\tilde{h}_m^{(i)}}{\sigma_{m,i}^2} \tag{5.20}$$

where $\sigma_{m,i}^2$ is the variance of the equivalent noise and given by

$$\sigma_{m,i}^2 = \gamma \sum_{j\neq m}^{M_u} |\tilde{h}_j^{(i)}|^2 + 1 \tag{5.21}$$

Note that the MRC solution only consider the buffered signal which contain the layer m to be decoded and does not take into account the correlation between the equivalent channel coefficients $\tilde{h}_j^{(i)}$. The SINR at the output of the combiner can be calculated by substituting the combining solution in the SINR expression of Equation (5.17).

5.5.2 MMSE detector

Under the minimum mean square error (MMSE) detection, the linear weighting vector for the detection of the m-th layer is given by

$$\mathbf{f}_m^H = \sqrt{\gamma}\mathbf{h}_m^H \left(\mathbf{I} + \gamma \mathbf{H}\mathbf{H}^H\right)^{-1} \tag{5.22}$$

Consequently, the SINR at the output of the combiner is given by

$$\xi_m^{\text{mmse}} = \frac{\mu_m^2}{\sigma_\eta^2} = \frac{\mu_m}{1-\mu_m} = \gamma \mathbf{h}_m^H \left[\mathbf{I} + \gamma \sum_{j\neq m}^{M_u} \mathbf{h}_j \mathbf{h}_j^H\right]^{-1} \mathbf{h}_m \tag{5.23}$$

where the last equality can be obtained by applying the matrix inversion lemma on the expression of $\mathbf{f}_m^H$.

5.6 Adaptive HARQ Protocol for two-layer transmission

In this section, we investigate the best choice for linear coefficients at the current transmission in order to minimize the average packet error rate over all layers assuming perfect channel coding and Gaussian source distribution.

For multiple transmissions, the instantaneous channel capacity C is given by

$$C = \log_2 \left(\det \left[\mathbf{I} + \gamma \mathbf{H} \mathbf{H}^H \right] \right)$$

The instantaneous capacity C gives an upper bound on the total reliable transmitting rate giving the channel state $\mathbf{H}$. Since the transmitting rate using M layers is Mr, where r is the transmitting rate per layer, the maximum number of layers which can be supported by the channel is $M = \lfloor \frac{C}{r} \rfloor$. For block fading channels, due to the limited observations of channel states in one data block, the outage probability is commonly used as a measure of performance limit. It is shown in [87], that maximizing the average outage probability is equivalent to equally distribute the available channel capacity over different layers. Let P_m^{out} be outage probability for the m-th layer. Then, the optimum is achieved when all layers have equal error protection, i.e. $P_1^{\text{out}}(\gamma) = P_2^{\text{out}}(\gamma) = \cdots = P_M^{\text{out}}(\gamma)$.

For simplicity, we restrict ourselves to the simplest case of two-layer transmission with PL-HARQ protocol where only erroneous packets are retransmitted ($M_n = 0$) in order to avoid the effect of the dropped packets on the detection performance.

5.6.1 First transmission

Suppose that the receiver buffer is initially empty, the first transmission of two packets is performed using the linear coefficients $\alpha_1^{(1)}$ and $\alpha_2^{(1)}$ with $|\alpha_1^{(1)}| > |\alpha_2^{(1)}|$. The SINR for the first layer using successive decoding is

$$\xi_1^{(1)} = \frac{\gamma |h^{(1)}|^2 |\alpha_1^{(1)}|^2}{1 + \gamma |h^{(1)}|^2 |\alpha_2^{(1)}|^2} \tag{5.24}$$

and for the second layer assuming correct decoding of the first layer

$$\xi_2^{(1)} = \gamma |h^{(1)}|^2 |\alpha_2^{(1)}|^2 \tag{5.25}$$

We can verify that this transmission scheme can achieve the channel capacity

$$\log_2(1 + \xi_1^{(1)}) + \log_2(1 + \xi_2^{(1)}) = \log_2(1 + \gamma |h^{(1)}|^2)$$

From (5.24) and (5.25), the outage probabilities for both layers are given by

$$\begin{aligned} P_1^{\text{out}}(\gamma) &= \Pr\left(\log_2(1+\xi_1^{(1)}) < r\right) \\ &= F_{|h|^2}\left(\frac{\xi_0}{\gamma(|\alpha_1^{(1)}|^2 - \xi_0|\alpha_2^{(1)}|^2)}\right) \qquad (5.26) \\ P_2^{\text{out}}(\gamma) &= \Pr\left(\log_2(1+\xi_2^{(1)}) < r\right) \\ &= F_{|h|^2}\left(\frac{\xi_0}{\gamma|\alpha_2^{(1)}|^2}\right) \qquad (5.27) \end{aligned}$$

where $\xi_0 = C^{-1}(r) = 2^r - 1$, and $F_X(x) \triangleq \Pr(X < x)$. As it is previously noted, the maximum average outage is achieved when $P_1^{\text{out}}(\gamma) = P_2^{\text{out}}(\gamma)$. This leads to the following solution

$$|\alpha_1^{(1)}|^2 = (\xi_0 + 1)|\alpha_2^{(1)}|^2,$$

which is independent of γ and the fading distribution. Since $|\alpha_1^{(1)}|^2 + |\alpha_2^{(1)}|^2 = 1$, we get

$$|\alpha_1^{(1)}|^2 = \frac{\xi_0 + 1}{\xi_0 + 2}, \text{ and } |\alpha_2^{(1)}|^2 = \frac{1}{\xi_0 + 2}. \qquad (5.28)$$

Since the source is assumed complex Gaussian, the phases of the linear coefficients can be arbitrary chosen. Therefore, we assume that $\alpha_1^{(1)}$ and $\alpha_2^{(1)}$ are positive reals. For example, for a transmission rate per layer $r = 1$ bit/cu which can be realized by using a rate-1/2 error correction code with QPSK modulation, we obtain $|\alpha_1^{(1)}|^2 = \frac{2}{3}$ and $|\alpha_2^{(1)}|^2 = \frac{1}{3}$. The intersection point between $\xi_1^{(1)}$ and $\xi_2^{(1)}$ takes place at the outage threshold $\gamma|h^{(1)}|^2 = \xi_0(\xi_0 + 2)$.

5.6.2 Second transmission

There are two possible cases for error in the first transmission which are discussed below.

5.6.2.1 Case of two errors

If the first transmission falls in outage ($\gamma|h^{(1)}|^2 < \xi_0(\xi_0 + 2)$), the transmitter resends both layers with new linear coefficients $\alpha_1^{(2)}$ and $\alpha_2^{(2)}$. The channel matrix for both transmission is then

$$\mathbf{H} = \begin{bmatrix} \alpha_1^{(2)}h^{(2)} & \alpha_2^{(2)}h^{(2)} \\ \alpha_1^{(1)}h^{(1)} & \alpha_2^{(1)}h^{(1)} \end{bmatrix}$$

We investigate the best choice for $\alpha_1^{(2)}$ and $\alpha_2^{(2)}$ that maximize the average outage knowing that the first transmission was in outage.

The instantaneous channel capacity C for both transmission can be upper bounded by using Hadamard's inequality [88] as

$$C = \log_2 \det \left[\mathbf{I} + \gamma \mathbf{H}\mathbf{H}^H\right] \tag{5.29}$$

$$\leq \log_2(1+\gamma|h^{(1)}|^2) + \log_2(1+\gamma|h^{(2)}|^2) \tag{5.30}$$

with equality for a diagonal matrix, i.e. $\alpha_1^{(2)}(\alpha_1^{(1)})^* + \alpha_2^{(2)}(\alpha_2^{(1)})^* = 0$ leading to the following retransmission solution

$$\alpha_1^{(2)} = (\alpha_2^{(1)})^*, \quad \alpha_2^{(2)} = -(\alpha_1^{(1)})^* \tag{5.31}$$

This solution maximizes C, but is it compliant with the minimization of the average outage per layer? To answer this question, we derive in the following the solution which minimize the average outage probability.

According to Equation (5.18), the MMSE-SIC receiver selects the layer having the highest SINR. It can be shown by direct evaluation of (5.23) that the output SINR if the MMSE detector starts with the first layer

$$\xi_1^{(2)} = \frac{\gamma||\mathbf{h}_1||^2 + \gamma^2\Delta^2|h^{(1)}|^2|h^{(2)}|^2}{1+\gamma||\mathbf{h}_2||^2}, \; \xi_2^{(2)} = \gamma||\mathbf{h}_2||^2 \tag{5.32}$$

Inversely, if the MMSE detector starts with the second layer, we obtain

$$\xi_2^{(2)} = \frac{\gamma||\mathbf{h}_2||^2 + \gamma^2\Delta^2|h^{(1)}|^2|h^{(2)}|^2}{1+\gamma||\mathbf{h}_1||^2}, \; \xi_1^{(2)} = \gamma||\mathbf{h}_1||^2 \tag{5.33}$$

where $\Delta^2 \triangleq |\alpha_1^{(1)}\alpha_2^{(2)} - \alpha_2^{(1)}\alpha_1^{(2)}|^2$.
We observe from (5.32) and (5.33) that the first detected layer is the layer with the maximum received SNR $||\mathbf{h}_m||^2$ (this is only true for the case of two-layer transmission). Since the linear coefficients in the first transmission are reals, we remark also that the SINR is maximized with respect to the linear coefficients phases in the second transmission when $\alpha_1^{(2)}$ and $\alpha_2^{(2)}$ are reals with opposite signs because this maximizes Δ^2. Note that when $\Delta^2 = 0$ we have $\alpha_1^{(1)}\alpha_2^{(2)} = \alpha_2^{(1)}\alpha_1^{(2)}$. This means that the retransmission uses the same linear coefficients as in the first transmission. In this case, maximum ratio combining can be performed between the two received signals before successive decoding starting by the first layer. This solution provides the same outage probability for both layers independently of channel realizations. However, it does not exploit the total capacity of the channel.

Suppose that the SIC receiver selects layer 1 to be first decoded ($||\mathbf{h}_1||^2 > ||\mathbf{h}_2||^2$). Then, having γ and $h^{(1)}$, the outage probabilities at the second transmission can be computed from (5.32) as

$$P_1^{\text{out}}(\gamma) = \Pr(\log_2(1+\xi_1^{(2)})) < r) \qquad = F_{|h|^2}(\beta_1) \tag{5.34}$$

$$P_2^{\text{out}}(\gamma) = \Pr(\log_2(1+\xi_2^{(2)})) < r) \qquad = F_{|h|^2}(\beta_2) \tag{5.35}$$

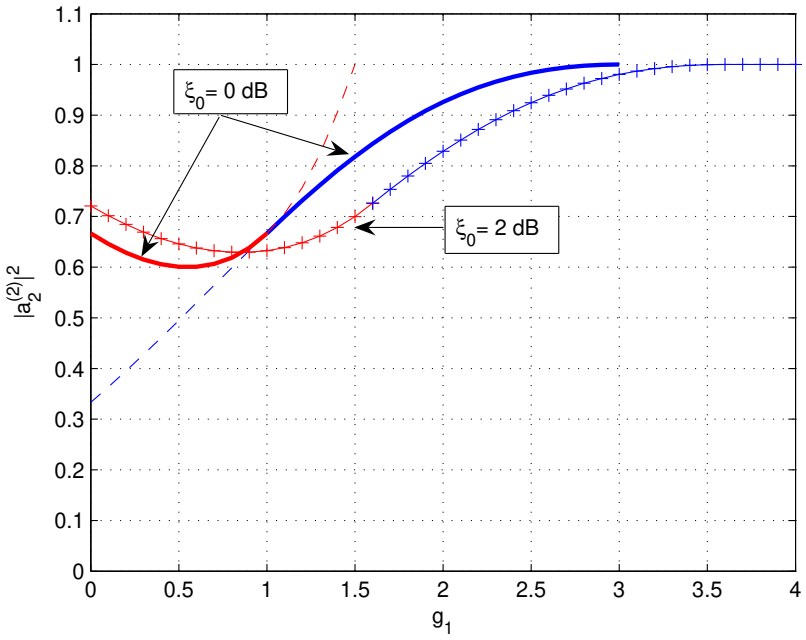

FIGURE 5.6: Optimum value for $|\alpha_2^{(2)}|^2$ as function of g_1.

where

$$\beta_1 = \frac{\xi_0 + ((\xi_0+1)|\alpha_2^{(1)}|^2 - 1)g_1^2}{\gamma(1-(\xi_0+1)|\alpha_2^{(2)}|^2 + \Delta^2 g_1^2)} \tag{5.36}$$

$$\beta_2 = \frac{\xi_0 - |\alpha_2^{(1)}|^2 g_1^2}{\gamma|\alpha_2^{(2)}|^2} \tag{5.37}$$

where $g_1^2 \triangleq \gamma|h^{(1)}|^2$. Using the optimum solution for the first transmission in (5.28), the optimum solution for the second transmission can be found by solving $\beta_1 = \beta_2$ with respect to $|\alpha_2^{(2)}|^2$ under the constraint $\xi_1^{(2)} > \xi_2^{(2)}$ for $g_2 \triangleq \gamma|h^{(2)}|^2 > \beta^\star$, where $\beta^\star$ is the intersection value. This leads to solve the following equation

$$(\xi_0+2)|\alpha_2^{(2)}|^2 = 1 + \Delta^2 g_1^2. \tag{5.38}$$

Obviously, the solution of (5.38) depends on the channel gain in the first transmission g_1^2 except if $\Delta^2 = 0$. By solving (5.38) we obtain the following solution

$$|\alpha_2^{(2)}|^2 = \frac{(g_1^2+\xi_0+2)^2}{(\xi_0+2)((g_1^2-\xi_0)^2+4\xi_0+4))} \tag{5.39}$$

In the other case when layer 2 is selected, we follow the same steps to obtain the corresponding solution. By combining both cases, we obtain the results shown in Figure

5.6. We remark that the second layer is allocated more power in the second transmission. When g_1 is sufficiently high, the retransmission power is mainly allocated to the second layer.

For practical modulation and coding, our analysis is still applicable by replacing the value of ξ_0 by the SNR value which corresponds to the target error probability, such as $P_e = 10^{-3}$ for example. This value can be empirically determined from the performance of the error correcting code over AWGN channel. For example, the corresponding retransmission coefficient for $\xi_0 = 2$ dB is also shown in Figure 5.6.

5.6.2.2 Case of one error

Since the two layers are equally protected in the first transmission, this case would not occur under ideal conditions. However, if this happens in real situations, the erroneous packet is retransmitted alone using the total power.

Now, before continuing the adaptive retransmission strategy for following transmissions, we evaluate the performance of the proposed adaptation scheme for only two allowable transmissions.

5.6.2.3 Numerical results

In order to verify the advantage of the proposed adaptive HARQ protocol, we have simulated the FER performance in the system for $T - \max = 2$ over Rayleigh fading channel using a regular Low density parity check code (LDPC) with $K = 506$, $N = 1024$ given in [89] (with up to 50 internal iterations). By numerical simulations, we find that the empirical values of ξ_0 for this code with QPSK modulation is about $\xi_0 \approx 1.58 \approx 2$ dB instead of 0 dB for a perfect code with same rate and Gaussian modulation. Using this new value, we found from (5.28) that the optimum power allocation for the first transmission is $|\alpha_1^{(1)}|^2 = 0.72$.

Figure 5.7 shows the FER performance for the adaptive HARQ protocol using MMSE detection. We observe that at the first transmission, the FER performance of the two layers are not exactly the same. This is related to the successive decoding method with imperfect channel code. Actually, let P_1 denotes the FER for the first layer, and P_2 denotes the FER for the second layer assuming that the first layer is correct. Since the second layer is not decoded until the successful decoding of the first layer, the actual FER for the second layer would be $P_1 + (1 - P_1)P_2$. Thus, even if $P_1 = P_2$, the FER for the second layer would be $2P_1 - P_1^2$ which explains the difference in FER for each layer.

For the second transmission using the swept coefficients, the detection order can alternate between the two layers depending on the channel realizations in the first and in the second transmission. Consequently, the effect of imperfect coding is distributed equally over both layers. This is why the two FER curves are almost identical.

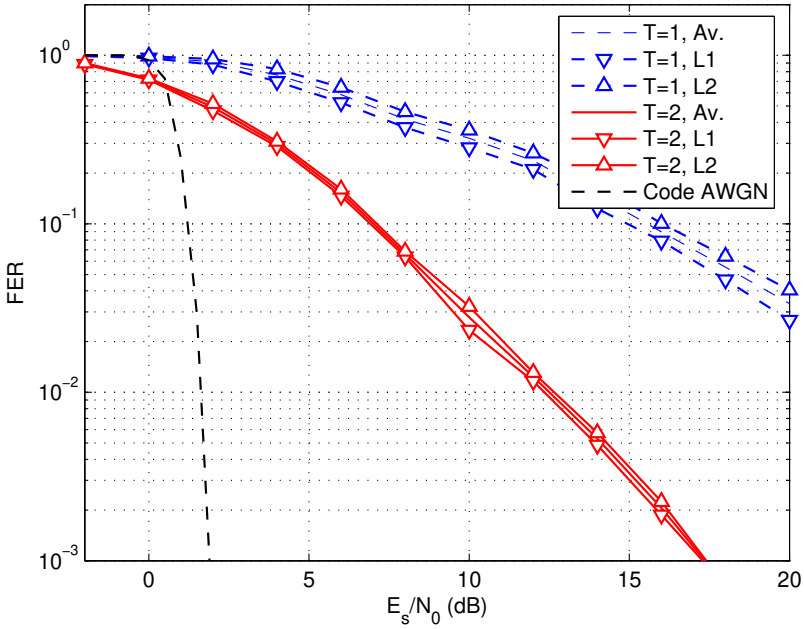

FIGURE 5.7: Performance of the optimized layered HARQ protocol for $T_{\max} = 2$.

Figure 5.8 shows the average FER performance comparison between the adaptive retransmission scheme with identical retransmissions using the superposition coefficients given by (5.28). Note that the case of a single error is treated in the same manner for both scheme. We observe several points: First the better performance of MMSE detection in comparison with MRC for the adaptive scheme. Second, the adaptive HARQ protocol for multi-layer retransmission provides about 1.5 dB of gain in comparison with static HARQ protocol at the second transmission. Third, we have simulated the average FER for the simple retransmission solution given by (5.28) which maximizes the instantaneous channel capacity. Interestingly, the performance loss is only about 0.1 dB compared with the optimal solution which minimize the average outage probability. This is actually the rational behind the proposed sub-optimal solution for later retransmissions in section 5.6.3.

5.6.3 Third and following retransmissions

For the third retransmission, similar analysis can be performed as in the case of two transmissions. However, this task becomes more complicated. Instead, we propose a sub-optimal solution as follows: For the current transmission T ($T > 2$), let T_0 be the index of the previous transmission that has the largest channel gain. We adapt the coefficients at the current transmission with the transmission T_0 based on (5.31), i.e.

$$\alpha_1^{(T)} = \alpha_2^{(T_0)}, \ \alpha_2^{(T)} = -\alpha_1^{(T_0)} \tag{5.40}$$

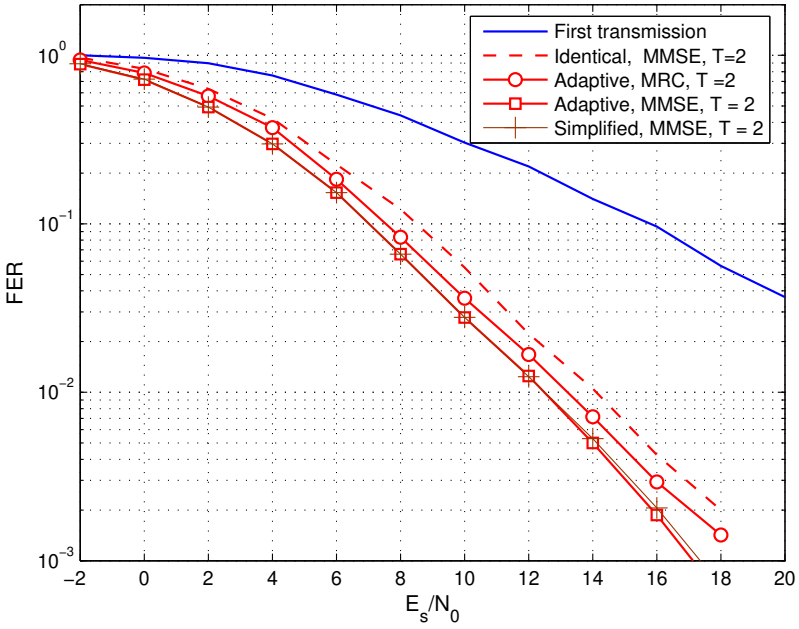

FIGURE 5.8: Performance of the optimized HARQ protocol using MRC and MMSE combining methods for $T_{\max} = 2$.

where

$$T_0 = \arg\max_{1 \le t \le T-1}(g_t) \tag{5.41}$$

Indeed, by adopting this solution, we only need the knowledge of the index of the best previous transmission T_0 instead of complete CSI.

5.6.4 Simplified adaptive HARQ protocol

In light of the previous analysis, we propose the following sub-optimal but simple adaptive HARQ protocols for layered transmissions:

- First transmission is determined from Equation (5.28).

$$|\alpha_1^{(1)}|^2 = \frac{\xi_0 + 1}{\xi_0 + 2}, \text{ and } |\alpha_2^{(1)}|^2 = \frac{1}{\xi_0 + 2}.$$

- Second transmission is determined from Equation (5.31).

$$\alpha_1^{(2)} = (\alpha_2^{(1)})^*, \quad \alpha_2^{(2)} = -(\alpha_1^{(1)})^*$$

- Third and later transmissions are determined from Equation (5.40).

$$\alpha_1^{(T)} = \alpha_2^{(T_0)}, \ \alpha_2^{(T)} = -\alpha_1^{(T_0)}$$

using the value of $T0$ returned by the receiver.

- For any retransmission request for a single layer, only the erroneous packet is retransmitted in a single layer with the full power.

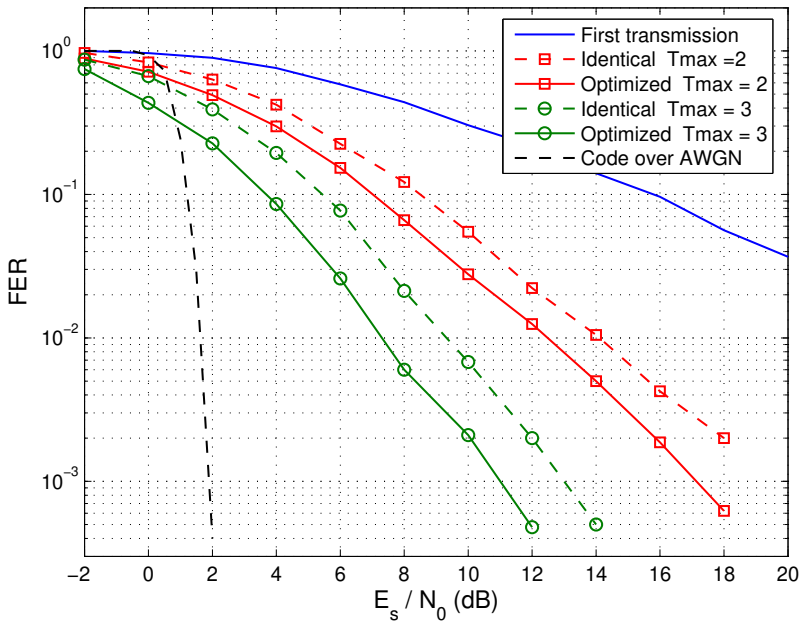

FIGURE 5.9: FER performance of the adaptive layered HARQ protocol for $T_{\max} = 1, 2$, and 3.

Figure 5.9 shows the FER performance of the proposed HARQ protocol for a maximum number of retransmissions per packet $T_{\max} = 3$ using the same simulation parameters as in Figure 5.7. We observe that, in comparison with identical retransmission, the adaptive HARQ protocol for multi-layer retransmission provides about 2 dB of gain at the third transmissions.

5.7 Conclusions

We presented in this chapter an adaptive HARQ protocol for multi-layer transmission over block-fading channels with feedback. With the same coding rates for all layers, we have optimized the superposition coefficients at each HARQ transmission in order to minimize the average frame error rate. We have shown in the case of a two layer retransmission scheme, that maximizing the instantaneous channel capacity is almost optimal for the minimization of average FER. The obtained solution consists of power swapping and sign inversion which is very similar to Alamouti space-time diversity scheme [5]. For long-term static channel, this solution allows the separation of the two layers into two parallel channels. Multi-layer transmission with adaptive HARQ

protocols provides the same protection for all transmitted bits. This can be viewed as modulation diversity applied on a modified 16-QAM constellation. However, the successive decoding simplifies the demapping and results in a lower decoding latency since the decoding of lower layers is aborted if the upper layer is not decoded successfully.

The MMSE MIMO detection method has been generalized for multi-layer HARQ transmissions over frequency-selective channels in our published paper in [90] conference (see publications below). A potential perspective of this work is the generalization for a frequency-selective channels including phase-precoding within each layer.

The results presented in this chapter have led to the following publications:

1. A. Assimi, C. Poulliat, and I. Fijalkow, "Packet combining for multi-layer hybrid-ARQ over frequency-selective fading channels," in *Eur. Signal Process. Conf. (EUSIPCO)*, Glasgow, Scotland, August 2009, pp. 671-675.

2. A. Assimi, C. Poulliat, and I. Fijalkow, "Reliable communications using multi-layer transmission," in *EuropeComm*, London, UK, August 2009.

Conclusions and perspectives

We have considered in this thesis the problem of reliable data packet transmission using single-carrier signaling over frequency-selective fading channels. The main question was how to optimize the HARQ retransmission protocols at the link layer of the communication network with the signal processing at the physical layer including channel equalization. We mainly focused on Chase Combining HARQ protocols due to their implementation simplicity.

We have seen in the first chapter that IR-HARQ protocols outperform in general CC-HARQ protocols, especially for high initial coding rate over slow time-varying flat fading channels. For frequency-selective channels, the comparison between the two HARQ protocols must also involves the performance of signal detection. Using maximum ratio combining at the bit level after separate equalization of each received packet would lead to the same relative performance between CC and IR. However, the performance of CC can be improved by using joint equalization for packet combining which has better performance than maximum ratio combining. Even though, the performance of CC are still behind the performance of IR.

From these results, we wondered if it is possible to further improve the performance of CC-HARQ protocols by introducing some modifications to the retransmission scheme while keeping, in the same time, the relative simplicity of CC-HARQ protocols.

In order to answer this question, we have analyzed the performance of the transmission scheme using an ideal maximum likelihood receiver in order to find out the different factors that affect the system performance. From this analysis we have found the following results:

On one hand, the error sequence plays a similar role to that of the channel response on the Euclidean distance distribution. This suggests that the retransmitted signal must provide the required diversity if the communication does not. However, the amplitude of the transmitted sequence is determined by the chosen constellation with a specific PAPR at the input of the power amplifier at the transmitter. In order create retransmission diversity while keeping unchanged the PAPR level of the original constellation, we propose to introduce phase-precoding diversity among subsequent CC-HARQ retransmission. The latter diversity scheme can be viewed as a generalized form of the already known cyclic-frequency diversity in the frequency-domain for OFDMA systems. The introduced phase-precoding at the transmitter can be handled with a modified

version of a joint equalizer without any significant additional complexity in comparison with joint equalization for identical retransmissions. Phase-precoding allows to smartly decorrelate error sequences which results in reduced output Euclidean distance fluctuations around the average. This results in enhanced joint equalization performance. However, the performance limits of the phase-precoding diversity remains the same as for identical retransmissions without precoding. This means that using a sophisticated receiver including iterative equalization and decoding, no performance improvement can be expected.

For frequency-selective channels, we have seen that turbo-equalization is an efficient technique which provides a near maximum-likelihood performance. However, this requires an additional computational complexity at the receiver and therefore an increased latency. However, phase-precoding helps the turbo-equalizer to converge faster. only 2 or 3 turbo-iterations are required to achieve most of the turbo-equalization gain. Hence, a lower receiver complexity for the same performance between the precoded and the non-precoded systems when using an iterative receiver structure.

On the other hand, the Euclidean distance variance is inversely proportional to the interleaving length. For T HARQ transmissions, beside the superior coding gain, IR benefit from T times larger interleaving length in comparison with CC. Therefore, we study in Chapter 3 the bit-interleaving diversity in order to recover this loss for the CC-HARQ scheme. Fortunately, this diversity scheme introduce also decorrelation (with a smaller degree than the optimized phase-precoding) between error sequences which improve the equalization performance. Furthermore, bit-interleaving provides also some modulation diversity for high order modulation. This leads to better performance limits than the classical retransmission scheme. Also, for MIMO channels, bit-interleaving benefits from spatial channel diversity. Both inherent diversities which result from the bit-interleaving are subject to further improvement by a proper choice of the used interleaver in order to provide the same degree of protection for all transmitted bits. From our comparative study between bit-interleaving diversity and phase-precoding diversity, we conclude that phase-precoding is suitable for not-iterative detection and decoding while bit-interleaving is suitable for an iterative receiver and high order modulations.

The retransmission protocols with transmit-diversity have better throughput performance for low to medium SNR range. For high SNR values, the data throughput is mainly determined by the FER at the first transmission. When the transmitter knows the average SNR value, the modulation and the coding scheme can be adapted accordingly. The adaptation is performed for a finite number of quantized SNR values. In rapidly time-varying conditions, no adaptation can be performed due to the unpredictable channel gain. For this, we have turned our attention in the last chapter to the multi-layer transmission scheme.

Multi-layer transmission can improve the throughput performance by carrying many packets on the transmitted signal. The receiver decodes the totality of these packets or a part of them depending on the instantaneous channel gain. In order to optimize the HARQ retransmission protocols, we first modeled multiple multi-layer transmissions

with an equivalent MIMO channel model. Then, based on this model, we proposed an adaptive retransmission protocol that minimizes the average FER per layer. This work was performed over a flat fading channel.

Perspectives

Multiple HARQ transmissions is considered in this thesis as SIMO transmissions with the difference that the number of transmitting antennas varies from one packet to another. According to this modernization, the phase-precoding diversity technique decorrelates the equivalent channels between various receive antennas. It would be interesting to extends this technique to MIMO transmissions in order to combat both of inter-symbol interference and inter-channel interference.

One can view IR as a form of code diversity as it is exactly the case when using self-decodable code at each HARQ transmission. We observe that, we have better performance when the diversity is introduced earlier in the transmission scheme since this inherently generates the diversity of the later blocks in transmitter scheme. This leads to think that it is possible to obtain further improvement if we introduce some kind of diversity to the information data before channel coding such as applying a different interleaver at each HARQ transmission before channel coding. This is another possible perspective of this thesis.

Multi-transmission was studied in this thesis over flat fading channels. The extension to frequency-selective channels and the possibility for the integration of the studied diversity techniques are among of the perspectives of this thesis because the propagation channels between various layers are inherently correlated.

Appendixes

Appendix A: Proof of Lemma 1

The OSED is given by,

$$\Delta = d_E^2(\mathbf{e}) = \|\mathbf{h} * \mathbf{e}\|^2 = \sum_{n=0}^{N_s-1} \left| \sum_{i=0}^{L-1} h_i e_{n-i} \right|^2$$

By developing the squared sum, we obtain,

$$\Delta = \sum_{n=0}^{N_s-1} \sum_{i=0}^{L-1} \sum_{j=0}^{L-1} h_i h_j^* e_{n-i} e_{n-j}^*$$

By changing the order of summation and introducing the new variable $n' = n - i$, the previous equation becomes

$$\Delta = \sum_{j=0}^{L-1} \sum_{i=0}^{L-1} h_i h_j^* \sum_{n'=-i}^{N_s-1-i} e_{n'} e_{n'+i-j}^*$$

Now, by performing the change of variable $\ell = j - i$, and recalling that $e_{-i} = e_{Ns-i}$ due to the cyclic-prefix insertion, we obtain

$$\Delta = \sum_{\ell=-L+1}^{L-1} \sum_{i=0}^{L-1} h_i h_{i+\ell}^* \sum_{n'=0}^{N_s-1} e_{n'} e_{n'-\ell}^*$$

with $h_i = 0$ for $i \notin [0, \cdots, L-1]$. This yields to

$$\Delta = \sum_{\ell=-L+1}^{L-1} R_{-\ell}(\mathbf{h}) R_\ell(\mathbf{e})$$

Finally, by using the hermitian symmetry of the autocorrelation function $R_{-\ell}(\mathbf{h}) = R_\ell^*(\mathbf{h})$, we obtain the desired result.

Appendix B: Proof of Proposition 1

Assuming uniform interleaving, the error symbols are considered as identically distributed but not independent due the constraint on the sum of their Hamming weights. However, any two error symbols are conditionally independent knowing their respective Hamming weights. The coded and interleaved packet contains N_b bits which are modulated to N_s symbols. The error packet contains d errors which are assumed uniformly distributed over the packet. The probability that a symbol e_n has a Hamming weight $d_H(e_n) = k$ is given by

$$\Pr(d_H(e_n) = k) = \binom{Q}{k}\binom{N_b - Q}{d-k} / \binom{N_b}{d} \tag{42}$$

where Q is the number of bits per symbol. The average squared amplitude μ_e can be calculated as

$$\mu_e(d) = E[||\mathbf{e}||^2|d] = N_s \sum_{k=1}^{Q} m_2(k) \Pr(d_H(e_n) = k) \tag{43}$$

$$= N_s \binom{N_b}{d}^{-1} \sum_{k=1}^{Q} \binom{Q}{k}\binom{N_b - Q}{d-k} m_2(k) \tag{44}$$

where $m_2(k) = E[|e_n|^2|k]$ for $k = 1, \cdots, Q$ is the conditional mean of $|e_n|^2$ giving its Hamming weight k.

The variance σ_e^2 can be similarly calculated as follows:

$$\sigma_e^2(d) = E[(||\mathbf{e}||^2 - \mu_e)^2|d] = E[||\mathbf{e}||^4|d] - \mu_e^2(d) \tag{45}$$

with

$$E[||\mathbf{e}||^4|d] = N_s \overline{m}_4(d) + N_s(N_s - 1)\varrho_2(d) \tag{46}$$

where

$$\overline{m}_4(d) = E[|e_n|^4|d] = \binom{N_b}{d}^{-1} \sum_{k=1}^{Q} \binom{Q}{k}\binom{N_b - Q}{d-k} m_4(k) \tag{47}$$

$$\begin{aligned} \varrho_2(d) &= E[|e_{n_1}|^2|e_{n_2}|^2|d] \\ &= \binom{N_b}{d}^{-1} \sum_{\substack{k_1,k_2=1 \\ k_1+k_2 \le d}}^{Q} \binom{Q}{k_1}\binom{Q}{k_2}\binom{N_b - 2Q}{d-k_1-k_2} m_2(k_1) m_2(k_2) \end{aligned} \tag{48}$$

for $n_1 \neq n_2$, where $m_4(k) = E[|e_n|^4|k]$. The conditional moments m_2 and m_4 can be computed directly from the modulation and the mapping scheme.

Appendix C: Proof of Proposition 2

The autocorrelation coefficient of the error sequence for lag ℓ is by definition, $R_\ell(\mathbf{e}) = \sum_{i=0}^{N_s-1} e_i e_{i-\ell}^*$. Then, we have

$$\begin{aligned} E(R_{\ell_1}(\mathbf{e})R_{\ell_2}^*(\mathbf{e})) &= E\left(\sum_{i=0}^{N_s-1}\sum_{j=0}^{N_s-1} e_i e_{i-\ell_1}^* e_j^* e_{j-\ell_2}\right) \\ &= \sum_{i=0}^{N_s-1}\sum_{j=0}^{N_s-1} E(e_i e_{i-\ell_1}^* e_j^* e_{j-\ell_2}) \end{aligned}$$

For given absolute values for error elements, their phases are independent for different indexes. Since $\ell_1 \neq \ell_2$, we can verify that $E(e_i e_{i-\ell_1}^* e_j^* e_{j-\ell_2}) = 0$ for all possibilities of i and j.

Appendix D: Proof of Proposition 3

This follows by direct evaluation of (2.29) using the result of Proposition 2.

Appendix E: Proof of Proposition 4

For BPSK modulation, we have $N_s = N_b = N$ Since autocorrelation coefficients are identically distributed, we determine the p.m.f of $R_1(\mathbf{e})$. For this, we define a new variable $S = \sum_{i=1}^{N-1} |z_i|$ where $z_i = e_i e_{i+1}/4$. The introduced variable S gives the number of non-zero terms in the autocorrelation definition. Note that the signs of the non-zero variable z_i are independent due to the conditional independence of error elements (assumption A2).

We evaluate the p.m.f of $R_1(\mathbf{e})$ as the marginal probability of $R_1(\mathbf{e})$ conditionally to the variable S,

$$\Pr(R_1) = \sum_{s=0}^{d-1} \Pr\left(R_1 | S = s\right) \Pr(S = s). \tag{49}$$

For $\ell = 1$, S is the number of consecutive non-zero elements in the error sequence $\mathbf{e}$.

We first determine $\Pr(S = s)$ which is the number of consecutive non-zero elements in a circular error sequence of length N with Hamming weight d. There are $\binom{d-1}{m-1}$ distinct decompositions of a sequence of d elements into m subsequences, each of length at least 1. The number of configurations in which these subsequences can occur in a circular sequence of length N, with consecutive subsequences separated by at least one position, is given by $\frac{N}{m}\binom{N-d-1}{m-1}$. For given m, we have $s = d - m$. This leads to the

following hyper-geometric p.m.f. of S

$$\Pr(S=s)=\frac{\binom{d-1}{s}\binom{N-d}{d-s}}{\binom{N-1}{d}}. \tag{50}$$

For a given value of $S=s$, we have $R_1(\mathbf{e})=4(s-2n)$ where n is the number of negative elements z_i. Since there is $\binom{s}{n}$ different possibilities out of 2^s to select n negative elements from the s non-zero elements, we find the conditional probability $\Pr(R_1(\mathbf{e})|S=s)$, after defining $k=s-2n$, is

$$\Pr(R_1=4k|S=s))=\frac{\binom{s}{n}}{2^s}=2^{-s}\binom{s}{\frac{s-k}{2}}, \tag{51}$$

with the convention $\binom{i}{j}=0$ for non integer values of j. By substituting equations (50) and (51) in (49) we obtain the p.m.f of $R_1(\mathbf{e})$,

$$\Pr(R_1=4k)=\frac{1}{\binom{N-1}{d}}\sum_{s=|k|}^{d-1}2^{-s}\binom{d-1}{s}\binom{N-d}{d-s}\binom{s}{\frac{s-k}{2}}. \tag{52}$$

This completes the proof of the proposition.

Appendix F: Statistics of error blocks for MIMO transmission

For an error block $\mathbf{e}_j$ from the error sequence which corresponds to the transmitted block on the j-th antenna, the statistics of its squared amplitude $||e_j||^2$ can be calculated as follows.

For the mean, we have

$$\mu_e \triangleq \mu(||\mathbf{e}_j||^2)=\sum_{d_j=1}^{d}E(||\mathbf{e}_j||^2|d_j)\Pr(d_j) \tag{53}$$

where $E(||\mathbf{e}_j||^2|d_j)$ is given by Proposition 2 in Chapter 2 for a block length $M=N_b/N_t$ and a Hamming error weight d_j. The probability $\Pr(d_j)$ is the probability of having a e Hamming weight d_j in the j-th error block and is given by

$$\Pr(d_j)=\binom{N_b}{d}^{-1}\binom{M}{d_j}\binom{N_b-M}{d-d_j}. \tag{54}$$

Let $\mu_e(d_j)\triangleq E(||\mathbf{e}_j||^2|d_j)$, then the variance is calculated in a similar manner as

$$\sigma_e^2 \triangleq \sigma^2(||\mathbf{e}_j||^2)=\sum_{d_j=1}^{d}E(||\mathbf{e}_j||^4|d_j)\Pr(d_j)-\mu_e^2 \tag{55}$$

The cross-correlation statistics is calculated based on the conditional independence of error blocks as

$$\rho_e \triangleq E((||\mathbf{e}_i||^2 - \mu_e)(||\mathbf{e}_j||^2 - \mu_e)) \tag{56}$$

$$= \sum_{\substack{d_i,d_j=1 \\ d_i+d_j\leq d}}^{d} E(||\mathbf{e}_i||^2||\mathbf{e}_j||^2|d_i,d_j)\Pr(d_i,d_j) - \mu_e^2 \tag{57}$$

$$= \sum_{\substack{d_i,d_j=1 \\ d_i+d_j\leq d}}^{d} E(||\mathbf{e}_i||^2|d_i)E(||\mathbf{e}_j||^2|d_j)\Pr(d_i,d_j) - \mu_e^2 \tag{58}$$

$$= \sum_{\substack{d_i,d_j=1 \\ d_i+d_j\leq d}}^{d} \mu_e(d_i)\mu_e(d_j)|d_j)\Pr(d_i,d_j) - \mu_e^2 \tag{59}$$

where the joint probability of Hamming weights is

$$\Pr(d_i,d_j) = \tbinom{N_b}{d}^{-1}\tbinom{M}{d_i}\tbinom{M}{d_j}\tbinom{N_b-2M}{d-d_i-d_j}. \tag{60}$$

This completes the statistics of error blocks for MIMO transmission.

Bibliography

[1] S. Lin, D. Costello, and M. Miller, "Automatic-repeat-request error-control schemes," *IEEE Commun. Mag.*, vol. 22, no. 12, pp. 5–17, 1984.

[2] D. Chase, "Code combining–a maximum-likelihood decoding approach for combining an arbitrary number of noisy packets," *IEEE Trans. Commun.*, vol. COM-33, no. 5, pp. 385–393, 1985.

[3] B. A. Harvey and S. B. Wicker, "Packet combining systems based on the viterbi decoder," *IEEE Trans. Commun.*, vol. 42, no. 2/3/4, pp. 1544–1557, 1994.

[4] J. Hagenauer, "Rate-compatible punctured convolutional codes (RCPC codes) and their applications," *IEEE Trans. Commun.*, vol. 36, no. 4, pp. 389–400, 1988.

[5] S. M. Alamouti, "A simple transmit diversity technique for wireless communications," *IEEE Journal on Selected Areas in Communications*, vol. 16, no. 8, pp. 1451–1458, 1998.

[6] L. Zheng and D. N. C. Tse, "Diversity and multiplexing: a fundamental tradeoff in multiple-antenna channels," *IEEE Trans. Inf. Theory*, vol. 49, no. 5, pp. 1073–1096, 2003.

[7] C. Zhongren, U. Tureli, and Y. Yu-Dong, "Deterministic multiuser carrier-frequency offset estimation for interleaved OFDMA uplink," *IEEE Trans. Commun.*, vol. 52, no. 9, pp. 1585–1594, 2004.

[8] 3GPP Technical Specification Group Radio Access Network E-UTRA (Release 8), "LTE Physical Layer - General Description," 3GPP TS 36.201 V8.3.0, March, 2009, [Online] Available:http://www.3gpp.org/ftp/Specs/html-info/36-series.htm.

[9] G. Huang, A. Nix, and S. Armour, "Decision feedback equalization in SC-FDMA," in *IEEE Int. Symp. Pers., Indoor Mob. Radio Commun.*, Cannes, France, 2008.

[10] H. G. Myung, J. Lim, and D. J. Goodman, "Single carrier FDMA for uplink wireless transmission," *IEEE Vehicular Technology Magazine*, vol. 1, no. 3, pp. 30 – 38, 2006.

[11] J. Forney, G., "Maximum-likelihood sequence estimation of digital sequences in the presence of intersymbol interference," *IEEE Trans. Inf. Theory*, vol. 18, no. 3, pp. 363–378, 1972.

[12] W. H. Sheen and G. L. Stuber, "MLSE equalization and decoding for multipath-fading channels," *IEEE Trans. Commun.*, vol. 39, no. 10, pp. 1455–1464, 1991.

[13] C. Douillard, A. Picart, P. Didier, M. Jézéquel, C. Berrou, and A. Glavieux, "Iterative correction of intersymbol interference: turbo-equalization," *European Transactions on Telecommunications*, vol. 6, no. 5, pp. 507–512, 1995.

[14] R. Koetter, A. C. Singer, and M. Tuchler, "Turbo equalization," *IEEE Signal Process. Mag.*, vol. 21, no. 1, pp. 67–80, 2004.

[15] S. Benedetto, D. Divsalar, G. Montorsi, and F. Pollara, "A soft-input soft-output app module for iterative decoding of concatenated codes," *IEEE Commun. Lett.*, vol. 1, no. 1, pp. 22–24, 1997.

[16] L. Bahl, J. Cocke, F. Jelinek, and J. Raviv, "Optimal decoding of linear codes for minimizing symbol error rate," *IEEE Trans. Inf. Theory*, vol. 20, no. 2, pp. 284–287, 1974.

[17] M. Tuchler, R. Koetter, and A. C. Singer, "Turbo equalization: principles and new results," *IEEE Trans. Commun.*, vol. 50, no. 5, pp. 754–767, 2002.

[18] T. Fujiwara, T. Kasami, A. Kitai, and L. Shu, "On the undetected error probability for shortened hamming codes," *IEEE Trans. Commun.*, vol. 33, no. 6, pp. 570–574, 1985.

[19] 3GPP, "Technical Specification Group Radio Access Network; Multiplexing and channel coding (Release 8)," 3GPP TS 36.212 V8.6.0, March 2009, [Online] Available:http://www.3gpp.org/ftp/Specs/html-info/36-series.htm.

[20] K. A. S. Abdel-Ghaffar, "A lower bound on the undetected error probability of block codes," in *IEEE Int. Symp. Inf. Theory*, 1995, p. 341.

[21] F.-W. Fu, T. Klove, and V. K. W. Wei, "On the undetected error probability for binary codes," *IEEE Trans. Inf. Theory*, vol. 49, no. 2, pp. 382–390, 2003.

[22] J. G. Proakis, *Digital Communications*, 4th ed. Boston: McGraw Hill, 2001.

[23] C. Berrou, A. Glavieux, and P. Thitimajshima, "Near shannon limit error-correcting coding and decoding: Turbo-codes. 1," in *IEEE Int. Conf. Commun.*, vol. 2, Geneva, Switzerland, 1993, pp. 1064–1070.

[24] R. Gallager, "Low-density parity check codes," Ph.D. dissertation, MIT Press, 1963.

[25] D. J. MacKay and R. M. Neal, "Near Shannon limit performance of low density parity check codes," *Electr. lett.*, 1996.

[26] S. Dolinar and D. Divsalar, "Weight distribution for turbo codes using random and non-random permutations," Jet propulsion Lab, Tech. Rep., August 1995.

[27] K. V. Koutsouvelis and C. E. Dimakis, "A low complexity algorithm for generating turbo code s-random interleavers," *Wireless Personal Communications*, vol. 46, no. 3, pp. 365–370, 2007.

[28] 3GPP Technical Specification Group Radio Access Network E-UTRA (Release 8), "Base Station (BS) radio transmission and reception," 3GPP TS 36.104 V8.5.0, March, 2009, [Online] Available: http://www.3gpp.org/ftp/Specs/html-info/36-series.htm.

[29] D. G. Brennan, "Linear diversity combining techniques," *Proc. IEEE*, vol. 91, no. 2, pp. 331–356, 2003.

[30] D. N. Rowitch and L. B. Milstein, "On the performance of hybrid FEC/ARQ systems using rate compatible punctured turbo (RCPT) codes," *IEEE Trans. Commun.*, vol. 48, no. 6, pp. 948–959, 2000.

[31] G. Caire and D. Tuninetti, "The throughput of hybrid-ARQ protocols for the Gaussian collision channel," *IEEE Trans. Inf. Theory*, vol. 47, no. 5, pp. 1971–1988, 2001.

[32] H. El Gamal, G. Caire, and M. O. Damen, "The MIMO ARQ channel: Diversity-multiplexing-delay tradeoff," *IEEE Trans. Inf. Theory*, vol. 52, no. 8, pp. 3601–3621, 2006.

[33] J.-F. Cheng, "Coding performance of hybrid ARQ schemes," *IEEE Trans. Commun.*, vol. 54, no. 6, pp. 1017–1029, 2006.

[34] S. Kallel, "Complementary punctured convolutional (CPC) codes and their applications," *IEEE Transactions on Communications*, vol. 43, no. 6, pp. 2005–2009, June 1995.

[35] M. Patzold and F. Laue, "Statistical properties of Jakes' fading channel simulator," in *Proc. IEEE 48th Veh. Technol. Conf., VTC'98*, 1998, pp. 712–718.

[36] D. S. Baum, J. Hansen, and J. Salo, "An interim channel model for beyond-3G systems: extending the 3GPP spatial channel model (SCM)," in *Veh. Techn. Conf.*, vol. 5, Zurich, Switzerland, 2005, pp. 3132–3136.

[37] D. Baum and et al., "3GPP Spatial Channel Model Extended (SCME)," 2008, [Online] Available:http://www.ist-winner.org/3gpp_scme.html.

[38] "Spatial channel model for multiple input multiple output (MIMO) simulations," 3GPP TR 25.996 V8.0.0, December, 2008, [Online] Available:http://www.3gpp.org/ftp/Specs/html-info/25996.htm.

[39] A. Dejonghe and L. Vandendorpe, "Turbo-equalization for multilevel modulation: an efficient low-complexity scheme," in *IEEE Int. Conf. Commun.*, vol. 3, 2002, pp. 1863–1867.

[40] M. Tuchler, A. C. Singer, and R. Koetter, "Minimum mean squared error equalization using a priori information," *IEEE Trans. Signal Process.*, vol. 50, no. 3, pp. 673–683, 2002.

[41] F. Vogelbruch and S. Haar, "Improved soft ISI cancellation for turbo equalization using full soft output channel decoder's information," in *IEEE Global Telecommun. Conf.*, vol. 3, 2003, pp. 1736–1740.

[42] M. Tuchler and J. Hagenauer, "Linear time and frequency domain turbo equalization," in *IEEE Veh. Technol. Conf.*, 53rd, Ed., Rhodes, Greece, 2001, pp. 1449–1453.

[43] S. ten Brink, "Convergence behavior of iteratively decoded parallel concatenated codes," *IEEE Trans. Commun.*, vol. 49, no. 10, pp. 1727–1737, 2001.

[44] J. Hagenauer, "The exit chart : Introduction to extrinsic information transfer in iterative processing," in *European Signal Processing Conference*, Vienna, Austria, September 2004, pp. 1541–1548.

[45] H. Samra and Z. Ding, "A hybrid ARQ protocol using integrated channel equalization," *IEEE Trans. Commun.*, vol. 53, no. 12, pp. 1996–2001, 2005.

[46] T. Shi and L. Cao, "Combining techniques and segment selective repeat on turbo coded hybrid ARQ," in *IEEE wirel. Commun. Netw. Conf.*, vol. 4, 2004, pp. 2115–2119.

[47] J. Forney, G., "Lower bounds on error probability in the presence of large intersymbol interference," *IEEE Trans. Commun.*, vol. 20, no. 1, pp. 76–77, 1972.

[48] S. Benedetto, D. Divsalar, G. Montorsi, and F. Pollara, "Serial concatenation of interleaved codes: performance analysis, design, and iterative decoding," *IEEE Trans. Inf. Theory*, vol. 44, no. 3, pp. 909–926, 1998.

[49] M. Oberg and P. H. Siegel, "Performance analysis of turbo-equalized partial response channels," *IEEE Trans. Commun.*, vol. 49, no. 3, pp. 436–444, 2001.

[50] A. Ghrayeb and M. El-Tarhuni, "On the performance of turbo equalization for precoded ISI channels," *Wirel. Commun. Mob. Comput.*, vol. 6, no. 4, pp. 431–438, 2006.

[51] S. M. Kay, A. H. Nuttall, and P. M. Baggenstoss, "Multidimensional probability density function approximations for detection, classification, and model order selection," *IEEE Trans. Signal Process.*, vol. 49, no. 10, pp. 2240–2252, 2001.

[52] N. Sellami, A. Roumy, and I. Fijalkow, "A proof of convergence of the MAP turbo-detector to the AWGN case," *IEEE Trans. Signal Process.*, vol. 56, no. 4, pp. 1548–1561, April 2008.

[53] S. A. Raghavan, J. K. Wolf, and L. B. Milstein, "On the performance evaluation of ISI channels," *IEEE Trans. Inf. Theory*, vol. 39, no. 3, pp. 957–965, 1993.

[54] M. H. Quenouille, "The joint distribution of serial correlation coefficients," *The Annals of Mathematical Statistics*, vol. 20, no. 4, pp. 561–571, 1949.

[55] A. Steinhardt and J. Makhoul, "On the autocorrelation of finite-length sequences," *IEEE Transactions on Acoustics, Speech, and Signal Processing*, vol. 33, no. 6, pp. 1516–1520, 1985.

[56] F. Hoppe and M. Nediak, "Fréchet optimal bounds on the probability of a union with supplementary information," *Statistics and probability letters*, vol. 78, no. 3, pp. 311–319, 2008.

[57] J. Li, K. R. Narayanan, and C. N. Georghiades, "An efficient algorithm to compute the Euclidean distance spectrum of a general intersymbol interference channel and its applications," *IEEE Trans. Commun.*, vol. 52, no. 12, pp. 2041–2046, 2004.

[58] W. Ser, K.-C. Tan, and K.-C. Ho, "A new method for determining "unknown" worst-case channels for maximum-likelihood sequence estimation," *IEEE Trans. Commun.*, vol. 46, no. 2, pp. 164–168, 1998.

[59] E. Malkamaki and H. Leib, "Evaluating the performance of convolutional codes over block fading channels," *IEEE Trans. Inf. Theory*, vol. 45, no. 5, pp. 1643–1646, 1999.

[60] H. Harashima and H. Miyakawa, "Matched-transmission technique for channels with intersymbol interference," *IEEE Trans. Commun.*, vol. 20, no. 4, pp. 774–780, 1972.

[61] J. Forney, G. D. and M. V. Eyuboglu, "Combined equalization and coding using precoding," *IEEE Commun. Mag.*, vol. 29, no. 12, pp. 25–34, 1991.

[62] H. Samra and Z. Ding, "Symbol mapping diversity in iterative decoding/demodulation of ARQ systems," in *IEEE Int. Conf. Commun.*, vol. 5, Anchorage, Alaska, USA, 2003, pp. 3585–3589.

[63] H. Samra, H. Sun, and Z. Ding, "Capacity and linear precoding for packet retransmissions," in *IEEE Int. Conf. Acoust. Speech Signal Process.*, vol. 3, Pennsylvania, Philadelphia, USA, 2005, pp. 541–544.

[64] T. Strohmer, R. Heath Jr., and A. Paulraj, "On the design of optimal spreading sequences for cdma systems," in *Asilomar Conference on Signals, Systems and Computers*, vol. 2, 2002, pp. 1434 – 1438.

[65] L. Welch, "Lower bounds on the maximum cross correlation of signals," *IEEE Trans. Inf. Theory*, vol. 20, no. 3, pp. 397–399, 1974.

[66] J. L. Massey and T. Mittelholzer, "Welch's bound and sequence sets for code-division multiple-access systems," in *Sequences II, Methods in Communications, Security and Computer Science*, Springer-Verlag, New York, NY, USA, 1993, pp. 63–78.

[67] G. N. Karystinos and D. A. Pados, "New bounds on the total squared correlation and optimum design of DS-CDMA binary signature sets," *IEEE Trans. Commun.*, vol. 51, no. 1, pp. 48–51, 2003.

[68] D. Falconer, S. L. Ariyavisitakul, A. Benyamin-Seeyar, and B. Eidson, "Frequency domain equalization for single-carrier broadband wireless systems," *IEEE Commun. Mag.*, vol. 40, no. 4, pp. 58–66, 2002.

[69] R. Visoz, A. Berthet, and S. Chtourou, "Frequency domain block turbo-equalization for single-carrier transmission over MIMO broadband wireless channel," *IEEE Trans. Commun.*, vol. 54, no. 12, pp. 2144 – 2149, 2006.

[70] T. Ait-Idir, H. Chafnaji, and S. Saoudi, "Joint hybrid ARQ and iterative space-time equalization for coded transmission over the MIMO-ISI channel," in *Wirel. Commun. and Net. Conf.*, Las Vegas, USA, 2008, pp. 622 – 627.

[71] K. Balachandran and J. B. Anderson, "Mismatched decoding of intersymbol interference using a parallel concatenated scheme," *IEEE J. Sel. Areas Commun.*, vol. 16, no. 2, pp. 255–259, 1998.

[72] J. Nelson, A. Singer, and R. Koetter, "Linear turbo equalization for parallel ISI channels," *IEEE Trans. Commun.*, vol. 51, no. 6, pp. 860–864, 2003.

[73] D. N. Doan and K. R. Narayanan, "Iterative packet combining schemes for intersymbol interference channels," *IEEE Trans. Commun.*, vol. 50, no. 4, pp. 560–570, 2002.

[74] X. Cheng, C.-X. Wang, D. Yuan, and H.-H. Chen, "A novel iterative method for turbo equalization," in *IEEE wirel. Commun. Netw. Conf.*, Hong Kong, China, 2007, pp. 488–492.

[75] T. Abe and T. Matsumoto, "Space-time turbo equalization in frequency-selective MIMO channels," *IEEE Trans. Veh. Technol.*, vol. 52, no. 3, pp. 469–475, 2003.

[76] T. Koike, H. Murata, and S. Yoshida, "Hybrid ARQ scheme suitable for coded MIMO transmission," in *IEEE Int. Conf. Commun.*, vol. 5, Paris, France, 2004, pp. 2919–2923.

[77] J. Wang, M. Tu, K. Zheng, and W. Wang, "Hybrid ARQ scheme with antenna permutation for MIMO systems in slow fading channels," in *Networking Conference*, Coimbra, Portugal, 2006, pp. 1222– 1227.

[78] A. Steiner and S. Shamai, "Multi-layer broadcasting hybrid-ARQ strategies for block fading channels," *IEEE Trans. Wireless Commun.*, vol. 7, no. 7, pp. 2640 – 2650, 2008.

[79] L. Hang, C. Jason, M. Tao, and R. S. Cheng, "Optimal power allocation scheme on generalized layered space-time coding systems," in *Proc. IEEE Int. Conf. on Comm., ICC 2001*, 2001, pp. 1706–1710.

[80] X. Ma and L. Ping, "Power allocations for multilevel coding with sigma mapping," *Electr. lett.*, vol. 40, no. 10, pp. 609 – 611, 2004.

[81] K. Wu, L. Ping, and W. Leung, "Multi-layer turbo space-time codes for high-rate applications," in *GLOBECOM '04*, Dallas, Texas, 2004, pp. 3758– 3762.

[82] K. Kansanen, C. Schneider, T. Matsumoto, and R. Thoma, "Multilevel-coded QAM with MIMO turbo-equalization in broadband single-carrier signaling," *IEEE Trans. Veh. Technol.*, vol. 54, no. 3, pp. 954 – 966, 2005.

[83] F. Etemadi and H. Jafarkhani, "Optimal rate and power allocation for layered transmission with superposition coding," in *Data Compression Conference*, Washington, DC, USA, 2007, pp. 380–389.

[84] A. Nakajima and F. Adachi, "Throughput performance of iterative frequency-domain SIC with 2D MMSE-FDE for SC-MIMO multiplexing," in *Veh. Techn. Conf.*, 2006, pp. 1–5.

[85] J. Tong and L. Ping, "Iterative decoding of superposition coding," in *int. Symp. Turbo Codes*, Munich, Germany, 2006, pp. 1–5.

[86] P. Wolniansky, G. Foschini, G. Golden, and R. Valenzuela, "V-BLAST: an architecture for realizing very high data rates over the rich-scattering wireless channel," in *International Symposium on Signals, Systems, and Electronics*, Pisa, Italy, 1998, pp. 295–300.

[87] B. Lu and X. Wang, "Design of multilayer coded modulation for nonergodic block-fading channels," *IEEE Trans. Commun.*, vol. 55, no. 1, pp. 205–215, 2007.

[88] R. A. Horn and C. Johnson, *Matrix Analysis*. Cambridge University Press, Cambridge, 1985.

[89] D. MacKay, "Encyclopedia of sparse graph codes," 2006, [Online] Available:http://www.inference.phy.cam.ac.uk/mackay/codes/data.html.

[90] A. Assimi, C. Poulliat, and I. Fijalkow, "Packet combining for multi-layer hybrid-ARQ over frequency-selective fading channels," in *Eur. Signal Process. Conf.*, Glasgow, Scotland, 2009, pp. 671–675.

Résumé

Nous considérons dans cette thèse le problème de la transmission fiable de données par paquets en utilisant une transmission mono-porteuse sur des canaux sélectifs en fréquence à évanouissements. Notre objectif est de concevoir des couples émetteurs-récepteurs permettant d'améliorer les performances de la détection en l'absence d'information sur le canal à la transmission et ceci en exploitant la diversité temporelle disponible dans le cadre des protocoles de retransmission hybrides (HARQ).

En analysant les performances du système de transmission avec un récepteur à maximum de vraisemblance, nous établissons un critère pertinent pour l'étude des performances du système basé sur les statistiques de la distance Euclidienne à la sortie du canal sélectif en fréquence. A partir de ce cadre théorique, nous proposons un nouveau schéma de diversité entre les différentes retransmissions, nommé précodage de phase, qui permet de combattre l'interférence entre symboles pour les canaux lentement variables dans le temps. Puis, à l'aide de nos outils d'analyse, nous revisitons un autre schéma de diversité qu'est la diversité d'entrelacement. En particulier, nous soulignons le double avantage offert par ce schéma, à savoir la diversité de modulation et la réduction de l'interférence entre symboles. Nous réalisons ensuite une étude comparative entre les deux schémas de diversité précédents sous traitement itératif ou non itératif au récepteur. Enfin, nous introduisons un nouveau protocole de retransmission adaptative pour les transmissions dîtes multi-couches afin de réduire l'interférence entre couches pour les canaux rapidement variant dans le temps utilisant des informations de retour limitées.

Abstract

In this thesis, we consider the problem of reliable data packets transmission using single-carrier signaling over frequency-selective fading channels. Our objective is to design enhanced transceivers with improved detection performance in the absence of channel state information at the transmitter by exploiting the available time-diversity in Chase combining Hybrid Automatic Repeat reQuest (HARQ) protocols.

By analyzing the performance of the transmission scheme using an optimal maximum-likelihood receiver, we establish a suitable criterion for the study of system performance based on the statistics of the Euclidean distance at the output of a frequency-selective channel. From this theoretical framework, we propose a novel transmit-diversity scheme between subsequent HARQ transmissions, called phase-precoding, which allows the mitigation of intersymbol interference for slow time-varying channels. Then, with the help of our analytical tools, we revisit another transmit-diversity scheme which is the bit-interleaving diversity scheme. In particular, we emphasize the double advantage offered by this diversity scheme including the inherent modulation diversity in addition to the intersymbol interference reduction. Subsequently, we perform a comparative study between phase-precoding and bit-interleaving diversity schemes under iterative and non-iterative receiver structures. Finally, we introduce a new adaptive retransmission protocol for a multi-layer transmission scheme for the mitigation of inter-layers interference for rapidly time-varying channels using limited feedback information.